Ghent University:
Analitycal chemistry

Sapienza University of Rome:
Materials and Raw Materials Engineering

Joint Ph.D in:
Materials and Raw Materials Engineering and Analitycal chemistry

Corrosion behavior of bronze alloys exposed to urban and marine environment: an innovative approach to corrosion process understanding and to graphical results presentation.

Liliana Gianni

Promoters: Prof. Annemie Adriaens
Prof. Mauro Cavallini

Ghent - Rome
2011

Purpose of the Research

This research follows two main directions: the study of bronze corrosion in urban and marine environments and a new approach to the interpretation of data obtained from a set of techniques that are used in the field of diagnostics and conservation of cultural heritage.

In the framework of the first aim, the attention was focused on the analysis of the influence of tin content on corrosion behavior of bronzes.

Three bronze samples with different percentages of tin were selected to represent different kinds of artifacts that can be found in our hinterland or coastal cities.

The samples were exposed to natural urban and marine environments and monitored to understand the ongoing corrosion processes, their specific rates and to identify the patina composition, evolution, stratigraphy and properties.

Two cities were selected for the urban in field exposure in order to evaluate the corrosion due to each different air quality, temperature and humidity.

Natural environments were also reproduced artificially in laboratory with the intent of imitating the corrosion conditions and analyzing the effects of the surface exposure to wet and dry cycles, as well as to the effects of a long wet period. Different wet periods represent different situations that can be found on a same artifact or associated to different environmental conditions.

The data gathered allowed us to propose a corrosion model for bi-component bronzes in specific urban and marine environments tested, with the aim of predicting bronzes evolution and estimate the risks for artifacts.

The in field exposure results and the laboratory tests were compared to give a correct interpretation of the corrosion processes on the three alloys in each different environment of exposure. The comparison was also useful to associate the urban environment to the corresponding laboratory tests (wet and dry cycles or long wetness time) .

The second aim of this research was the improvement of the interpretation of some analytical techniques' results in the field of cultural heritage conservation sciences.

The use of electrochemical and optical methods and the comparison of their results were aimed to highlight the complementarity of the techniques, to find their new possible combinations, to gather more information about the artifact's conservation state, to ascertain the tight relationship between data and corrosion parameters and to support the interpretation of each technique.

Electrochemical impedance spectroscopy was one of the techniques used being a powerful tool in metallic heritage's diagnosis also if its application in this field is still difficult. The application of EIS in the cultural heritage analysis requires specific precautions in its use in order to be less invasive as possible. This aspect has been considered by testing the aggressiveness of the electrolytic solutions frequently used in EIS measurements in order to select the less dangerous for the bronze. However the main focus of this work has been the evaluation of reproducibility and sensibility of the EIS measurements on complex cases of

corrosion. Those were evaluated in order to understand what values differences can be distinguished and therefore which is the best application of the techniques for specific results needs.

The research also attempted to facilitate the interpretation and translation in equivalent circuits of the Nyquist curves. This aim was pursued by associating the specific physical or chemical aspects of the corrosion process or corrosion patina properties to the equivalent circuit elements

Moreover, the cases analyzed in this work will be collected with other EIS analysis done on copper and copper alloys exposed to different environments to build an impedance collection.

The impedance cases collected can be consulted to support the interpretation of the corrosion phenomenon in similar environmental conditions, to help in the translation in equivalent circuit the graphs and to explain and describe the corrosion of a specific material in a specific environment.

With a wide range of cases analyzed, the collection could be used as an information tool on the corrosion phenomenon in different environments for different metals. This tool could be consulted in many cultural heritage professions to plan a restoration or conservation activity and to set up an emergency restoration scale knowing the conservative state of artefacts.

An innovative data elaboration was also pursued for the spectrocolorimetric technique, which is frequently used on paintings' and pigments' characterization but less for metal artefacts.

In this research an innovative use of the spectrocolorimetry was pursued using colorimetry not only to characterize the patina colour but also to describe the corrosion's evolution. Colorimetric parameters were associated to specific corrosion indexes. The correct relationships between colour parameters and corrosion description were evaluated comparing the colorimetry results and interpretations with the results and interpretations obtained with other techniques.

Moreover, in order to expand the spectrocolorimetry use in the analysis of metallic artefacts, a new data elaboration was developed to identify corrosion's products. In this research a first step to reach this goal was done: spectrocolorimetry measures combined with XRD analysis were collected and studied to find colour parameters characteristics as fingerprints of corrosion products. In order to deduce this information the transformation of the graphs and data from the λ domain to the energy and the derivation the reflectance curves in relation to the energy was suggested, obtaining the adsorption edge of the patina. The energy reflected from the patinas, when radiated from the spectrophotometer, is also computable by integration of this curve. Also these values will be considered to characterize the patina.

The research proposes also an innovative graphical results' presentation useful to summarize and simplify the techniques' interpretation and contribution. The graphical results' presentation was suggested to be consulted by professionals of different disciplines. This aim was pursued by realizing a "damage scale" of three bronze alloys in each urban environment of exposure and also taking into account the stability or the passive properties of the patinas formed.

1. Background

1.1 Bronze

1.1.1 Bronze in the history of art

The Latin word for copper, "cuprum", comes from "aes Cyprius", which literally means "metal from Cyprus". In the antique age of Romans, Cyprus was a region famous for its supply of copper [1]. In the modern era this connection between copper and Cyprus has been retained in the chemical abbreviation for copper, Cu.

Copper is the most important metal in artistic metallurgy, both for its availability and for its properties of hardness, malleability, resistance to atmosphere and quality of its alloys: bronzes and brasses. Copper has a quite high melting temperature (1085 °C) as well as a low fluidity. It is not suitable to be cast in molds, and for this reason metals such as tin, zinc and lead are added to form castable alloys. The melting temperature then is lowed and the liquid becomes more homogeneous [1].

The use of native copper goes back in time to thousands of years ago and occurred in most geographical areas at a very early period in human prehistory. When Neolithic cultures first began to use it, around the 8^{th} millennium B.C., they worked the metal into small ornaments and simple copper blades [2]. At the beginning the metal was treated with cold hammering to produce plates to apply on wood or stone models, and, only for small sculptures, used to be cast in molds [3]. The late use of metals in sculptures, usually made of wood or stone, was due to a lack of knowledge of the materials and to the difficulties of metallurgical technology. Those aspects were exceeded with some innovation as the "lost wax" technique ("a cera persa") was known in Mesopotamia and in Egypt since the second millennium B.C. and was currently used in Greece since the 5^{th} century B.C.[1].

The most frequently used alloy has been bronze, sometimes referred to as "bronzes" for the great variety of its possible set of compositions. The most important alloying component in the bronze is tin. With this element the alloy becomes more fluid but it is also harder and brittle in its solid state. The alloys with a low concentration of tin (with a copper presence of more than 90%) can be easily cold hammered, however, the fluid liquid is heterogeneous and the solid product could be crrupted. On the other hand, alloys with higher concentrations of tin show a good fluidity of the liquid and are easy to be cast into shapes but do not to be handled at cold temperatures [3].

The white alloying elements, as tin, lead and zinc, were also added to give a specific coloration to the bronze. As a results, over time the use of the alloying elements changed to follow aesthetics and material needs [4].

Generally the prehistoric and pre-classic bronzes (Mesopotamian, Egyptian, Cretan etc) were poor of tin: they had a 90%-95% concentration of copper. Also in Greece the tin content was low and some lead was usually added [1]. Only in the ancient Roman period the bronze alloys were used with higher concentration of tin. The concentration of copper was lower, around 70%, and occasionally part of tin was replaced by lead and zinc. Lead was also alloyed to lower the costs of the alloy whilst the zinc favored the gilding, common during the Roman empire. The percentage of 70% of copper and 30% of white element reached in the classic age were also common during the Middle Ages. At the beginning the lead was preferred to tin, but became more used specially in the belts casting. The copper content increased during the Renaissance, when the zinc alloyed with copper to produce brass was discovered [3].

1.1.2 Material microstructure

The phase diagram for the copper-tin system is rather complex (Figure 1.1). Tin bronzes may be conveniently divided into two regions: low-tin bronzes and high-tin bronzes. Low-tin bronzes are those in which the tin content is less than 17%. This is the maximum theoretical limit of the tin solubility in the copper rich solid solution. In practice, the usual limit of solid solution is nearer to 14%, although it is rare to find a bronze with this tin content in a homogeneous phase.
Figure 1.1 shows a peritectic structure at 798 °C (25.5% of tin) and two eutectoid structures at 586 °C (24.6% of tin) and at 520°C (27% of tin). The phases present in the copper-tin phase diagram are [5]:

- The α phase is a solid solution with face-centered cubic crystalline structure. The maximum solubility of tin in this phase as a function of the temperature is as follows: 15.8% at 520 °C, 10.7% at 320°C and 1% at 100°C;
- The β phase is a meta-stable phase with body-centered cubic crystalline structure. It is formed by the peritectic reaction between α and the residue liquid;
- The γ phase is a meta-stable phase with face-centered cubic crystalline structure and at 520°C is transformed into a eutectoid of α + δ;
- The δ phase has an intermetallic compound: $Cu_{31}Sn_8$;
- The ε phase is an orthorhombic structure with the following formula: Cu_3Sn. It formed for the slow eutectoid transformation of δ to α + ε. However the reaction is too slow and the micro-structure is a mixture of α + δ.

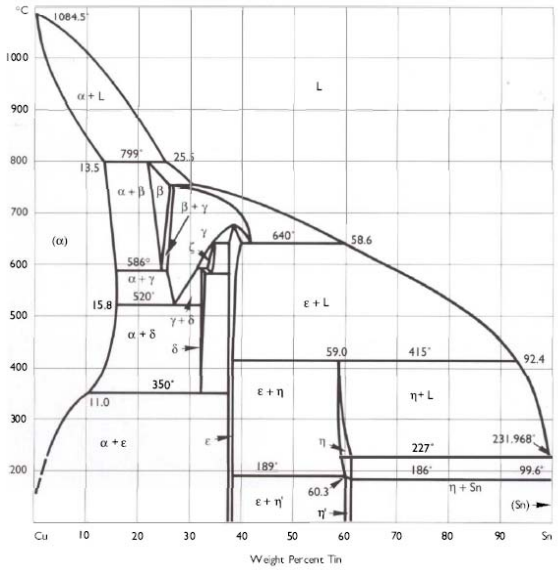

Fig. 1.1: Phase diagram of Cu-Sn [5].

When a tin bronze is cast the alloy is extensively segregated, usually with cored dendritic growth, and the alpha + delta eutectoid surrounds the dendritics arms. The center of the dendritic arms are copper-rich, since copper has the higher melting point, and the successive growth of the arms results in the deposition of more tin. At low tin contents, for example, between 2% and 5%, it may be possible for all the tin to be absorbed into the dendritic growth. This varies considerably depending on the cooling rate of the bronze and the kind of casting involved. If the cooling rate is very slow, there is greater chance of reaching equilibrium, and amount of interdendritic delta phase will reduce or disappear entirely [6]. Figure 1.2 (a) shows a low-tin bronze where no separated tin-rich phase is evident. All tin is in solid solution in copper. The small blue inclusions are copper sulfides from the melting processes. Working and annealing of face centered cubic structure metals creates twinned crystals when the metal re-crystallizes [4].

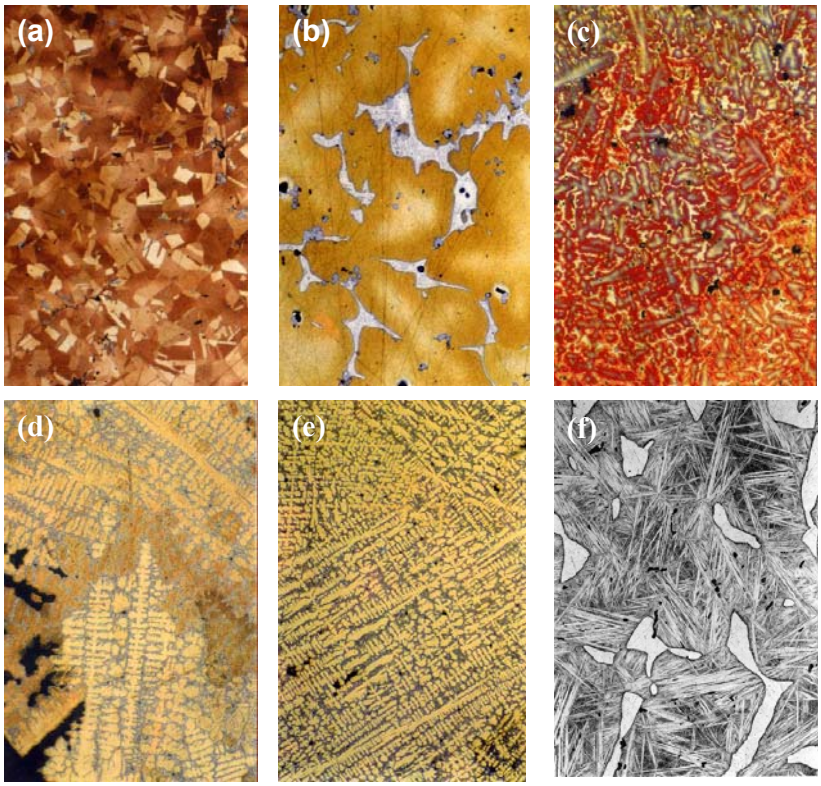

Fig 1.2: Bronze alloy with (a) 5% tin bronze of axe from Bronze Age Iran, x130; (b) 9% tin bronze of axe from Bronze Age, x210; (c) 10% tin bronze of Austrian axe, x120; (d) 16% tin bronze, x100 (e) 18% tin bronze, x100; (f) 18% tin bronze, x280. Images of David A. Scott [4].

At a tin content of about 10% it is very unusual in antique castings to get an absorption of the delta phase. The dendrites will usually be surrounded by a matrix of the alpha phase + delta eutectoid. As the tin content increases, the portion of interdendritic eutectoid also increases [4,6]. Figure 1.2 (b) and (c) show respectively a bronze with 9% and 10% of tin. In image (c) the $\alpha + \delta$ phase appears, where the α phase is red or orange.

From 14% to 19% it has been found that the alloy cannot be worked. A film of delta phase forms and this brittle phase then coats the grain boundaries with the result that the alloy breaks up into pieces. However with a 19% concentration tin bronzes can be hot-worked. Bells and mirrors in the antiquity were often made of ternary tin bronzes consisting of about 20-25% tin, 2-10% lead and the remainder being copper [4-6]. Figure 1.2 (d) and (e) show a bronze with 16% and 18% of tin. In (d) coarse dendrites of the α phase with an extensive infill of $\alpha + \delta$ phase are visible. More fine are the dendrites of α phase in figure (e).

Binary bronzes containing more than 17% of tin often have about 23% of tin, which corresponds closely to the equilibrium value of beta phase of the bronze system is shown in figure (f) (Quenched high tin bronze mirror from java, composition 21.3% tin, 78.3% copper). The alpha phase is occasionally twinned from hot-working. The background of acicular needles is a typical quenched beta phase bronze. The beta phase range is between 650-750°C [4;6].

1.1.3 Stability of bronze in different environments: Pourbaix diagram

In the field of corrosion, and generally in order to know the behavior of a metal in aqueous solutions a diagram is used: Pourbaix diagram. Pourbaix diagrams or E-pH diagrams depict the stability of a metal when exposed to a given environment as a function of potential and pH. The Pourbaix diagram is a type of predominance diagram: it shows the predominant form in an element that will exist under a given set of environmental condition.

These diagrams give a visual representation of the oxidizing and reducing abilities of the major stable compounds of an element and are used frequently in geochemical, environmental and corrosion applications. Kinetics is not incorporated [7].

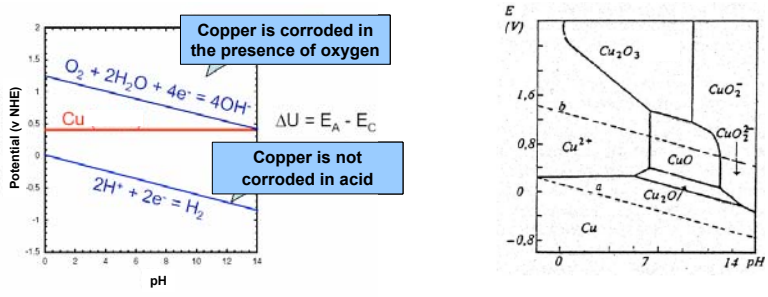

Fig 1.3: Pourbaix diagram of copper in water [8].

The usefulness of a Pourbaix diagram is enhanced by superimposing on it the domain enclosing the combinations of the parameters, E and pH for which water is stable. This is defined by blue lines on the diagram (Figure 1.3 on the left) representing the decomposition of water by evolution of hydrogen by reaction 1 or of oxygen by reaction 2:

$2H^+ + 2e^- \rightarrow H_2$ $\quad E^0 = 0.000$ V SHE (1)

$\frac{1}{2} O_2 + 2H^+ + 2e^- \rightarrow H_2O$ $\quad E^0 = +1.228$ V SHE (2)

The two blue lines enclose a domain within which water is stable. For combinations of potential and pH above the top line, water is unstable and decomposes evolving oxygen. For combinations below the bottom line, it is also unstable and decomposes evolving hydrogen.

Copper has a standard potential between the two lines, $E°Cu^{2+}/Cu = +0.33$ V SHE, so the copper is not corroded in acid solutions without O_2 but is damaged in aerated acid and basic solutions.

Figure 1.3 (in the right part of the image) shows the Pourbaix diagram for copper immersed in water. Where CuO is formed, copper is protected and the area is passive. In the areas where the copper is in its ionic form, the corrosion is in act. whilst the copper is immune to the alkaline environment (at the bottom of the Figure 1.3) [8].

Some differences can be noted in the Pourbaix diagrams where also other compounds are present in the system. The Figure 1.4 is a diagram of the system Cu-SO_4^{2-}-H_2O. In the passivity area of the diagram the tenorite (CuO) always occurs, close to the cuprite zone (Cu_2O). The products occurring in the corrosion area are: antlerite, formed with more acid pH and brochantite, formed with less acid values (as will be shown in the following paragraphs).

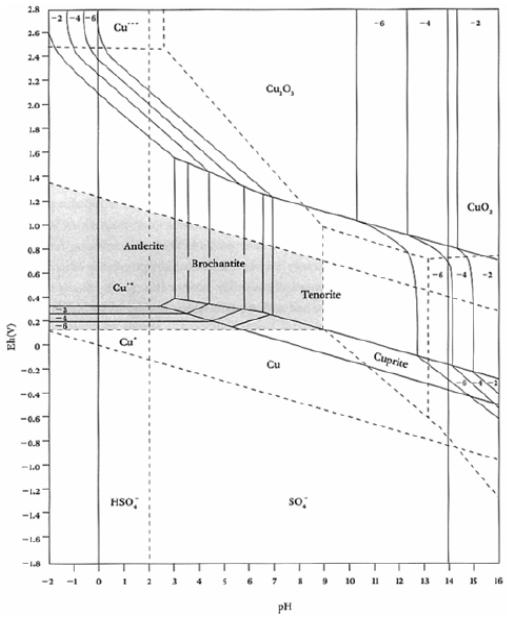

Fig. 1.4: Pourbaix diagram for the Cu-SO_4^{2-}-H_2O system [2].

Figure 1.5 shows the Pourbaix diagrams for the system Cu-Cl- H_2O for different concentrations of chloride: in (a) at 35 ppm, in (b) at 350 ppm, in (c) at 3550 ppm and in (d) at 35500 ppm.

The passivity regions are characterized by the presence of tenorite (CuO) which is produced with a higher potential than cuprite (Cu_2O) but in the same pH area. Nantokite (CuCl) and atacamite ($Cu_2Cl(OH)_3$) occur in the area where corrosion is in act. When the chloride concentration increases, the passivity areas decrease, whilst the stability of both nantokite and atacamite increases. The chloride environment keeps the corrosion active producing non-passive layers of copper chloride [4].

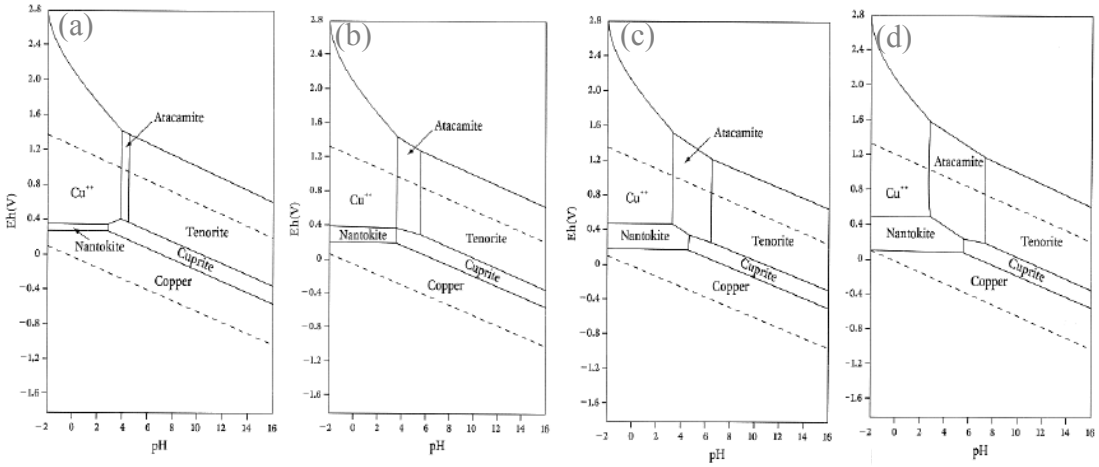

Fig. 1.5: Pourbaix diagrams of the Cu-Cl- H_2Osystem at chloride concentrations of: (a) 35 ppm; (b) 350 ppm; (c) 3550 ppm; (d) 35500 ppm [2].

1.2 Atmospheric corrosion of metals

1.2.1 General description of corrosion aspects

It is well known that the corrosion is a natural phenomenon that cannot be stopped. The thermodynamic law states that every material tends to reach its lower energy state. That for metals, such as copper, corresponds to the compound state from which they are extracted. The corrosion is also referred to as *metallurgy in reverse* [8].

In order for copper to corrode, there are four essential constituents: an anode, a cathode, the metal itself and an electrically conducting solution. The anode is the site where the copper is corroded; the electrolyte solution is the corrosive medium; the cathode forms the other electrode of the cell and is not consumed in the corrosion process.

At the anode, the corroding copper goes into solution as positively charged ions, releasing electrons that participate in the cathodic process. Generally the corrosion cells are very small, numerous and distributed in a random manner over the surface of the metal and the effects are more or less a uniform attack on the surface.

The anodic and cathodic reaction are the following:

$Cu \rightarrow Cu^{2+} + 2e^-$ Anodic reaction

$O_2 + 2H_2O + 4e^- \rightarrow 4OH^-$ Cathodic reaction

However, at low pH environments, hydrogen evolution may take place as cathodic reactions on the metal surface [8]:

$2H^+ + 2e^- \rightarrow H_2$ (g)

1.2.2 Influence of gaseous pollutants

The metal corrosion is due to the reactions shown in previous paragraph but an important role in atmosphere is also played by pollutants. The effect of a pollutant on the atmospheric corrosion of metals depends on several important pollutant properties: water solubility, chemical reactivity and acidity. Another important factor for enhancing the sensitivity of a metal to a specific gaseous pollutant is the deposition velocity, defined as the ratio of the rate of deposition of the gas towards the metal surface and its concentration in the atmosphere. Table 1.1 displays the solubility, in terms of Henry's laws constant, and the deposition velocity for a number of important gaseous corrosion stimulators [9].

Pollutant	H^* (mol L^{-1} atm^{-1})	Deposition velocity † (cm s^{-1})	
		Outdoor	Indoor
H_2S	0.10	0.38	0.03
SO_2	1.2	0.01-1.2	0.05
NO_2	0.007	0.02-0.8	0.006
O_3	0.012	0.05-1	0.036
HNO_3	2.1×10^5	0.1-30	0.07

* Henry´s law constant

Tab. 1.1: Solubility and deposition velocity for atmospheric pollutants [9].

The main gas pollutants are: SO_2, SO_3, H_2S, NH_3, NO_2, CO, CO_2 and other minor organic products.
Sulfur dioxide is an acid gas. Its dry deposition is influenced by the temperature and the relative humidity, those being the main factors that determine the thickness of the moisture layer and therefore the ability to dissolve gasses that have a specific solubility. Sulfur dioxide reacts with water and produces sulfuric acid (H_2SO_4) which is together with HNO_3 the major acid component of acid rain [10-12].
Great efforts have been done to limit SO_2 emissions and to reduce the acid rain effects. The interest in the effects of SO_2 on atmospheric corrosion derives to a large extent from its role as one source for sulfate. Sulfates are common corrosion products when metals are exposed to outdoor environments, as

many works demonstrate [9; 13-17]. Moreover, as shown with the Pourbaix diagrams, the sulfates compounds keep the process active. Despite the decrease in SO_2 levels in many countries, sulfates are still a major corrosion product found on copper and its alloys indicating that SO_2 still plays a very important role for the atmospheric corrosion and in the corrosion rate. The corrosion mechanism is usually attributed to the acidification effect, as is shown in literature [10-12]. In absence of an additional oxidant, SO_2 produces copper sulfite as main reaction product and the oxidation of these copper sulfite layers to sulfate is quite slow. For this reason the atmospheric concentration of nitrogen dioxide (NO_2) and ozone (O_3) is also important. They are indeed the most important oxidants in the atmosphere and are able to accelerate the corrosion in the presence of SO_2 [9;18-21].

$$SO_2 + H_2O \rightarrow H^+ + HSO_3^- + O_3 \rightarrow 2H^+ + SO_4^{2-} + O_2$$

As is shown in the above reaction, SO_2 is an acidifying pollutant and the acidification of the water layer accelerates the corrosion process. In the atmosphere, however, the levels of SO_2 are usually smaller in comparison to the levels of the oxidation agents, which therefore determine the corrosion rate. Synergic effects of pollutant mixtures have been demonstrated in laboratory tests (Figure 1.6), where single and combined corrosion effects can be simulated and controlled [18-21]. Interpretation of the results of real cases, in the other hand, is more complicated.

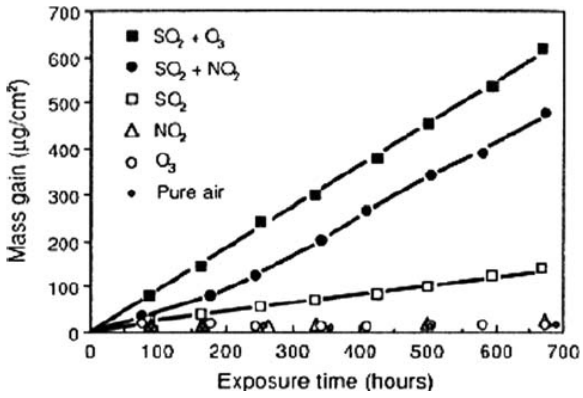

Fig 1.6: Mass gain of zinc samples exposed in air at 95% RH [18].

Nitrogen dioxide, NO_2, is also a very important gaseous pollutant, not only because it is among the most important trace oxidants in the atmosphere, and is therefore able to accelerate atmospheric corrosion in the presence of SO_2, but also because it can be oxidized and can form nitric acid (HNO_3) which is a very corrosive substance [22-24]. Moreover, whilst sulfur dioxide levels seem to be decreasing in the last ten years, this cannot be said for the nitric acid levels that play an increasingly important role in the atmospheric corrosion.

1.2.3 Influence of sodium chloride (NaCl)

Other dangerous atmosphere components for metals' conservation are represented by saline particles. Atmospheric salinity is a parameter related with the amount of marine aerosol present. Saline particles, such as the sodium chloride, the most important airborne particle, accelerates the metallic corrosion process, increasing the amount of soluble corrosion products [19].

The main source for chlorine in the atmosphere is the sea salt aerosol. The wind and the evaporation of drops of seawater are responsible for the salinity in the atmosphere.

Nevertheless, sodium chloride is frequently present also in urban environments at lower concentrations in comparison to that in marine sites. Distance from the seashore is not always by itself a determinant factor influencing the corrosion rate. The latter also depends on the topography and orography of the land, as well as the intensity and direction of prevailing wind etc.

Chlorides dissolved in the layer of moisture also considerably raise the conductivity of the electrolyte layer on the metal and tend to destroy any passive film existing on the metallic surface [25]. Chloride does not reduce the pH of the electrolyte on the metal surface but provides a rather corrosive electrolyte with high conductivity. For their hygroscopic property, sodium chloride lowers the critical relative humidity from 100% to 75%. Moreover, the ionic content of the particles stretches the time of wetness also by affecting the freezing point, thereby enabling the formation of moisture levels below [19].

Lindström et all. [26] showed that the corrosion rate of zinc was strongly dependent on the nature of the cation. When sodium chloride (NaCl) is present, also in the case of bronze materials the corrosion rate in humid air increases. Sodium chloride (NaCl), combined with O_3 and SO_2, increases the corrosion rate proportionally with its concentration. But in presence of a small amount of NaCl, the corrosion rate slows down when SO_2 is added. The corrosion rate is high with $O_3 + SO_2$ without NaCl but decreases with small amounts of NaCl particles present on the surface. Research indicates that the corrosion in a multi-pollutant situation in combination with NaCl particle deposition is complicated and that the rate controlling factors are different with and without electrolyte forming particles present on the surface [27-28].

1.2.4 Influence of the relative humidity and the temperature

The relative humidity (RH) in the atmosphere plays an important role and affects directly the amount of water on the metal surface. It was reported that the atmospheric corrosion rate of metals increases with the relative humidity during the environmental atmosphere exposure as Figure 1.7 shows.

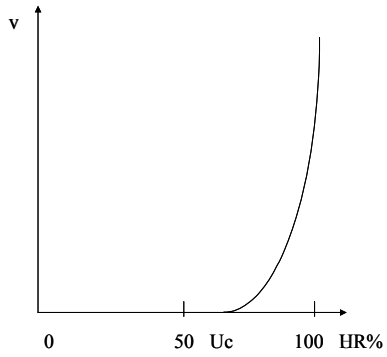

Fig. 1.7: Corrosion rate related to the Relative Humidity

At low relative humidity (20%) the thickness of the water layer is less than two mono-layers and water is tightly bound to the surface. At higher relative humidity (75%), the thickness is in the range of ten or more mono-layers and is more loosely bound enabling to act as an ionic medium for dissolving pollutants [29].

Some studies relate the temperature and the relative humidity to the corrosion rate of the metals [30-33]. Figure 1.8 shows the corrosion with respect to the relative humidity and to the temperature for an SO_2 polluted environment.

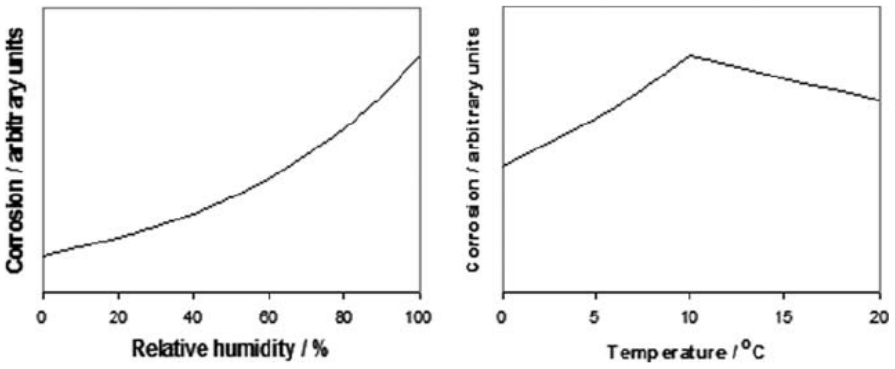

Fig. 1.8: Effects of the relative humidity (left) and the temperature (right) on metal corrosion in a SO_2 polluted environment [19].

Whilst the corrosion increases with the humidity, the temperature has a different effect. At annual temperatures below 10 °C, the corrosion increases with the temperature and this can be related to the increased wetness time, defined as the time when the relative humidity is higher than 80% and the temperature simultaneously above 0°C. The decreasing part above 10°C is attributed to a faster evaporation of the moisture layers after rain or dew periods and a surface temperature above the environment temperature due to sun radiation which results in a decrease of the surface time of wetness [19].

Otherwise the corrosion is proportional to the relative humidity and the temperature in the diagrams in chloride environments (Figure 1.9).

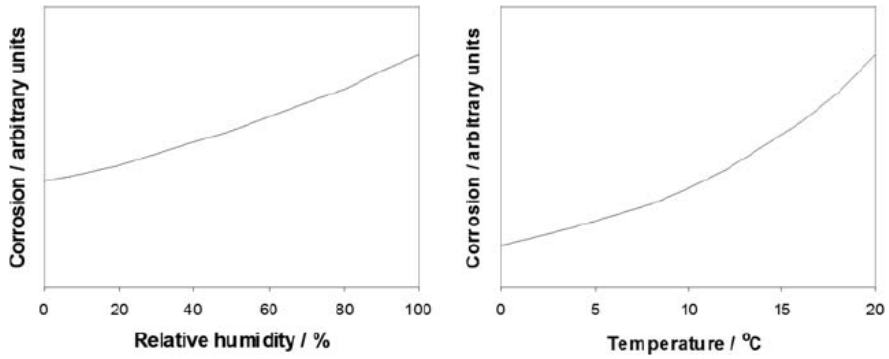

Fig. 1.9: Effects of relative humidity (left) and temperature (right) on metal corrosion in NaCl environment [19].

The formation of a non-uniform surface electrolyte in the form of droplets may occur during the deposition of aerosols and hygroscopic particles on metal surface. The droplets create a situation with a differential aeration cell with the anode in the center of the droplet and cathodic areas in the peripheral parts of the droplet. A secondary spreading of the electrolyte outside the initially formed droplet was observed. The secondary spreading includes transport of cations to the spreading area outside the droplet but not of anions [34].

In the presence of SO_2, a small secondary spreading effect of NaCl electrolyte on copper surface from edge of droplet was observed [34].

1.3 Corrosion products

1.3.1 Environment-bronze-corrosion product system

1.3.1.1 Corrosion products mechanism of layers formation

Some studies have shown the general reaction schemes that describe the evolution of copper patina as a result of variations in environmental pollutants [35-36].

Some stages have been developed to explain the mechanism of corrosion. In the absence of the corrosive gas species, a reactive metal exposed to air develops a thin protective film, often composed of oxides or hydroxides which have low ionic transport properties. This creates a barrier to further corrosion. On exposure to moist air above a critical relative humidity, a thin monolayer adsorbs water on the surface. The absorption of atmospheric gases, the dissolution of ionic species on the surface and the deposition of airborne particulates into the water layer control the composition of the electrolyte. For the corrosion to initiate, the protective layer on the metal surface needs be changed to a non-protective one that has substantial ionic transport [37]. The non-protective layer with high ionic transport typically remains thin and becomes inner layer of a duplex film of corrosion products. A

thicker outer layer develops through the precipitation of soluble species and through further reaction of the corrosion products with the atmosphere. The outer layer is porous or cracked and can permit the penetration of water and gases. Cations are produced by the oxidation of metal in the metal/inner layer interface. Cations and/or anions move through the non-protective film. The critical factors are therefore: the competition between protective and non-protective layer; the ionic and electronic transport properties and the composition and structure out of the layer [37-38].

1.3.1.2 Corrosion products

Figure 1.10 represents the sequence of the corrosion products formed on copper exposed to urban environment characterized by the presence of SO_2 and exposed to marine sites where the chloride presence is predominant.

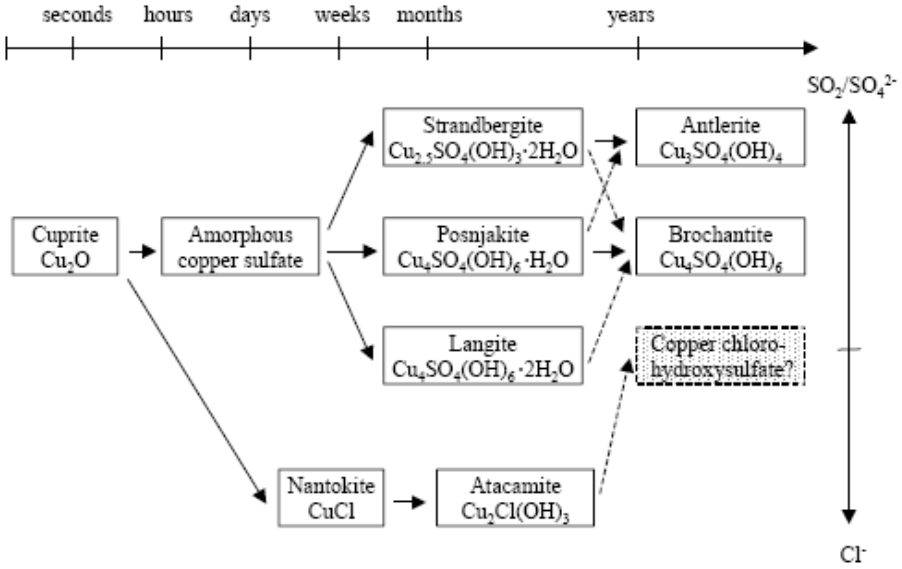

Fig. 1.10: A scheme for patina formation of copper exposed to sulfate or chloride environments [39].

The most common constituents of the patina (both unsheltered and sheltered) of a copper roof in an urban environment include cuprite (Cu_2O) in the inner layer and posnjakite ($Cu_4SO_4(OH)_6\ H_2O$), which is the less steady precursor of brochantite ($Cu_4SO_4(OH)_6$), both in the external layer. Strandbergite ($Cu_{2.5}SO_4(OH)_3\ 2H_2O$) and antlerite ($Cu_3SO_4(OH)_4$) can form in more polluted environments with higher levels of SO_2. Nantokite (CuCl) and atacamite ($Cu_2Cl(OH)_3$) primarily form in chloride containing environments such as traffic or marine atmospheres. The figure also includes langite ($Cu_4SO_4(OH)_6\ 2H_2O$), a precursor phase, that seems to exist in less polluted sites with more humid and wet conditions. The total thickness of the patina depends on the exposure time and the environment and varies typically between 10 and 70 µm [39].

To study the copper behavior in aqueous solution, stability diagrams were developed. This allowed to show the weather conditions where the above-mentioned corrosion products form in the specific

pollutant environment. It is important to note that the following diagrams represent a chemical balance condition and are correlated to a pure system that not frequently is present in atmosphere [40].

Figure 1.11 shows the diagram for the Cu-SO_3-H_2O system with indication of the pH range and the SO_4^{2-} concentration of the rain and the fog. It is clear that brochantite ($Cu_4SO_4(OH)_6$) is stable during the rain period. When the water on the surface starts to evaporate the sulfate concentration increases and the pH decreases: the antlerite is favoured.

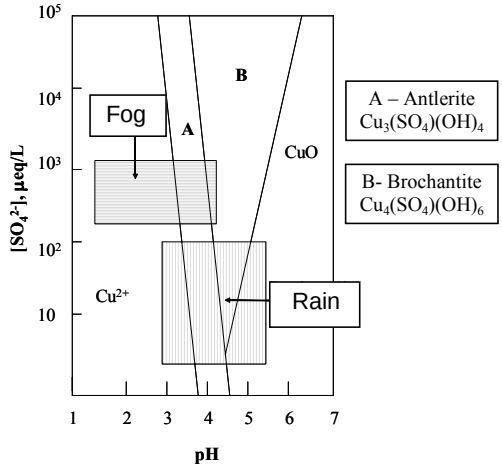

Fig. 1.11: Stability diagram of the Cu-SO_3-H_2O system [40].

The diagram of the Cu-NO_3^--H_2O system shows that gerhardtite ($Cu_2(NO_3)(OH)_3$) is stable when the nitrate concentration is high, and can be found as a component of the patina in case the pollutants are concentrated in the environment.

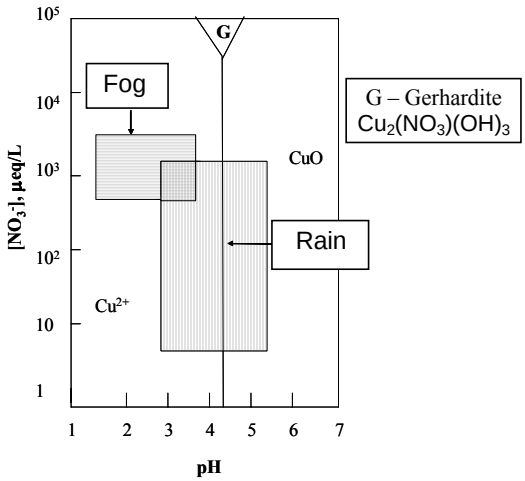

Fig. 1.12: Stability diagram of the Cu-NO3--H2O system [40].

Figure 1.13 shows the conditions of the formation of malachite in the Cu-CO_2-H_2O system. This product is stable for high concentration of dioxide carbon (CO_2).

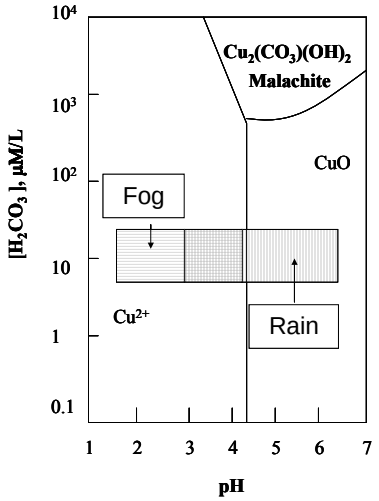

Fig. 1.13: Stability diagram of the Cu-CO_2-H_2O system. [40].

The diagram of the Cu-Cl-H_2O system is represented in Figure 1.14. Atacamite $Cu_2Cl(OH)_3$ is stable for high chloride concentrations present in the rain. The formation is helped by the evaporation. Otherwise it is unfavorable during the fog period due to the acidity of the environment. In any case, rain or fog, the atacamite is only partially stable.

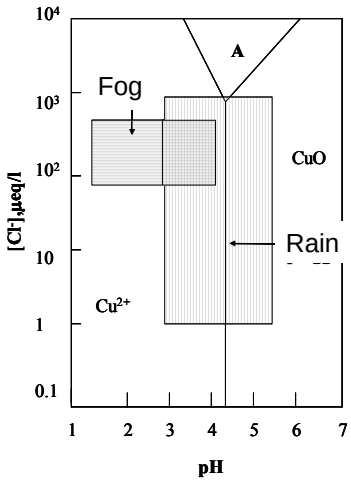

Fig. 1.14: Stability diagram of the Cu-Cl-H_2O system [40]

1.3.2 Corrosion morphologies

Generally all the corrosion products present on a metallic surface are indicated as "patinas" without mentioning and distinguishing the different possible compounds, layers and morphologies. There are plenty of morphologies and they are very important because they indicate different corrosion processes, different patina properties and different conservation states of the metal [6;8].
In this paragraph we report the most important corrosion morphologies that occur on bronze. They are summarized in Figure 1.15 [6].

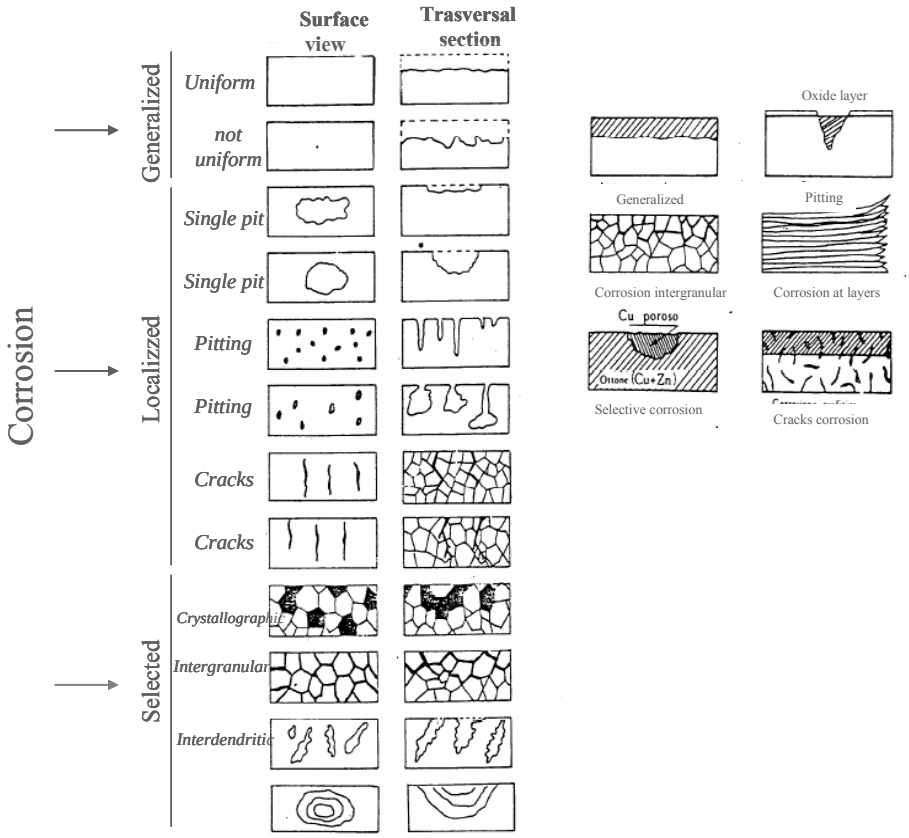

Fig 1.15: Corrosion morphologies [6].

1.3.2.1 Patina

Patina can be composed of mono-layers or stratified corrosion products. In general it can be considered as a continuous evolution of products and can reach the thickness of several micrometers.
The encountered corroded surface can be classified into two categories of corrosion patterns: Type I and II [41]. Both categories can be observed on one and the same artifact.
Type I is flat and the aspect of the object is preserved whilst in the Type II, or on a rough surface, the shape and the surface are strongly damaged.

Type I patinas are formed as a consequence of a generalized corrosion that produces a passive layer that slow down and even stops the process [40]. The surface is very protective and shows different colors (blue, green, grey) and for its passive propriety and esthetic aspect it is called “noble patina”. Generally the Cu/Sn ratio is stable in the patina but is related to the artifact. That means that the corrosion products formed are not a mix of copper and tin but are compounds of copper and tin separately.

Type II of patinas are the result of localized and generalized corrosion due to the high metal dissolution. The patina is rough and powdery with a high concentration of chloride between the metal and its inner corrosion layer [41]. Tin is present with a high concentration for the phenomena of decuprification of the alloy (selective copper dissolution) whilst the chloride is in contact with the metal. The formation of structure II is regulated by three steps: the dissolution of the alloy, the propagation for mass transport through the deposits and consequent attenuating of the process and the re-start of the corrosion [37]. A phenomenon common to both structures is decuprification but a slow dissolution of the alloy produces a layer rich of tin so the structure will be I in case whilst at high dissolution rates, cooper and tin dissolution should occur without formation of protective layers (Type II). The passage between the structure Type I to Type II is lead by the role of transport properties in the corrosion products as shown in the previous paragraph [37].

1.3.2.2 Pitting

As Fig 1.16 shows, in a chloride environment the first product formed is CuCl. May [42- 43] was one of the first researchers to understand the role of nantokite (CuCl) in copper pitting. Nantokite fences the inner part of the pit avoiding the oxygen diffusion and the formation of a protective patina of cuprite (Cu_2O). The low solubility maintains the copper ions activity at low levels favoring the anodic reaction of the metal. The pitting is helped by high concentrations of sulfate and sodium ions, low concentrations of nitrates and little oxygen in the solution at acid pH.

Pourbaix showed that when oxygen is present in the solution the stable corrosion product is malachite ($CuCO_3 \cdot Cu(OH)_3$), whilst cuprite (Cu_2O) is formed when there is less oxygen present. Pourbaix also demonstrated that in the pit copper of the alloy, cuprite and nantokite are all present in contact with a solution of 234 ppm Cu^{++} and 270 ppm Cl^- [44]. The diagrams in Figure 1.16 represent this system where the green point represents the **Cu/Cu_2O**, **$Cu_2O/CuCl$** and **CuCl/Cu** coexistence (for 10^{-2} g Cl^- ioni/ L). This system is valid not only for localized corrosion [44].

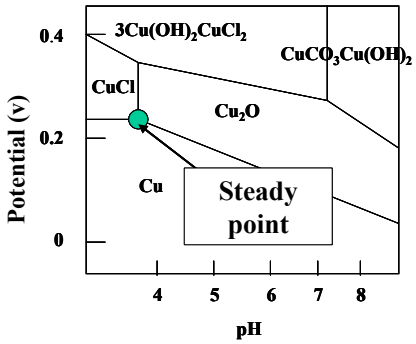

Fig 1.16: Pourbaix diagrams of Cu_2O-H_2O-HCl system for chloride ions activity of 10^{-2} M and a partial pressure of CO_2(g) at $10^{-3.5}$ Pa [44].

1.3.2.3 Bronze disease

The term "bronze disease" is used in conservation literature to describe the oxidation and hydrolysis of CuCl into copper trihydroxychloride.

The presence of CuCl is not a instable index because it can stay inactive for a long time before reacting with oxygen and humidity. Organ [45] following the research of Berthelot [46], suggested the mechanism of chloride attack as summarized in Figure 1.17.

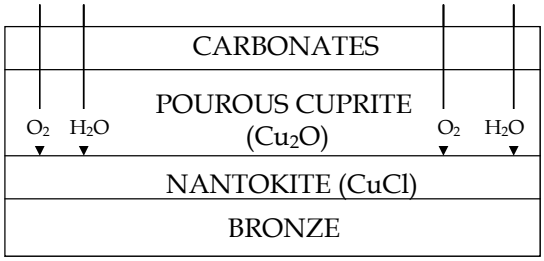

Fig. 1.17: Bronze corrosion by bronze disease [45].

The first reaction is between the cuprite (Cu_2O) and nantokite (CuCl) in water:

$$\mathbf{2CuCl + H_2O \leftrightarrow 2HCl + Cu_2O} \quad (1)$$

Then the process continues on the surface of the metal in contact with the CuCl. The copper of the reaction comes from the alloy whilst hydrochloric acid was formed in the first reaction.

$$\mathbf{2HCl + 2Cu + \tfrac{1}{2}\, O_2 \rightarrow 2CuCl + H_2O} \quad (2)$$

The second reaction is very fast and the water formed moves in diffusion towards the first site to be consumed again so the equilibrium of the reaction (1) is more balanced towards the cuprite formation.
The hydrochloric acid can move towards the inner layer only if it is concentrated enough to diffuse through the nantokite (CuCl) [37]. Scott [47] suggested that in the mineral layers there are some faults so air and humidity can get through and transform nantokite (CuCl) to copper trihydroxychloride ($Cu_2Cl(OH)_3$) on the metal surface. These products are bulky and break the corrosion layer to go towards the exterior creating a way for the penetration of oxygen and water.
When nantokite is in contact with the metal and receives water it generates copper chloride. The three isomer are: atacamite, paratacamite and botallackite

$$\mathbf{4CuCl + O_2 + 4H_2O = 2Cu_2Cl(OH)_3 + 2H^+ + 2Cl^-} \quad (3)$$

Paratacamite ($Cu_2Cl(OH)_3$) is thermodynamically the more stable phase and comes from the crystallization of atacamite at ambient temperature. The conversion of nantokite (CuCl) to paratacamite ($Cu_2Cl(OH)_3$) depends on the relative humidity, temperature, oxygen concentration and partial pressure as is shown in Figure 1.18 [48].

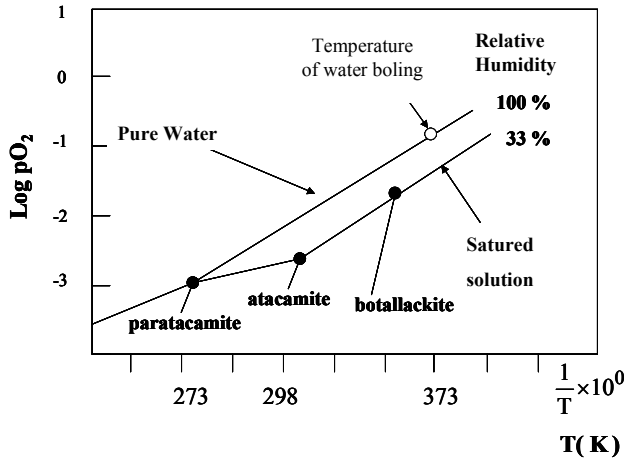

Fig. 1.18: 1/T- log pO_2 diagram for different partial pressures of the water. The different stable condition corrosion products [48].

Botallackite is meta-stable. It is the first form but quickly re-crystallizes. The rate of crystallization of atacamite is higher in solution with high concentration of $[CuCl^+]$ / $[Cu^{2+}]$ and low concentration of $[Cu^{2+}]$ / $[H^+]$ [49]. The reactions are reported below [50]:

$$\mathbf{Cl^- + Cu(s) \rightarrow CuCl\ (s) + e^-} \quad (4)$$

$$\mathbf{2CuCl(s) + H_2O \rightarrow Cu_2O + 2H^+ + 2Cl^-} \quad (5)$$

$$CuCl \rightarrow Cu^{2+} + Cl^- + e^- \quad (6)$$

$$Cu^{2+} \rightarrow Cu_2Cl(OH)_3 \quad (7)$$

The Pourbaix diagram in Figure 1.19 represents the chloride ion activity: for neutral pH the nantokite forms cuprite. In the pits due to bronze disease the condition is acid (pH 3-5) and in this environment the nantokite can be oxidized to $3Cu(OH)_2 \cdot CuCl_2$-γ.

At potential of 0.238 V and pH of 3.94, the formation of atacamite is slower than paratacamite and this reaction gets towards the botallackite until the paratacamite.

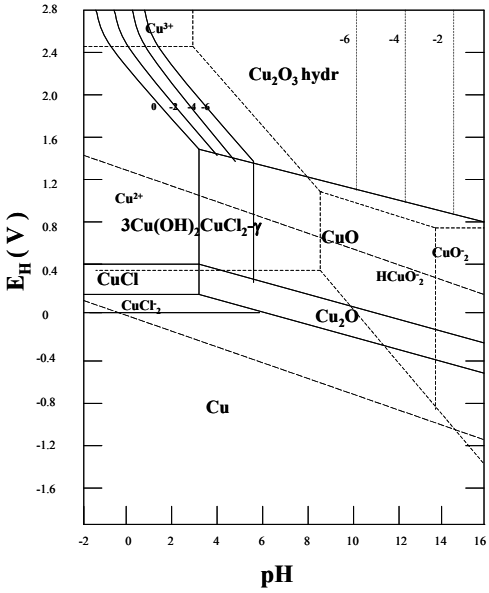

Fig. 1.19: Pourbaix diagram for the Cu-Cl-H_2O system at 25°C and at a chloride ions concentration of 10^{-2} g ions Cl^-/L (3550 ppm) [2].

1.4 Tin influence on bronze corrosion behavior

The corrosion process (as was shown in previous paragraphs) and the corrosion products composition are related to the conservative environments of the artifacts. Many studies analyzed the conservation state of historical bronzes [4; 15; 50-54], the patina composition [2; 4; 9; 12-16; 27; 35; 37; 39; 45-46], the corrosion process in urban [9;10; 12; 14-24; 29-36; 40; 52; 53] or marine environment [25; 26; 28; 46; 49; 52; 53]; very few investigated the influence of the material composition on the bronzes corrosion behavior [11; 13, 55; 56].

De Ryck et al. [55] studied the corrosion layer of a group of samples of the Cu-Sn alloy. The research underlined that the patina consisted of a single well adhering corrosion layer with (for some samples) a second loosely adherent layer evidenced. According to the SEM-EDX analysis the corrosion layer consists

primarily of tin and oxygen, which indicates that the layer is composed of tin oxides and tin hydroxides, as mentioned in literature [57]. In the case of a few samples, a second layer containing chlorine between the corrosion and the metal could be observed. For the Sn-Cu alloy it appeared that during the corrosion process the Cu of the Cu metallic inclusions were not diffused/dissolved into the corrosion layer. This meant that distinct copper inclusion remained visible in the corrosion layer.

Dos Santos et al. [58] researched the effects of synthetic seawater on Cu-13Sn alloy underlining the different properties of the patina formed in buffered and non-buffered media and in deoxygenated and oxygenated solutions. Many studies analyzed the corrosion behavior of specific bronze alloys in specific conservative environments [10; 57-63]. Some research evaluated the corrosion process on different statuary alloys [15; 64] and on new bronze alloys [11] but few comparative and systematic investigations were carried on. As an example, Gallese et al.[56] studied the corrosion of bronzes composed by more than four alloying elements, whilst Various Cu-Sn alloys were tested in sulfphuric acid by Surme et al.[65].

The aim of this research, departing from these mentioned studies, is the comparative study of bronze alloys corrosion in urban and marine environment, focusing on the analysis of the tin influence on bronze corrosion behaviour. Three by-component bronzes, with different percentage of tin, were selected to represents different kind of artifacts (that can be found in our hinterland or coastal cities) and were systematically tested in natural and artificial urban and marine environment.

References

[1] G. Giubbini, *"Le Tecniche Artistiche – La Scultura in Metallo"*, Ed. Mursia, 2004;

[2] D.A. Scott, " *Copper and Bronze in Art: Corrosion, Colorants, Conservation"*, Ed. Getty Institute Publication, 2002;

[3] F. Habashi, "*A history of metallurgy"*, Ed. F. Habashi Departement of Mining & Metallurgy Laval University, Quebec City, Canada, G1K 7P4;

[4] D.A. Scott, Jerry Podany, Brian B. Considine, *"Ancient & Historical Metals: Conservation and Scientific Research"*, Getty Institute Publication, (1994);

[5] E.G. West, *"Copper and its alloys"*, American Society of Metals, Ellis Horwood Limited, Chichester, UK (1982);

[6] D.A. Scott, " *Metallography and Microstructure of Ancient and Historic Metals"*, Ed. Getty Institute Publication, (1991);

[7] M. Pourbaix, *"Rapport Technique CEBELCOR"*, vol. 109, R.T. 160, 1969;

[8] P. Pedeferri, *"Corrosione e Protezione dei Materiali"*, Ed. Polipress, (2010);

[9] C. Leygraf, *"Atmospheric corrosion. Corrosion Mechanism in Theory and Practice"*, 2nd Edition, Ed. By Philippe Marcus, 529-562, (2002);

[10] L. Morselli, E. Bernardi, C. Chivari, G. Brunoro, *"Corrosion of 85-5-5-5 bronze in natural and synthetic acid rain"*, Applied Physisc A 79, 363-367 (2004);

[11] C. Chiavari, A. Colledan, A. Frignai, G. Brunoro, *" Corrosion evaluation of traditional and new bronzes for artistic casting"*, Materials Chemistry and Physics 95, (2006), 252-259;

[12] R.P.B. Hernandez, Z. Paszti, H.G. De Melo, I.V. Aoki, "*Chemical characterization and anticorrosion properties of corrosion products formed on pure copper in synthetic rainwater of Rio de Janeiro and Sao Paulo"*, Corrosion Science 52 (2010), 826-837;

[13] G.P. Cicileo, M.A. Crespo, B.M. Rosales, *"Comparative study of patinas formed on statuary alloys by means electrochemical and surface analysis techniques"*, Corrosion Science 46, (2004) 929-953;

[14] M. Watanabe, Y. Higashi, T. Ichino, *"Surface observation and profiling analysis studies of corrosion products on copper exposed outdoors"*, Journal of the Electrochemical Surface, 150 (2) B37-B44 (2003);

[15] C. Chiavari, K. Rahmouni, H. Takenouti, S. Joiret, P. Vermaut, L. Robbiola, *" Composition and electrochemical properties of natural patina of outdoor bronze monument"*, Electrochemical Acta 52 (2007), 7760-7769;

[16] J.P. Faney, M.E. Davis, *"Metallographic studies of the copper patina formed in atmosphere"*, Corrosion Science, vol. 27, n. 7 659-668 (1987);

[17] M. Reid, J. Punch, L.F. Garfias-Mesias, K. Shannon, S. Belockapkine, D.A. Tanner, *"Study of Mixed flow gas exposure of copper"*, Journal of Electrochemical Society, 155 (4) C147-C153, (2008);

[18] J.E. Svensson, L.G. Johansson, "*A laboratory study of the effect of the ozone, nitrogen dioxide and sulphur dioxide on the atmospheric corrosion of the zinc"*, Journal of Electrochemical Society. vol. 140, n. 8, 2210-2216 (1993);

[19] J. Watt, J. Tidblad, V. Kucera, R. Hamilton, *"The effects of air pollution on Cultural Heritage"*, Ed. Springer (2010);

[20] S. Oeschen, M. Faller, "*Environmental effects on materials: the effects of the pollutants SO_2, NO_2, NO and O_3 on the corrosion of copper, zinc and alluminium. A short literature survey and results of laboratory exposure"*, Corrosion Science 39 (9), 1505-1530 (1997);

[21] H. Strandberg, L.G. Johansson, *"Role of O_3 in the atmospheric corrosion of copper in the presence of SO_2"*, Journal of the Electrochemical Society 144 (7), 2334-2342 (1997);

[22] F. Samie, J. Tidblad, V. Kurcera, C. Leygraf, *"Atmospheric corrosion effects of HNO_3"*, Journal of the Electrochemical Society, 154 (5) C249-C254, (2007);

[23] K.F. Khaled, M.A. Amin, *"Dry and wet lab studies for some benzotriazole derivates as possible corrosion inhibitors for copper in 1 M HNO_3"*, Corrosion Science 51, (2009) 2098-2106;

[24] J. Tidblad, C. Leygraf, *"Atmospheric Corrosion effects of SO_2 and NO_2: a comparison of laboratory and field exposed copper"*, Journal of the Electrochemical Society 142(3), 749-756;

[25] M. Morcillo, B. Chico, L. Mariaca, E. Otero, *"Salinity in marine atmospheric corrosion: its dependence on the wind regime existing in the site"*; Corrosion Science 42, 91-104 (2000);

[26] R. Lindstrom, J.E. Svensson, L.G. Johnnsson, *"The influence of salt deposits on the atmospheric corrosion of zinc"*, Journal of the Electrochemical Society 149 (2), B57 (2002);

[27] P. Eriksson, L.G. Johansson, J. Gullam, *"A laboratory study of corrosion reactions on statue bronze"*, Corrosion Science 34, 1083 (1993);

[28] Z.Y. Chen, S. Zakipour, D. Persson,, and C. Leygraf, *"Combined Effects of Gaseous Pollutants and Sodium Chloride Particles on the Atmospheric Corrosion of Copper"*, Corrosion Science, vol. 61,n. 11, (2005);

[29] C. Leygraf , T. E. Graedel, "*Atmospheric Corrosion"*, The electrochemical Society, INC. Pennington, New Jersey, 2000;

[30] S.D. Cramer, S.A Matthes, B.S. Jr Covino, S.J Bullard, G.R Holcomb, *"Environmental factors affecting the atmospheric corrosion of copper. Outdoor atmospheric corrosion",* ASTM STP 1421, Townsend, H.E., Ed American Society for Testing and Materials International, West Conshohocken, PA, 245-264, (2002);

[31] P.B. Philipps, W. Rice, *"The role of water in atmospheric corrosion"*, American Chemical Society 8, 236-2261 (1979);

[32] P.V. Strekalov, V.V Agafonov, N. Mikhailovki, *"Effect of temperature on the adsorption of moisture and the corrosion rate of zinc under atmospheric condition*", Protection of Metals 8, 521-523, (1972);

[33] F. Samei, J. Tidblad, V. Kurcera, C. Leygraf, *" Atmospheric corrosion effects of HNO_3 – Influence of temperature and relative humidity on laboratori exposed copper"*, Atmospheric Environment 41 (2007), 1374-1382;

[34] Z. Y. Chen, D. Persson, C. Leygraf, *"In situ studies of the effect of SO on the initial NaCl-induced atmospheric corrosion of copper"*, Journal of the Electrochemical Society (2006);

[35] T.E. Graedel, K. Nassau, J.P.Franey, "*Copper patina formed in the atmosphere – I."*, Corrosion Science, vol. 27, n. 7, 639-657, (1987);

[36] J. Tidblad, T.E. Graedel, "*Gildes model studies of aqueous chemistry. II. Initial SO_2 - induced atmospheric corrosion of copper"*, Corrosion Science, vol. 38, n. 12, 2201-2224 (1996);

[37] J.H. Payer, G. Ball, B.I. Rickett, H.S. Kim, *"Role of transport properties in corrosion product growth"*, Material Science & Engineering A198 (1995) 91-102;

[38] J. Sandberg, I. Odnevall Wallinder, C. Leygraf, N. Le Bozec, *"Corrosion induced copper runoff from naturally and pre-patinated copper in a marine environment"*, Corrosion Science 48 (2006), 4316-4338;

[39] A. Krätschmer, I. Odnevall Wallinder, Cristofer Leygraf, *"The evolution of outdoor copper patina",* Corrosion Science, 44 (2002), 425-450;

[40] T.E. Graedel, *"Copper patinas formed in the atmosphere – II. A qualitative assessment of mechanism"*, Corrosion Science, vol. 27, n. 7, (1987) 721-740;

[41] L. Robbiola, J.M. Blengini, C. Fiaud, "*Morphology and mechanisms of formation of natural patinas on archeological Cu-Sn alloys"*, Corrosion Science, vol. 40, n. 12 (1998) 2083-2111;

[42] L.L. Shreir, "*Corrosion. Volume I: metal-environmen reactions"*, G. Newnes-Butterworths, 2nd Edition (1976);

[43] V.F. Lucey, *"Developments leading to the present understanding of the mechanism of pitting corrosion in copper"*, British Corrosion Jornal, n. 7 (1972), 36-41;

[44] M. Pourbaix, *"Lectures on electrochemical corrosion"*, Plenum Press, New York-London (1973);

[45] R.M, Organ, *"Aspects of bronze patina and its treatment"*, Studies in Conservation, n. 8(1963), 1-9;

[46] D. A. Scott, *"Bronze Disease: a review of some chemical problems and the role of relative humidity"*, JAIC, vol. 29 (1990), n. 2, 193-206

[47] D.A. Scott, *"A review of copper chloride and related salts in bronze corrosion and as painting pigments"*, Studies in Conservation, n.45 (2000), 39-53;

[48] M. Pourbaix, *"Structured questions. Corrosion and Metal Artifacts: a dialogue between Conservators and Archeologists and Corrosion Scientists"*, National Bureau of Standars Special Pubblication n 479, Whashington D.C.M U.S. Departement of Commerce (1977), 215-216;

[49] T. Pollard, W. Pollard, *"The copper chloride system and corrosion: A complex interplay of kinetic and thermodynamic factors. Dialogue/89: The conservation of bronze sculptures in outdoor environment – A dialogue among Conservators, Curators, Enviromental Scientist and Corrosion*

Engineers", Ed. T. Drayman-Weisser, Huston, National Association of Corrosion Engineering, Texas (1992), 123-133;

[50] D.A. Scott, L.S. Dodd, *"Examination, conservation and analysis of gilded Egyptian bronze Osiris"*, Journal of Cultural Heritage 3 (2002) 333-345;

[51] G. D'Ercoli, G.Guida, M. Marabelli, V. Santin, *"Non-distructive testing by the Rp method of bronze monuments: three case studies"*, Cultural Heritage Conservation and Environment Impact Assessment by Non-Destructive Testing and Micro-Analysis, Van Grieken & Janssens (eds) 2005, Taylor & Francis Group, London ISBN 90 5809 6815;

[52] P. Letardi, I. Trentin, G. Cutugno, *"Monumenti in bronzo all'aperto. Esperienze di conservazione a confronto"*, Nardini Editore, Firenze 2004;

[53] P. Dilmann, G. Béranger, P. Piccardo, H. Matthiesen, *"Corrosion of metallic heritage artifacts. Investigations, conservations, and prediction for long-term behaviour"*, Woodehad publishing materials, Cambridge England 2007;

[54] H. Hassairi, L. Bousselmi, S. Khosrof, E. Tiki, *"Characterization of archeological bronze and evalutation of the benzotriazolenefficency in alkali medium"*, Material and Corrosion 2008, 59, No. 1;

[55] I. De Ryck, E. Van Biezen, K. Leyssens, A. Adriaens, P. Storme, F. Adams, *"Study of tin corrosion: the influence of alloying elements"*, Journal of Cultural Heritage 5, 2004, 189-195;

[56] F. Gallese, G. Laguzzi, L. Luvidi, V. Ferrari, S. Tackacs, G. Venturi Pagani Cesa, *"Comparative investigation into the corrosion of different bronze alloys suitable for outdoor sculpture"*; Corrosion science 50, (2008) 954-961;

[57] T. Stambolov, *"The corrosion and conservation of metallic antiquities and works of art"*, Central Research Laboratory of for Objects of Art and Science, Amsterdam 1985;

[58] L. M. Dos Santos, M.M. Lemos Salta, I.T.E. Fonseca, *"The elctrochemical behaviour of bronze in synthetic seawater"*, Journal of solid state electrochemistry (2007) 11: 259-266;

[59] S. I. Sherwood, *"Corrosion of bronze in outdoor environments"*, Cultural Heritage Conservation and Environment Impact Assessment by Non-Destructive Testing and Micro-Analysis, Van Grieken & Janssens (eds) 2005, Taylor & Francis Group, London ISBN 90 5809 6815;

[60] G. Laguzzi, L. Luvidi, G. Brunoro, *"Atmospheric corrosion of B6 bronze evacuate by the thin layer activation technique"*, Corrosion science 43 (2001) 747-753;

[61] E. Sidot, N. Souissi, L. Bousselmi, E. Triki, L. Robbiola, *" Study of the corrosion behaviour of Cu-10Sn bronze in aerated Na_2SO_4 aqueous solution"*, Corrosion science 48 (2006) 2241-2257;

[62] F.J. De Oliveira, D.C.B. Lago, L.F. Senna, L.R.M. De Miranda, E. D'Elia, *"Study of patina formation on bronze speciemens"*, Materials chemistry and physics 115 (2009) 761-770;

[63] N. Souissi, L. Bousselmi, S. Khosrof, E Triki, *"Electrochemical behaviour of archeological bronze alloy in various aqueous media: New method for understanding artifacts preservation"*, Materiallls and corrosion 54, 318-325 (2003);

[64] B. M. Rosales, R. M. Vera, J. P. Hidalgo, *"Characterisation and properties of synthetic patina on copper base sculptural alloys"*, Corrosion Science 52 (2010) 3212-3224;

[65] Y. Surme, A.A. Gurten, E. Bayol, E. Ersoy, *"Systematic corrosion investigation of various Cu-Sn alloys electrodeposited on mild steel in acid solution: dependence of alloy composition"*, Journal of alloys and compounds 485 (2009) 98-103;

2. Experimental

2.1 Methods

2.1.1 Electrochemical methods

In this research electrochemical methods were used to evaluate the kinetics and thermodynamics of the corrosion process under study, the corrosion products properties (passive, non-passive) and to estimate the thickness and morphologies of the film (porosity, adhesion to the substrate). The electrochemical techniques used are: the open circuit potential measurements (OCP) and electrochemical impedance spectroscopy (EIS).

2.1.1.1 Open circuit potential measurements

The open circuit potential (OCP), also referred to as the equilibrium potential, the rest potential or the corrosion reaction, is the potential at which there is no net current flow through the external circuit of the electrochemical cell. The OCP of a corroding metal/alloy is measured as a voltage between the metal/alloy (working electrode) that is the anode and the reference electrode.
Measurements of the OCP can provide:

- A means to determine whether the corrosion system is in active or passive state [1];
- A means to determine the potential on the surface [2]: the potential distribution on the corrosion surface on heterogeneous surface [3-5];
- A means to evaluate the surface modification by monitoring the OCP as a function of time evolution during the time. Estimate the corrosion product stability by the OCP evolution [6-11];
- A means to differentiate areas on a metal surface with different properties;
- A means to monitor the corrosion process;
- Qualitative analysis of metallic element of the objects [12].

The open circuit potential in this project was taken after 15 seconds before each Electrochemical Impedance Spectroscopy (EIS) measurement with an electrochemical three electrode cell. The reference electrode was Ag/AgCl (sat) and the electrolyte solution was 0.1M $NaSO_4$.
The OCP evolution are represented in graphs of E vs time with the aim of understanding the patina formation in terms of kinetic and barrier properties.
The measurements were carried out with a Autolab PGStat 20 instrument.

2.1.1.2 Electrochemical impedance spectroscopy

In EIS studies the impedance is the system response to the application of a periodic small amplitude ac signal. These measurements are carried out at different ac frequencies and, thus, the name impedance spectroscopy was later adopted. Analysis of the system response contains information about the solution-surface interface, the surface structure and the reactions taking place there [13-17] (Figure 2.1).

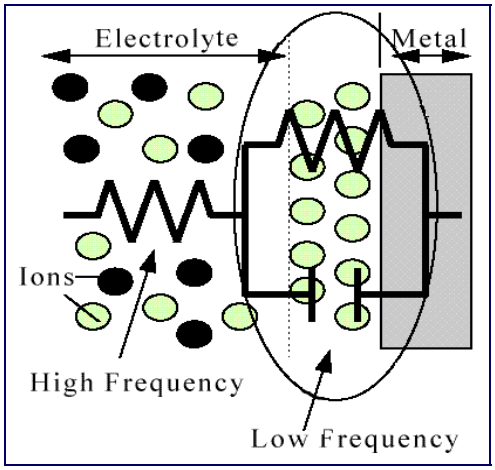

Fig.2.1: Electrochemical reaction inside an electrochemical cell [1].

When Z (impedance) is low in value, the current that flows in the circuit is high and the corrosion processes are facilitated. The value of Z at low frequencies can be used to estimate the corrosion rate [13;16-17].

Impedance data is typically represented in two kinds of plot: the Nyquist and the Bode plot.

The elaboration and interpretation of the spectra was done once the corresponding equivalent circuit that represent the cell system was found. The equivalent circuit allows the interpretation of the plot in terms of the resistance and the capacity belonging at specific electrochemical elements of the cell [16-17]:

- R_e: electrolyte resistance;
- C_g: geometric capacity of the cell;
- R_{ct}: charge transfer resistance;
- C_{dl} : double layer capacity

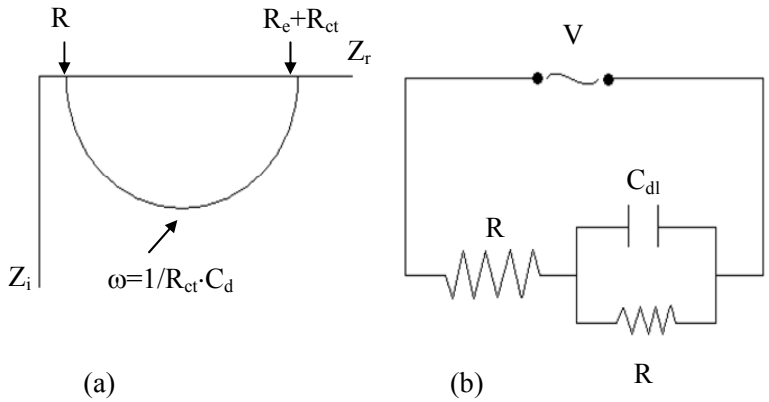

Fig. 2.2: Nyquist plot (a) and the corresponding equivalent circuit (b).

Equivalent circuits were used to understand the corrosion evolution, the patina growth and the film properties.

In this research the circuit elements were tightly correlated to specific corrosion indexes, in order to describe and quantify in detail the corrosion process and patina properties. The relationships between the circuit elements and corrosion indexes were deduced from different studies; this work collected and used all of them together.

The protection properties of the corrosion product was deduced from the resistance values as follows [18]:

$$R_p = Z_{75kHz} - Z_{1Hz}$$

where Z_{75kHz} (R_e) represents the resistance of the electrolyte and Z_{1Hz} ($R_e + R_{ct}$) is the sum of the solution and polarization resistance (Figure 2.2 on the left).

The film thickness was obtained from the following equation [19]:

$$T = \frac{1}{C_f}$$

where T represents the relative film thickness and C_f is the film capacity found with the equivalent circuit.

The porosity of the passive film can be extrapolated using the equivalent circuit element W (Warburg). That element is basic to understand whether the electrochemical behavior is governed by diffusion of charge carriers into or out of the film. The presence of Warburg can be assumed from the *n* index of capacitance. A value of *n* close to 0.5 indicates a possible presence of W [18].

Electrochemical impedance spectroscopy was carried out with a Autolab PGStat 20 instrument in a three electrodes cell: Ag/Ag/Cl (R), Pt (C) and bronze as working in a solution of 0.1 M of sodium

sulfate. The scan was preformed from 75 kHz to 1 Hz at 10 mV. The data elaboration was obtained with Autolab FRA Analyser and with EIS Spectrum Analyser [20-21].

2.1.2 Optical methods

In this research optical methods were used to evaluate the kinetics of the corrosion process under study, to evaluate the patina stability, to identify the corrosion products and to estimate the morphologies of the film. The electrochemical techniques used are: Spectrocolorimetry, Scanning electron microscopy with energy dispersive spectrometry (SEM- EDS) and X-ray diffraction spectroscopy.

2.1.2.1 Spectrocolorimetry

The basis of colorimetry is a set of standards defined by *Commision Internationale de l'Eclairage* (CIE) [23].

To define the color, its attributes are useful: hue, chroma and lightness. The hue (h°) is how we perceive an object so the color quality. The chroma (C*) describes the vividness or dullness of a color, in other words how close the color is to gray or to the pure hue. The lightness (L^{*}) is the luminous intensity of a color. Figure 2.3 show this attributes graphically [22;24-25].

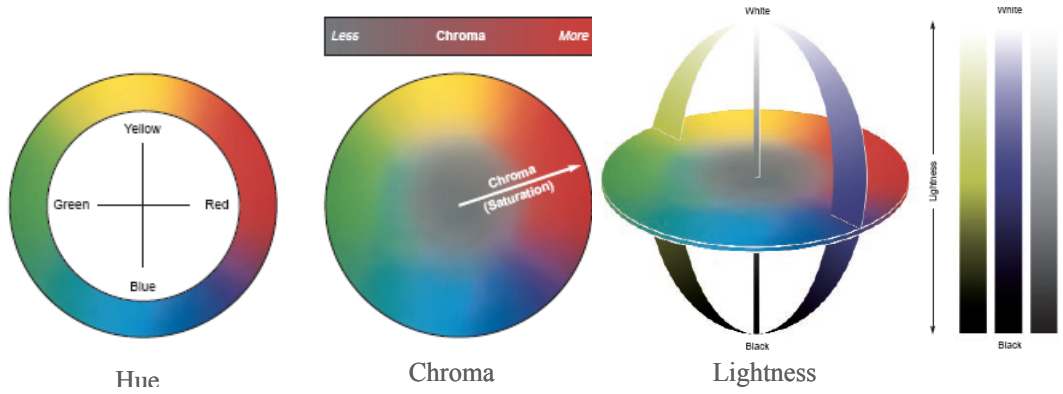

Fig. 2.3: Color attributes [26].

The color attribute are placed on a color spaces that CIE recommends: CIE L^{*} a^{*} b^{*} and CIE L^{*} C^{*} h°.

In this work the CIE L^{*} a^{*} b^{*} system was used (Figure 2.4). The parameter "a*" is the red/green ratio (a* is positive in the red region, negative in the green region) and "b*" is the blue/yellow ratio (b* is positive in the yellow region and negative in the blue region [22; 24-25].

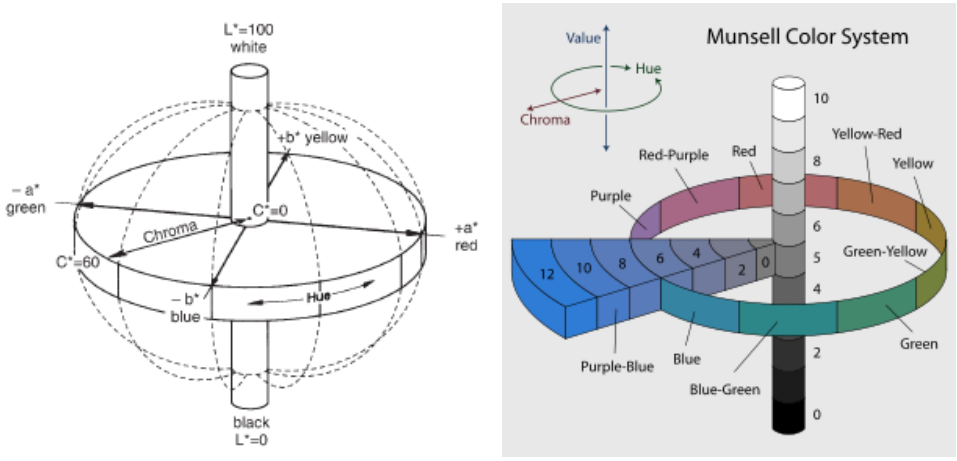

Fig. 2.4: CIE L^* a^* b^* color space [25].

The color difference (ΔE) between two colors can be calculated from the L^*, a^* and b^* values with the following equation [22; 24-26]:

$$\Delta E = \sqrt{\left(\Delta L^*\right)^2 + \left(\Delta a^*\right)^2 + \left(\Delta b^*\right)^2}$$

In this research a new relationship between colorimetric (L^*, a^*, b^*, C^*, h° and ΔE) and corrosion parameters was found.

The measurements were carried out with a portable sphere spectrophotometer X-Rite SP64 (measuring geometrics d/8°, illuminant types: C, D50, D65, D75, A, F2, F7,F11 & F12 and standard observers 2° & 10°.)

2.1.2.2 *Scanning electron microscopy with energy dispersive spectrometry (SEM- EDS)*

A Scanning Electron Microscope (SEM) analyzes a sample by scanning it with a high-energy beam of electrons in a raster scan pattern [27-30].

In this research SEM images (both backscattered as well as secondary) were taken to study the morphology of the corrosion products, their crystallinity, growth and stratification whilst the EDS analyses were done to identify the corrosion layers based on their elemental composition.

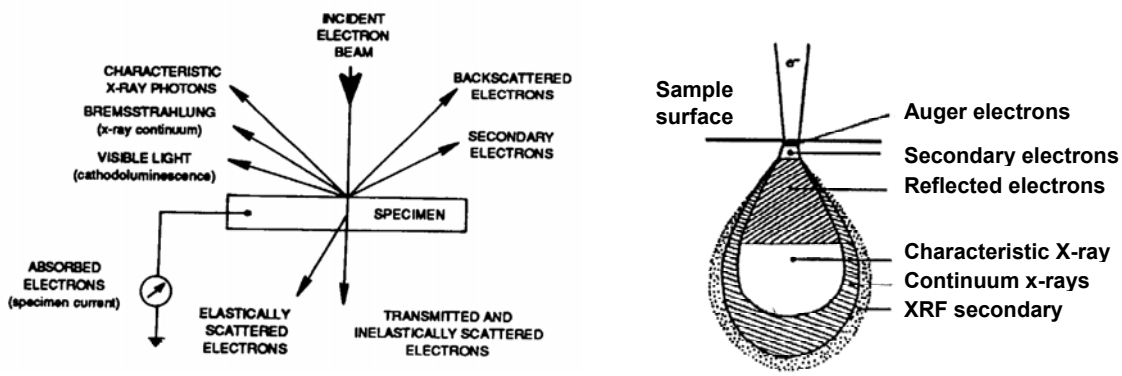

Fig. 2.5: Electron scattering and depth where are produced Auger, secondary and reflected electrons and X-rays on the sample [31].

The SEM-EDS instrument used in this research is a HITACHI S 2500 SEM, equipped with a LaB_6 electron source and a scintillation electron photo detector. The typical working pressure was 10^{-7} mbar.

2.1.2.3 X-ray diffraction spectroscopy

Diffraction is the phenomenon of wave interference that happens when the light passes across a crystalline object [32-33] (Figure 2.6). That phenomenon allows the identification of crystalline compounds. The diffractograms were used not only to characterize the corrosion products but also to understand the crystallinity and therefore the growth rate of the minerals on a surface.

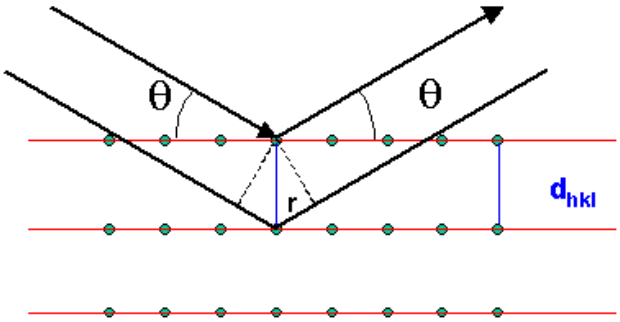

Fig. 2.6: Bragg model for the XRD [33].

A Thermo Scientific* ARL X'TRA powder diffractometer was used with the following setup: 40 kV, 40 mA, scanning 2θ from 10° to 80° grade, step width of 0.02° and counting time of 5 seconds per step.

2.2 Materials, sample preparation and test settings

2.2.1 Bronze alloys and their preparation

To understand the influence of the tin content on the bronze corrosion behavior, a low intermediate and high tin bronze were selected. The composition of the alloys is reported in Table 2.1.

Sample (tin concentration	Cu	Sn	Pb	As	Zn	Fe	Mn	Ni	S	Sb
3%	rest	3.0	0.2	0.2	0.2	0.2	0.2	0.2	0.2	0.2
7%	rest	7.0	0.2	0.2	0.1	0.3	0.3	0.5	0.5	0.7
20%	rest	22.5	0.2	0.2	0.2	0.2	0.2	0.2	0.2	0.2

Tab. 2.1: Composition of the three copper alloys used (in mass %) [34].

The samples were cut into disc shaped coupons with a diameter of 12 mm and a thickness of 2 mm. Their surface was polished with abrasive papers of 400–1200 grades. They were then cleaned with sulphuric acid at 10 %V/V, rinsed with distilled water and degreased with acetone.

2.2.2 Test settings

2.2.2.1 Field corrosion tests

The influence of the urban environment on the bronze corrosion was studied by exposing the three alloys for 5 weeks (from March 2010 to April 2010) at the Department of Analytical Chemistry (Ghent University, Belgium) towards the North-West. Others samples sets were exposed at the Faculty of Engineering (Sapienza University of Rome) towards South and at 45° of inclination from January 2011 to June 2011. The set-up is shown in Figure 2.7

Fig. 2.7: Photographs of the in field urban exposition in Ghent (left) and in Rome (right).

For the marine environment the samples were exposed in a coastal town (Fiumicino) from January 2011 to May 2011.The weather conditions during the exposure tests are reported in Table 2..

Months	Average °C	Min °C	Max °C	RH%	Average wind Km/h	Rain days	Storm days	Fog days
GHENT 2010								
March	7	3	11	72	14	15	2	3
April	10	5	16	64.8	11	10	0	2
ROME 2011								
January	7.6	4.3	12.1	83.5	4.8	13	3	/
February	7.3	3	13.9	72.2	4.4	5	3	3
March	10.2	6.1	14.8	79.4	6.4	12	6	2
April	14.5	9.4	20.2	73.8	5.3	10	3	1
May	18.2	12.3	24.3	69.3	6	8	8	0
Jun	22.6	17.3	27.9	68.1	6	7	3	0
FIUMICINO 2011								
January	8.5	4.7	12.7	83.6	6.8	16	1	5
February	7.8	2.8	13.4	74	8.8	6	3	6
March	10.7	6.5	14.6	79.8	9	11	2	2
April	14.6	9.1	19.7	76.2	7	10	1	3
May	18.1	11.9	23.5	73.2	8	9	2	4
Jun	22.1	16.9	26.5	75.6	8.1	8	2	1

Tab. 2.2: Weather condition from March to April 2010 of Ghent (weather station of Antwerp) and from January 2011 to June 2011 of Rome (weather station of Ciampino) and Fiumicino (weather station of Fiumicino) [35-36].

The samples were oriented towards the south and had an inclination of 45° following the ISO 9223 standard as in Rome [37]. Figure 2.8 shows the set-up.

Fig. 2.8: Rake expositor in field urban exposition in Rome and Fiumicino (Italy).

2.2.2.2 Laboratory tests

A chamber for the corrosion tests was assembled in order to have homogeneous vapor diffusion and deposition. The position of the vapor exit hole on the chamber (volume: 45 cm^3) from which the vapor was introduced, as well as the flow rate of the solutions vapor, was optimized to avoid the formation of water film on the surface and to obtain a drop deposition.
The circular coupons were installed on columns of 2 cm in height, inclined to 45° and 1.5 cm far from each other to avoid contamination between samples.

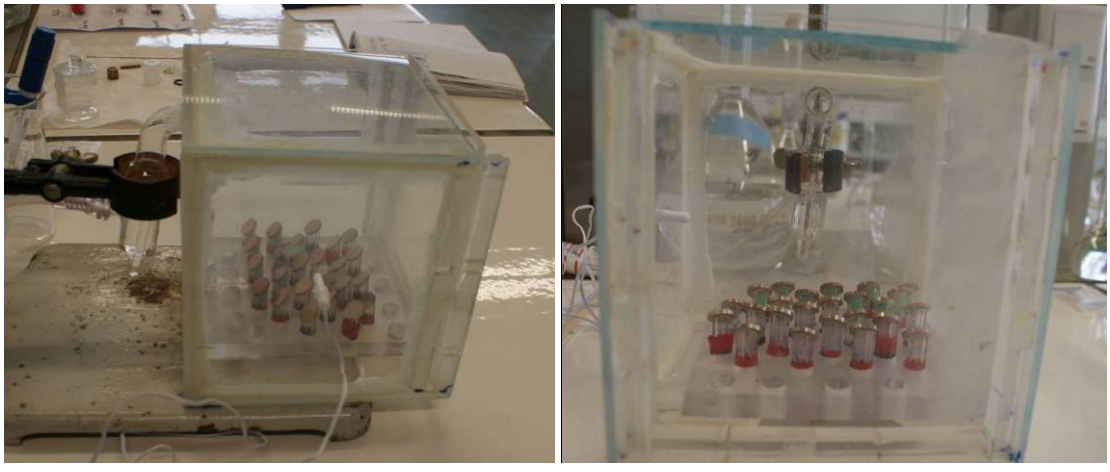

Figure 2.9: Chamber for the corrosion tests.

Wet and dry cycles were performed six times per day, spraying 0.66 mL of vapor per cycle.
The daily wet and dry cycles were carried out as follows: 30 minutes between the first three vaporizations; 2 hours between the 3rd and 4th hour; 30 minutes between the 4th-5th and 5th-6th hour; 17

hours between the last vaporization and the first vaporization of the following day. After seven days of cycles, the samples were dried for two days.

In order to simulate an urban environment, synthetic acid rain was sprayed on samples. In order to simulate a marine environment synthetic sea water was sprayed.

Figure 2.10 shows the graphs of the relative humidity (RH%) during the wet and dry tests performed at 25°C. The measurements were done after 2 hours, 4 hours, 24 hours, 48 hours, 96 hours, 240 hours as suggested by ISO 4536 [38].

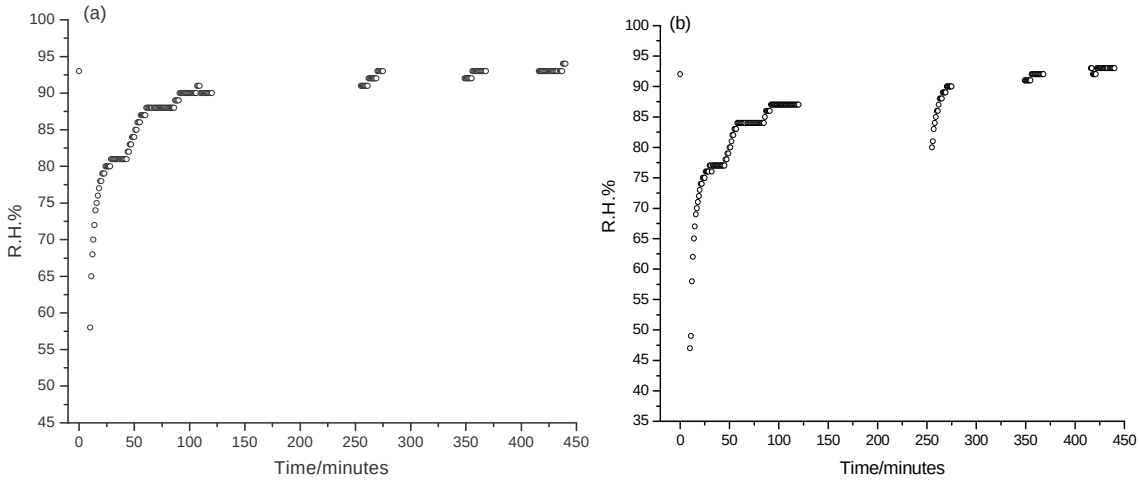

Fig. 2.10: R.H.% during the wet and dry tests in the vapor chamber. (a) during the week; (b) after the weekend.

The samples were vaporized with the above wet and dry cycles with a synthetic solution of acid rain [39] and synthetic sea water [40]. The compositions are reported in Table 2.3.

ACID RAIN		**SEA WATER**	
Component	**(mg/dm^3)**	**Component**	**(g/dm^3)**
H_2SO_4 (96%)	31.85	KBr	0.1
$(NH_4)_2SO_4$	46.20	KCl	0.7
$Na_2\ SO_4$	31.95	$CaCl_2$	1.3
HNO_3 (70%)	15.75	$Na_2\ SO_4$	4
$NaNO_3$	21.25	$MgCl_2\ 6H_2O$	10.7
NaCl	84.85	NaCl	23.5

Tab. 2.3: Synthetic acid rain and sea water solutions composition [39-40].

The effects on the bronze corrosion of long time wetness was tested with immersion in the solution of synthetic acid rain and in its major acid constituent (H_2SO_4 and HNO_3 both 0.1 M) for five weeks.

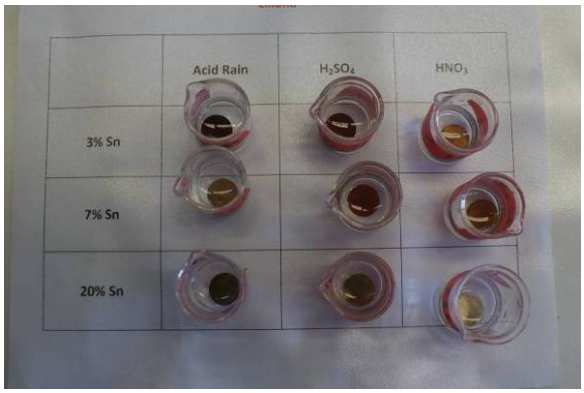

Figure 2.11: Immersion corrosion test in synthetic acid rain and in 0.1 M H_2SO_4 and 0.1 M HNO_3.

References

[1] J.A. Gonzales, M. Benito, S. Felin, *"Suitability of assessment method for identifying active and passive zones in renforzed concrete"*, Corrosion 51 (1995), 145-152;

[2] K. Leyssens, A. Adriaens, E. Pantos, C. Degrigny, *"Study of corrosion potential measurements as means to monitor the storage and stabilisation of archeological copper artefactcs"*, National Museum of Australia Camberra ACT, ABN 70 592 297 967 (2004);

[3] E. Heriz, R. Henkhaus, R. Rahmel, A. Rahmel, *"Corrosion Science: an experimental approach"*, Ellis Horwood Series in Corrosion and its Prevention, Chichester,UK (1992);

[4] H.W. Song, V. Saraswaathy, *"Corrosion monitoring of renforced concretestructure"*, Journal of Electrochemical Science 2 (1), 1-28 (2007);

[5] W.B. Stellwag, N. Wieling, *"Electrochemical corrosion testing."*, Ed. DECHEMA, Vol. 101, 17–26 (1986);

[6] M. Reid, J. Punch, L.F. Garfias-Mesias, K. Shannon, S. Belochapkine, D.A. Tanner, *"Study of mixed flowing gas exposure of copper"*, Journal of the electrochemical society 155 (4), C147-C153 (2008);

[7] F.j.r. de Oliveira, D.C.B. Lago, L.F. Senna, L.R.M. de Miranda, E. D'Elia, *"Study of the patina formation on bronze speciement"*, Materials Chemistry & Physics 115 (2009) 761-770;

[8] M. Sanchez, J. Gregori, C. Alonso, J.J. Garcia-Jareno, H. Takenouti, F. Vicente; *"Electrochemical impedance spectroscopy for studying passive layers on stell rebars immersed in alkaline solutions simulating concrete pores"*, Electrochemical Acta 52 (2007), 7634-7641;

[9] W.A. Badawy, r.m. El-Sherif, H. Shehata, *"Electrochemical behaviour of aluminum bronze in sulfate-chloride media"*, Journal of Applied Electrochemistry (2007) 37:1099-1106;

[10] E. Sidot, N. Souissi, L. Bousselmi, E. Triki, L. Robbiola, *"Study of the corrosion behaviour of Cu-Sn bronze in aerated Na_2SO_4 acqueous solution"*, Corrosion Science 48 (2006) 2241-2257;

[11] N. Souissi, L. Bousselmi, S. Khosrof, E. Triki, *"Electrochemical behaviour of an archeological bronze alloy in various aqueous media: New method for understanding artifacts preservation"*, Materials and Corrosion 54, 318-325 (2003);

[12] C. Degrigny, G. Guibert, S. Ramseyer, G. Rapp, A. Tarchini, *"Use of E vs time plots for the qualitative analysis of metallic elements from scientific and technical objects: the SPAMT Test Project"*, Journal of Solid State Electrochemistry, vol. 14, n. 3, 425-435 (2010);

[13] P. Letardi, I Trentini, G. Cutugno, *"Misure elettrochimiche per la caratterizzazione e il monitoraggio del potere protettivo di patine e rivestimenti: La tecnica EIS*, *Monumenti in bronzo all'aperto, esperienze di conservazione a confronto"*, Ed. Nardini, Firenze (2004), pp 119-126;

[14] M. Sanchez, J. Gregori, C. Alonso, J.J. Garcia-Jareno, H. Takenouti, F. Vicente, *"Electrochemical impedance spectroscopy for studying passive layers on steel rebars immersed in alkaline solutions simulating concrete pores"*, Electrochemical Acta 52, (2007) 7634-7641;

[15] E. Angelini, S. Grassini, S. Corbellini, G.M. Ingo, T. De Caro, P. Plescia, C. Ricucci, A. Bianco, S. Agostini, *"Potentialities of XRF and EIS portable instruments for the characterisation of ancient artefacts"*, Applied Physics Material Science & Processing 83 (2006) 643-649;

[16] A.J. Bard, L.R Faulkner, *"Electrochemical. Fundamentals and applications"*, Ed. Joy Wiley & Sons Inc Publications, (2000);

[17] J. Ross Macdonald, *"Impedance Spectroscopy. Theory, Experiment and Applications"*, Edited by E. Barsoukov, Wiley & Sons Inc Publications 2005;

[18] J. Sandberg, I.O. Wallinder, C. Leygraf, N. Le Bozec, *"Corrosion induced copper runoff from naturally and pre-patinated copper in marine environment"*, Corrosion Science 48 (2006) 4316-4338;

[19] W.A. Badawy, R.M. El-Sherif, H. Shehata, *"Electrochemical behavior of aluminum bronze in sulfate-chloride media"*, Journal Applied Electrochemistry (2007) 37:1099-1106;

[20] http://www.ecochemie.nl/export/Homepages/Autolab/download/NovaTutorials/Impedance_measurements_tutorial.pdf;

[21] http://www.abc.chemistry.bsu.by/vi/analyser/help.html;

[22] H.G. Volz, *"Industrial colour testing. Fundamentals and techniques"*, Wiley-VCH publication (2001);

[23] http://www.cie.co.at/index.php/Publications;

[24] D. Nystrom, *"Colorimetric and multispectra image acquisition"*, Linkoping University, Istitute of technologies, 2006;

[25] R. Cook, *"X-Rite: a guide to understanding color communication"*, X-Rite guide (2011);

[26] E. Franceschi, P. Letardi, G. luciano, *"Colour measurements on patinas and coating system for outdoor bronze monuments"*, Journal of Cultural Heritage 7 (2006), 166-170;.

[27] A. CASTELLANO, *"Elementi di archeometria: metodi fisici per i beni culturali"*, Casa editrice: Egea 2002;

[28] G GAVELLI, *"La Microscopia Elettronica a Scansione e la microanalisi elettronica nello studio delle opere d'arte"*, Casa editrice: Sansoni. Firenze 1982.

[29] D. Briggs, J. Brady, B. Newton, *"Scanning electron microscopy and X ray microanalysis"*, Jeol JSM 6400 guide (2000);

[30] B. Voutou, E.C. Stefananki, K. Giannakopoulos, *"Electron Microscopy. The basics"*, Aristotele University of Thessaloniki, Physics and advanced materials winter school 2008;

[31] http://www.vub.ac.be/META/toestellen_sem-edx.php?m=xpand&d=menu7

[32] A. Gilardoni, *"X-Rays in art"*, Casa editrice: Gilardoni. Como 1977;

[33] D. Halliday, *"Fondamenti di fisica"*, Ed Ambrosiana, Milano 1994;

[34] C. Ingelbrecht, A. Adriaens, E.A. Maier, Certification of Arsenic, Lead, Tin and Zinc (Mass Fractions) in Five Copper alloys CRM 691. EUR 19778/1, Office for Official Publications of the European Communities, Luxemburg, 2001, 53 pp., ISBN 92-894-0741;

[35] http://www.wunderground.com/history/airport/EBAW/2010/3/1/MonthlyHistory.html

[36] http://www.ilmeteo.it/portale/archivio-meteo/Roma;http://www.ilmeteo.it/portale/archivio-meteo/Fiumicino;

[37] International Organization for Standardization, ISO 9223: 1992, *"Corrosion of metals and alloys- Corrosivity of the atmospheres- Classification"*, www.iso.org;

[38] International Organization for Standardization ISO 4536: 1985, *"Metallic and non-organic coatings on metallic substrates- Saline droplets- Corrosion test(SD Test)"*, www.iso.org;

[39] C. Chiavari, A. Colledan, A. Frignani, G. Brunoro, *"Corrosion evaluation of traditional and new bronzes for artistic castings"*, Materials Chemistry and Physics 95 (2006) 252-259;

[40] A. Granic, H. O. Curkovic, E. Stupnisek – Lisac, M. Kharshan, AFurman, *"Bronze protection in artificial seawater"*, The Electrochemical Society 902, 1712 (2009), 35-48.

3. Urban effects on bronze corrosion: field exposure

The in field exposure of the samples was conduced to find a correlation between atmospheric parameters and the corrosion behavior of bronze alloys exposed to urban environment and to understand the corrosion process. As mentioned in the purposes, the evaluation was also focused on the analysis of the influence of tin content on bronze corrosion behavior. The research was carried out in two different urban environments: in Rome (Italy) and in Ghent (Belgium). The research aims to improve the results interpretation of EIS and spectrocolorimetry in the field of cultural heritage conservation sciences. In this framework, a tight correlation between electrochemical spectroscopy impedance parameters and corrosion aspects (index) will be pursued. Also a new approach to the use and interpretation of spectrocolorimetry results will be suggested. An illustration of graphical results will be introduced at the end of the chapter in order to summarize and simplify the results.
For each environment, only one sample of each alloy was analyzed to assess the innovative approach. However, the results could be considered representative because of the similar corrosion behavior observed in each alloy exposed to the seven different environments tested (2 natural urban environments, 1 natural marine environment and 4 synthetic solutions tested in laboratory). In any case, the research is still in progress aiming to improve this aspects.

3.1 Ghent: March-April 2010

During 2010 three bronze alloys (with 3% of tin, 7% of tin and 20% of tin each) were exposed for five weeks (from March 2010 to April 2010) at the Analytical Chemistry Department of Ghent University. In order to accelerate the corrosion process, the samples were positioned horizontally on the Northwest side of the Chemistry building. The corrosion evolution was monitored weekly with open circuit potential measurements and electrochemical impedance spectroscopy. These analyses were carried out with an Autolab PGStat 20 instrument with a three electrodes cell: Ag/Ag/Cl (R), Pt (C) and bronze (W) in a solution of 0.1 M of sodium sulfate. The impedance setup was performed from 75 kHz to 1 Hz at 10 mV.
At the end of the five weeks the samples were analyzed with spectrocolorimetry (measuring geometrics d/8° and standard observers 2° & 10°), SEM-EDS (LaB_6 electron source, 40 kV, 40 mA and 10^{-7} mbar) and XRD (40 kV, 40 mA, scanning 2θ from 10° to 80° grade, step width of 0.02° and counting time of 5 seconds per step).

3.1.1 Open circuit potential measurements

Figure 3.1 shows the OCP values during the five weeks of exposure. The 3% tin sample shows, up until the fourth week of exposure, a high increase of the electrode potential towards anodic values. The oxidation of the alloy generates a layer that during the last week of exposure dissolves with a cathodic process. The 7% tin sample shows a lower anodic process in the first weeks and - consequently - the patina slows down the corrosion phenomena, as the potential stabilizes. More or less the same happens for the 20% tin sample

The potential variation can be related to the absence and presence of SnO_2 (as will be shown later by the XRD data) as was also observed by De Oliveira et al. [1].

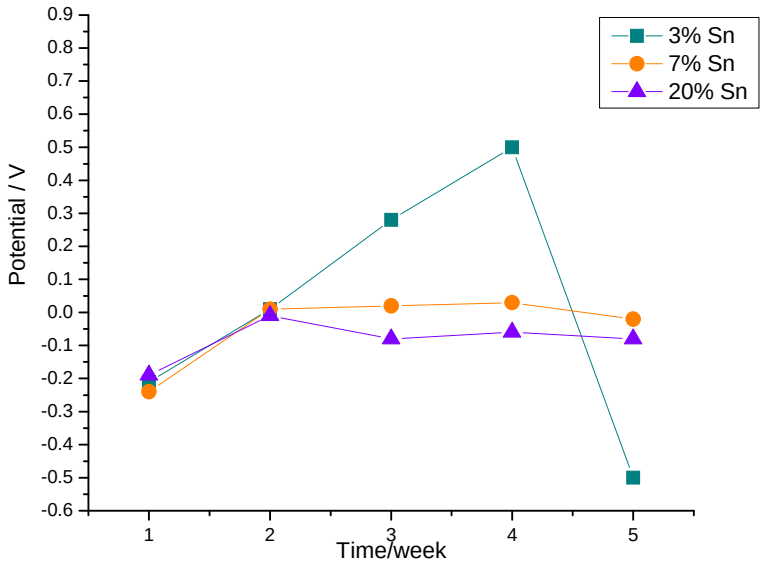

Fig 3.1: OCP measurements during 5 weeks of 3%, 7% and 20% tin alloys exposed to urban environment in Ghent from March to April 2010.

According to Cicileo et al. [2], the most protective products, that are adherent and non-porous at the surface, give a stable potential or a slight potential increase with time while, on the other hand, a potential decrease indicates less-protective products. In this case the most stable layers are produced on the samples containing 7% and 20% of tin. Figure 3.1 also shows that the layer formation is slower in the case of the 7% and 20 % tin samples compared to the 3% tin alloys, also because those films are more stable and protective as demonstrated by the potential stabilization.

3.1.2 Electrochemical impedance spectroscopy

The results obtained by impedance spectroscopy show the different corrosion behaviors of the three alloys exposed to urban environment (Figure 3.2).

Analyzing the Nyquist graphs 3% and 7% tin samples have a similar patina growth path: the layer grows on the surface but is not fixed to the surface so that the wet deposition dissolves the products exposing again the metal surface to aggressive agents. The extent of this process is different for the two samples because the protective propriety of the patina is higher in the 7% tin sample as the value of R highlights. Differently, in the Nyquist plot for the 20% tin samples the curves (in function of time) are very similar to each other. This indicates a low reaction with external factors and a passivation power of the corrosion layer.

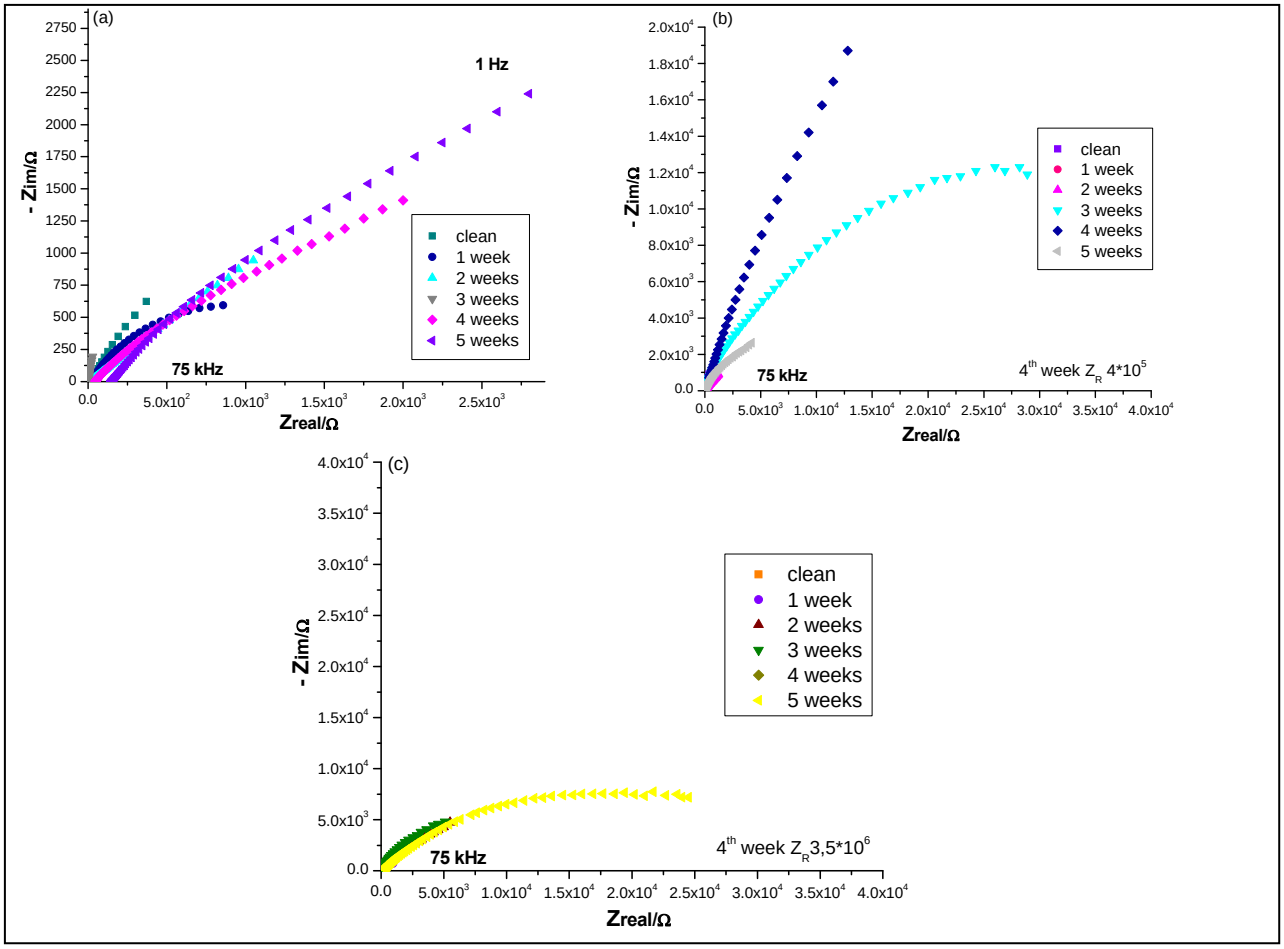

Fig 3.2: EIS results - samples exposed for 5 weeks to urban environment in Ghent from March to April 2010. (a) 3%, (b) 7% and (c) 20% tin samples.

Table 1 of Appendix 1 shows the equivalent circuits and the circuit element values of each alloy during the five weeks of exposure. The equivalent circuit was analyzed to describe in detail the corrosion process and the patina properties using the correlation found in many studies (Chapter 2, paragraph 2.1.1.2).

The CPE (Constant Phase Element) occurs frequently in the equivalent circuits. This element shows the inhomogeneous character of the system frequently considered as electrode roughness identification/attribution to the Q (capacitance) circuit element [3-4].

From the 1st week to 3rd week the CPE values of the 3% tin sample grow, indicating a patina formation. Until the 3rd week the CPE cannot be distinguished from the C (capacitance) of the film and the resistance elements (charge transfer resistance and film resistance) do not occur as single components.

On the other hand, the equivalent circuit of the 4th week impedance, is composed of multiple elements: $R_e(R_fC_f)(R_{ct}Q)W$. The (R_fC_f) are the resistance and capacity of the film that is porous and allows diffusion phenomena, as the elements Q (capacitance of charge transfer) and W (Warburg – transfer by diffusion) demonstrate. The Warburg element is commonly found in porous layers, therefore the element can also describe the porosity of the film [4]. The porosity and the diffusion processes are responsible for the patina dissolution (between the 4th-5th week of urban exposure) in the 3% tin sample, as already established by Payer et al [5]. This result is comparable with the OCP measurements.

The 7% tin sample has a different corrosion evolution and different equivalent circuits. From the first week a corrosion process occurs, although slower than the 3% tin sample, producing a patina that, from the second week, allows diffusion. From the 2nd to the 4th week the equivalent circuits are very similar (Appendix 1, Table 1): R(RQ)W or R(RC)W. The resistance increases and the capacities (C and Q) decrease, indicating a slow patina growth. A less rough patina (more stable) than the film of the 3% tin sample forms. The greater C presence, that is the capacity charge transfer, in the circuits can suggest this interpretation. However, the Warburg element demonstrates the presence of a diffusion process in progress during all the time of the exposure. The diffusion process may indicate that the corrosion mechanism is controlled not only by a charge transfer process but also by diffusion [6]. This diffusion process is a reversible dissolution which is accompanied by the formation of a porous film. On the 7% tin sample (where the Warburg element are present in almost all equivalent circuits) the formation of a passive film via dissolution-precipitation mechanism under open circuit condition is indicated from this parameter [6].

A small regression on the patinas formation can be observed between the 4th and 5th week, as already indicated from the OCP analysis.

The 20% tin sample shows a slow corrosion evolution with a small patina dissolution during the 3rd week (see also the OCP graph). The equivalent circuits are similar: in the first week a diffusion process produces a patina that increases slightly its resistance up until the 3rd week, when the capacity (Q) has a small increase due to the partial dissolution of the patina products.

The patina is less thick than the film of the 7% tin sample where the equivalent circuits are more complex but the protection properties are the same.

The patina relative thickness has been evaluated from the film capacity, when it is distinguished singularly in the equivalent circuit.

In the 3% tin sample the value of the relative thickness $(1/C_f)$ increases greatly from the 4th to the 5th week (from $2.43*10^3$ to $1.09*10^5$ F^{-1}) and so does the value of resistance.

In the 7% tin sample the relative thickness reaches higher values, from $5.02*10^{7}$ F^{-1} to $2.4*10^{8}$ F^{-1}. On the 20% tin sample this calculation cannot be done because the capacity of the film is not aside from the charge transfer capacity in the equivalent circuit.

In conclusion, the 3% tin sample forms a patina less stable than the 7% and 20% tin samples. The 7% produces a layer that slow down the process through a dissolution-precipitation mechanism. The 20% tin sample is less damaged even if the corrosion products are partially dissolved during the 3rd week.

3.1.3 Spectrocolorimetry

Figure 3.3 shows the reflectance curves for each alloy at the start of the experiment and after five weeks of exposure. In principle it would be interesting to compare the color difference of the 3% and 7% tin sample (the color difference is often difficult to distinguish for the human eye), but it would not be correct because the clean alloy already starts with a different color. Nevertheless, a comparison and an estimation of the changes (in the following referred to as "damage" in terms of color deviation from the natural color alloy) occurred on the samples can be estimated from the color difference (ΔE) between two measurements on the same sample.

When exposed to an urban environment the samples show different behaviors. The 3% tin sample has a large reflectance loss. Nevertheless, large differences in the trend of the reflectance curves cannot be observed. On the 7% tin sample the reflectance decrease is less significant and a peak can be observed on the reflectance curve. The color changes in the region of 450-500 nm. Even less difference is observed on the 20% tin sample. The reflectance is correlated to the patina formation that happens faster on the 3% tin sample. The peak on the 7% tin sample highlights the presence of corrosion products not detected on the 3% and 20% tin samples.

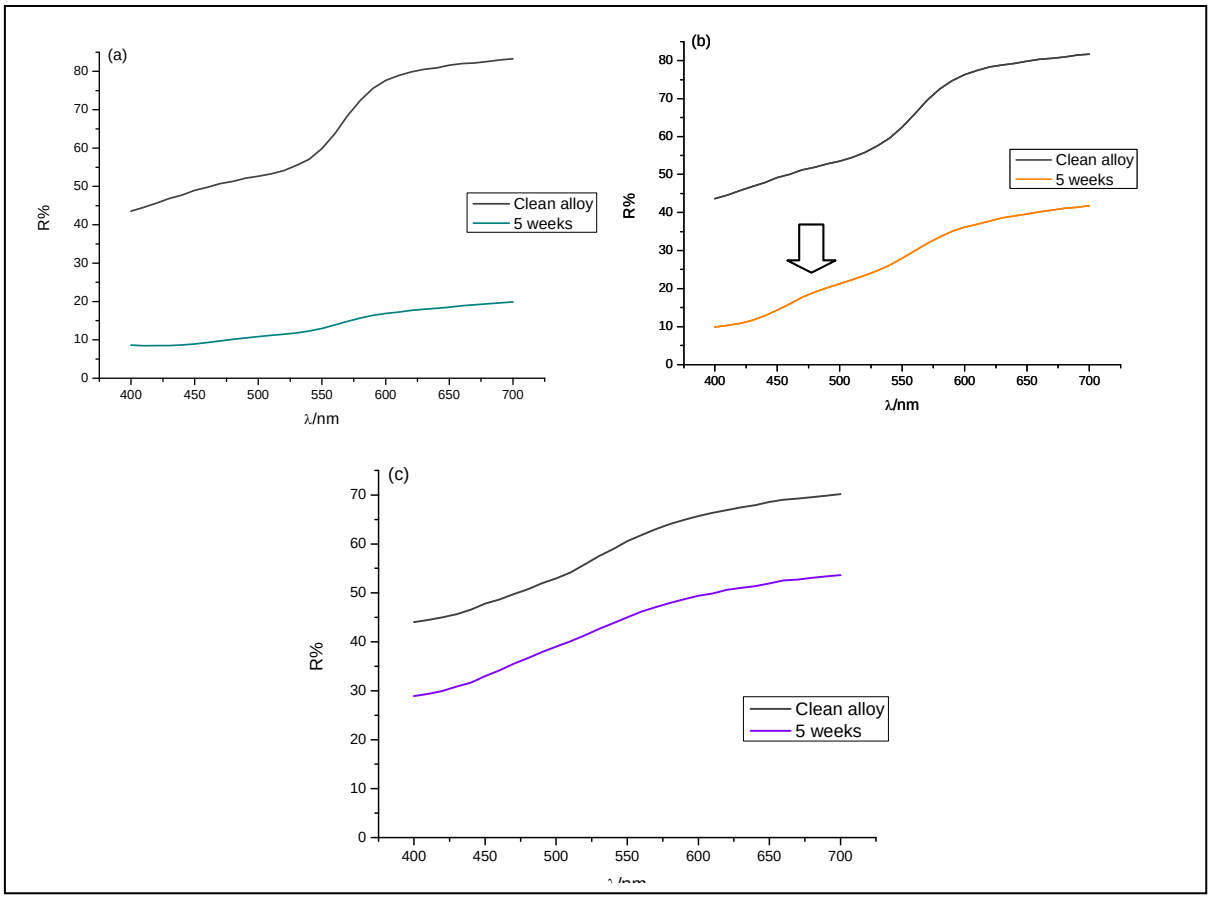

Fig 3.3: Reflectance measurements on (a) 3%, (b) 7% and (c) 20% tin samples exposed to urban environment in Ghent from March 2010 to April 210.

The color difference (ΔE) describes the different patina evolution of the three alloys. Figure 3.4 shows that the 3% tin sample has the biggest color difference (40.26), followed by the 7% tin sample (24.04) whilst the color changes of the order of 9.42. in the 20% tin alloy

The patina color change is stronger on the 3% and 7% tin samples whilst less damage occurs in the 20% tin sample.

	L^*	a^*	b^*	C^*	h°	ΔE
3%Clean	83.63	10.35	14.17	17.55	53.87	
3% Urban	43.61	6.22	12.59	14.04	63.7	40.26
7%Clean	84.07	8.26	14.63	16.8	60.55	
7% Urban	60.29	6.83	25.4	26.3	74.96	24.04
20%Clean	81.76	2.99	11.94	12.31	75.96	
20% Urban	72.57	2.39	13.96	14.16	80.31	9.42

Fig 3.4: Photographs (x1)of the 3%, 7% and 20% tin samples exposed to urban environment in Ghent from March to April 2010 and the color parameters table.

3.1.4 SEM-EDS and X-ray diffraction spectroscopy

SEM-EDS was used to analyze the morphology of the patina formed on the samples and to determine their elemental composition. The samples (3% tin sample, 7% tin sample and 20% tin sample) exposed in Ghent from March to April 2010 do not show a thick patina layer, as proven by the absence of a uniform crystalline patina (Figure 3.5).

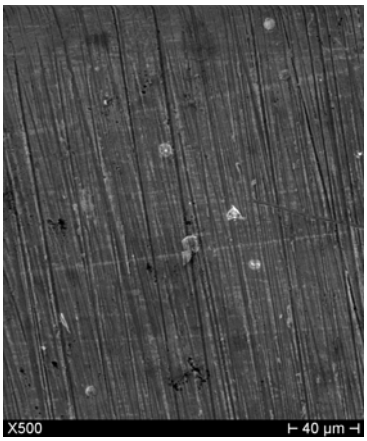

Figure 3.5: SEM secondary electrons image at x500 for the 3% tin sample exposed in Ghent from March to April 2010.

XRD was carried out at the end of the five weeks of exposure to the urban environment. The diffractograms show little peaks of tin oxide known as cassiterite (SnO_2) in each of the alloys, as shown in Figure 3.6.

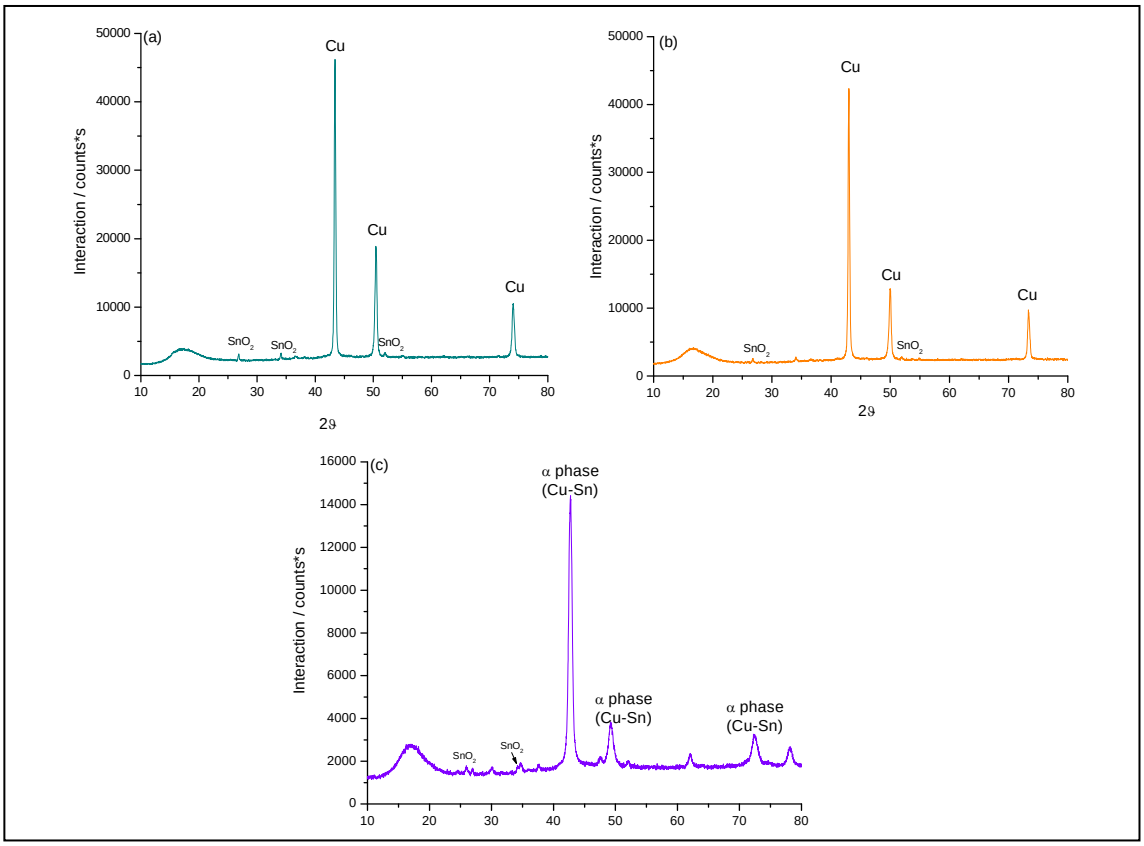

Fig. 3.6: XRD diffractograms of the 3% (a), 7% (b) and 20% (c) tin samples exposed for 5 weeks to urban environment in Ghent from March to April 2010.

3.2 Rome: January-June 2011

During 2011 three bronze alloys (with 3%, 7% and 20% of tin each one) were exposed for five months (from January to June 2011) at the engineering faculty of Sapienza University of Rome. Samples were exposed towards South at 45° of inclination following the ISO 9223 standard [6]. Spectrocolorimetry was conducted with the same measurement set-up of the previous experiments: measuring geometrics d/8° and standard observers 2° & 10°.

3.2.1 Spectrocolorimetry

During the exposure in Rome each alloy was analyzed with spectrocolorimetry twice per month. The reflectance curves are reported in Figure 3.7.

The biggest reflectance loss happened in the case of the 3% tin alloy (until the 6th week of exposure). Afterwards, the reflectance curves overlap. Base on these results we can assume that there is a fast corrosion process in the first few weeks, as proven by the big reflectance loss occurring. This process produces a patina that slows down the corrosion process as of the 8th week.

The 7% tin sample shows better resistance proprieties: until the 12th week the reflectance curves decrease progressively but less than in the 3% tin sample. After that an almost stable layer with that specific reflectance and color parameters occurs on the surface. On the curve trend of the 7% tin sample, from the second week, some peaks appear in the region of 450-500 nm and 550-600 nm. These wavelenghts correspond to the region of blue and green-yellow in the visible spectrum. Some corrosion products of this color are produced on the samples.

On the 20% tin samples the reflectance decrease is smaller than the reflectance decrease of the other alloys. The corrosion process is less strong on this surface than in the others

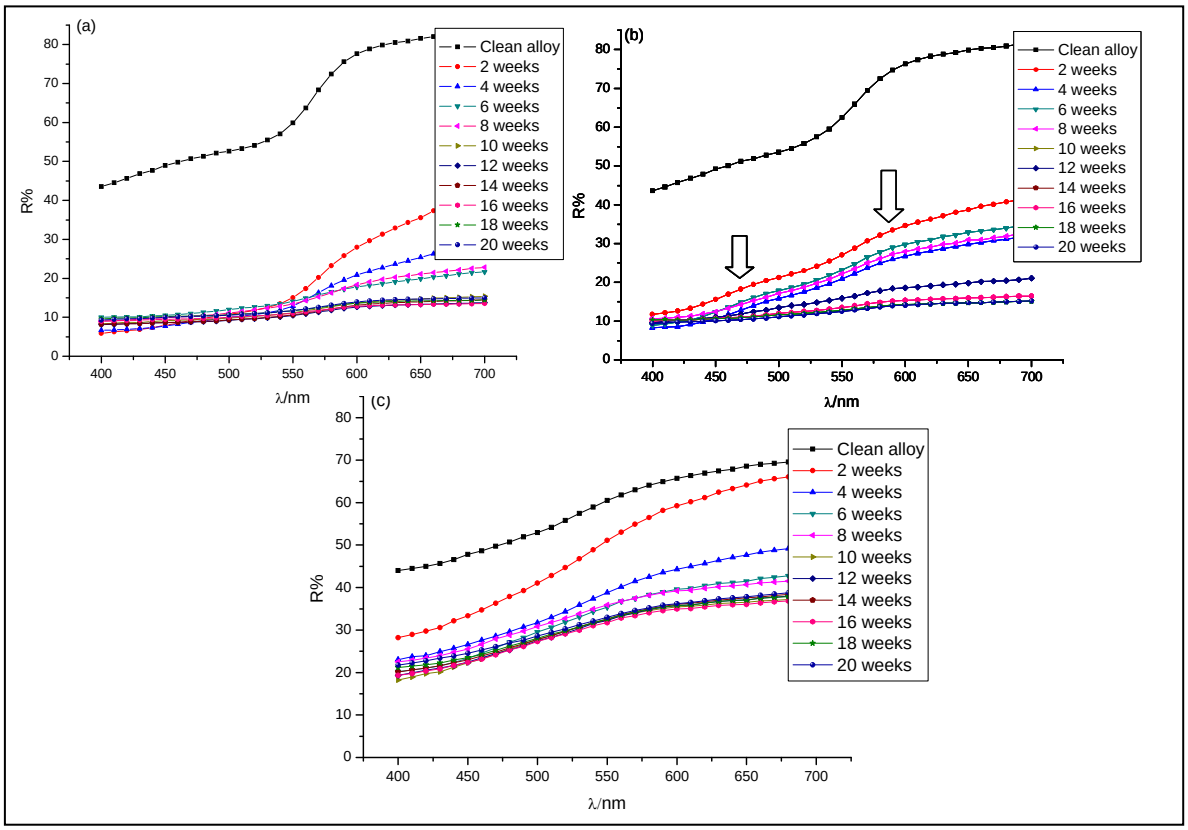

Fig 3.7: Reflectance measurements on (a) 3%, (b) 7% and (c) 20% tin samples exposed to urban environment in Rome from January to June 2011.

It is possible to better define the layer by using the CIEL* a* b* parameters. The color parameters are reported in the Tables below 3.1, 3.2 and 3.3

	L^*	a^*	b^*	C^*	h°	ΔE
clean	83.63	10.35	14.17	17.55	53.87	37.06
2 weeks	49.48	18.21	26.24	31.94	55.23	9.82
4 weeks	45.12	12.78	19.31	23.15	56.5	10.94
6 weeks	45.15	6.11	10.63	12.26	60.12	2.67
8 weeks	44.68	8.37	11.97	14.61	55.05	7.11
10 weeks	40.51	4.77	7.46	8.86	57.38	1.59
12 weeks	39.19	4.26	6.72	7.96	57.62	0.91
14 weeks	39.59	4.85	7.3	8.77	56.38	2.42
16 weeks	40.07	3.35	5.45	6.39	58.43	1.16
18 weeks	41.2	3.59	5.29	6.39	55.87	0.98
20 weeks	41.35	4.04	6.03	7.26	56.2	

Tab. 3.1: Cie $L^* a^* b^*$ parameters and ΔE values of the 3% tin samples exposed to urban pollution in Rome from January to June 2011.

For each alloy the lightness values decrease more evidently in the first weeks, which indicates that the corrosion in the first steps is faster than in the next weeks of exposure as underline also by the reflectance. Describing the patina quality formed on the 3% tin sample the red component (positive a^* values) and the yellow contribution (b^*) decrease progressively but not linearly during the exposure time. The color patina moves towards the green-blue region (see figure 2.4 and 2.6 of Chapter 2). The biggest change is observed between the first 8 weeks, after which the color differences are smaller. In these weeks the patina reaches its characteristic color properties and keeps it that way until the 20th week. The small values of ΔE during the last weeks indicates the stabilization of the corrosion products. On the other hand, the chroma shows a big decrease after the 8th week and these values, combined with the lightness decrease, represent the increasing darkness aspect of the surface layer. Other color components are hidden by chroma and lightness decrease.

The advanced corrosion of the 3% alloy is also underlined by the fact that the ΔE values are bigger than in the other alloys as well as greater are the lightness and reflectance decrease.

The greater change is observed between the first two weeks, after which the color difference values increase and decrease following the changes of the patina formation. Generally, the layers grow and reduce the lightness.

Table 2.2 reports the color parameters of the 7% tin samples.

	L^*	a^*	b^*	C^*	h°	ΔE
clean	84.07	8.26	14.63	16.8	60.55	**25.50**
2 weeks	59.58	6.98	21.64	22.74	72.12	**6.61**
4 weeks	53.16	6.14	22.96	23.76	75.02	**2.55**
6 weeks	55.7	6.32	22.77	23.63	74.5	**2.79**
8 weeks	54.48	6.25	20.26	21.2	72.86	**9.21**
10 weeks	49.61	4.01	12.76	13.37	72.56	**2.80**
12 weeks	46.98	3.39	12.02	12.49	74.25	**2.40**
14 weeks	45.32	3.98	10.38	11.11	69	**3.37**
16 weeks	43.69	2.82	7.66	8.76	69.82	**2.03**
18 weeks	42.57	2.39	6.03	6.47	68.82	**1.03**
20 weeks	42.17	2.7	6.91	7.41	68.67	

Tab. 3.2: Cie $L^* a^* b^*$ parameters and ΔE values of 7% tin samples exposed to urban pollution in Rome from January to June 2011.

The 7% tin sample has a patina with almost stable a^* values until the 8th week (Table 3.2). Afterwards the a^* values fall down towards the green region even if the decrease is not linear. The yellow values increase at the beginning (moving to the yellow part of the yellow-blue axis) to have a rapid drop after the 8th week; this decrease continues almost progressively. In the first 8 weeks the patina has a color different from the patina formed at the end of exposure time. The yellow component is dominant also because it is supported by high chroma values. After the patina growth and change, the color improves the green-blue component (more than the 3% tin sample). The lightness decrease and the a^* and b^* values indicate that the corrosion process is fast at the beginning, producing a patina on which (or changing this) is formed another layer from the 8th week as it was for the patina of 3% of tin.

The ΔE value of the 7% sample is smaller than in the 3% also if its ΔE never reaches the 0.91 or 0.98 of the 3% of tin sample that can be interpreted as high stability level of patina color. On the 7% tin sample there is a smaller but continuing corrosion aggression on the alloy. The color difference (ΔE) has an increase between the 8th to the 10th week, which indicates that the first patina formed slows the corrosion process that only later restarts.

	L^*	a^*	b^*	C^*	h°	ΔE
clean	81.76	2.99	11.94	12.31	75.96	**9.85**
2 weeks	76.44	5.29	19.91	20.6	75.13	**8.95**
4 weeks	68.35	4.34	16.18	16.75	75	**3.31**
6 weeks	65.65	2.46	16.59	16.77	81.58	**3.09**
8 weeks	65.99	1.84	13.58	13.71	82.28	**3.05**
10 weeks	63.23	1.27	14.76	14.81	85.08	**1.07**
12 weeks	63.24	2.19	14.21	14.37	81.26	**0.5**
14 weeks	63.5	2.24	13.78	13.96	80.78	**0.83**
16 weeks	62.82	1.76	13.75	13.86	82.71	**1.14**
18 weeks	63.49	2.04	12.86	13.02	80.98	**1.03**
20 weeks	63.89	2.33	11.95	12.17	78.97	

Tab. 3.3: Cie $L^* a^* b^*$ parameters and ΔE values of 20% tin samples exposed to urban pollution in Rome from January to June 2011.

The ΔE of the 20% tin sample is different. The patina progressively slow down the corrosion process. A small corrosion increase can be observed between the16th and the 18th week.

The largest decrease and difference in color values of the corrosion products can be deducted from the L^* values between the clean alloy and after the first weeks, as Table 2.3 shows. The red color values of the first 4 weeks are bigger than the red value of the clean alloy. After a decrease, the values "swing" around 2 for the a^* value and 13 for the b^* value. The chroma (the saturation color index) do not show relevant variations as in the case for the 7% and 3% tin samples.

Concluding the results of the 3% and 7% tin samples exposure show that the growth of the corrosion products could be divided into two big phases: between the first weeks and between the 8th to 10th week This can be explained with the weather condition of that period. From the 13th to 18th of March 2011 in Rome there was rain followed by 12 days of no precipitation. The acid solution deposit occurred with the rain and the consequent dry cycle energized the corrosion process, according to the models already shown in Chapter 1.

3.3 Conclusions

The results obtained from the in field exposure carried out in Ghent (paragraph 3.1) and Rome (paragraph 3.2), proved the discontinuity and complexity of the corrosion process in urban environments. The three alloys showed different corrosion behaviors and different properties of their corrosion products.

The open circuit potential monitoring evidenced that the 3% tin sample is the most damaged alloy. Then follows the 20% and 7% of tin alloys that shows similar OCP values. The 7% tin sample resistance to corrosion can be ascribed to the observed patina stability.

The electrochemical impedance spectroscopy allows a description of the patina properties evolution: even if the 20% tin sample seems to be the less damaged, also despite the patina instability, the 7% tin sample surface shows good passive properties.

Coherent with the OCP measurements, the EIS results indicate that on the 7% tin sample the corrosion produces a layer that is protective as much as the thinner patina observed on the 20% sample, but more stable.

The thickness of the 7% tin sample patina (determined with the C_f of the impedance measurements) is minor compared to the 3% tin sample patina.

The 3% tin sample features a porous and unstable patina that frequently tends to dissolve by environment attacks.

Colorimetric measurements suggest that the most significant color change is observed on the 3% tin sample, followed by the 7% and 20% tin samples (Figure 3.4). The 7% tin sample is more protected from its patina but shows a greater color change than the 20% tin sample (that features a thinner layer).

Moreover, it is worth to note that on the 7% tin samples the corrosion products create a peak of absorbance in the 475-500 nm region. This peak does not exist on the 3% tin sample reflectance curve.

The corrosion product formed on the three samples was characterized with XRD: cassiterite.

The graph on Figure 3.8 shows and summaries the analysis results of the electrochemical and colorimetric measurements.

The alloys are sorted on a "scale" that moves from negative to positive, respectively corresponding to "alloy's bad conservation condition" (more damaged or less protected alloys with a porous and not stable patina) to "alloy's best conservation condition".

Regarding the electrochemical measurements, the graph in Figure 3.8 takes into account the stability and passivity of the layers formed. For this reason the 7% tin sample (which shows a patina with good stability and barrier properties) is located near to the positive pole of the scale whilst the 3% tin sample appears to be more damaged.

The results of the colorimetric measure represented in the graphs are referred to the ΔE that can be correlated to the damage due to the formation of the patina which alters the natural color of the alloy .

The electrochemical and colorimetric results are not in contrast: it is clear that from a colorimetric point of view the thicker patina of the 7% tin sample generates more color damage at the surface than the slight but less protective film of the 20% tin sample.

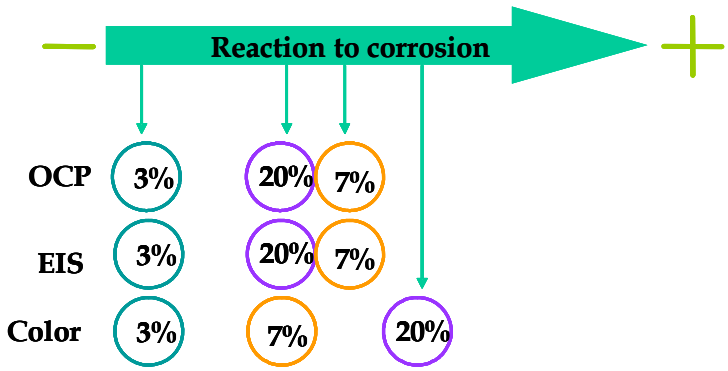

Fig.3.8: The "Damage scale" for the three alloys exposed in Ghent from March to April 2010.

The analysis results of the research carried out on the samples exposed in Rome from January to June 2011 are similar to the results obtained in Ghent. Color measurements indicate that the 3% tin sample is the most damaged, followed by the 7% and the 20% tin samples. In terms of ΔE between the clean alloy and after 5 month of exposure, the difference between the 3% and 7% tin samples is quite small ($\Delta E_{3\%}$=43.51; $\Delta E_{7\%}$=42.96; $\Delta E_{20\%}$=17.88).

Analyzing the variation of the ΔE during time it is possible estimate the patina evolution and stability. The color difference, indeed, can be correlated to the patina formation (which produces a change of color) or to the patina dissolution. The dissolution process occurring on the film is an indicator of the instability or the poor passivity property of the patina. Figure 3.9 shows the color variation during the exposure for the sample exposed in Rome.

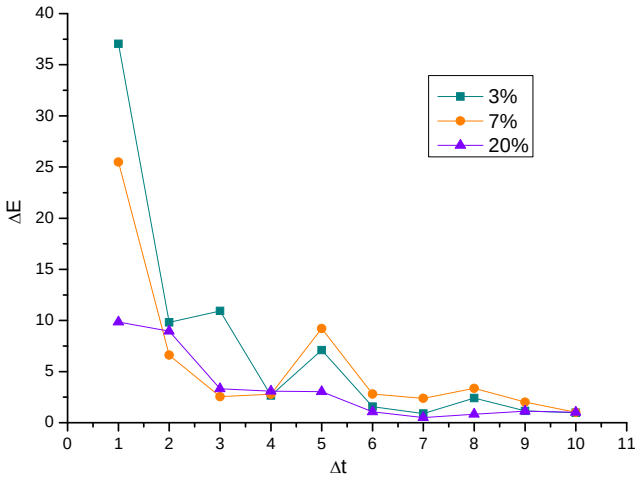

Fig. 3.9: Color differences during exposure for the three alloys exposed in Rome from January to June 2011.

As already understood, the corrosion process is fast in the first phases, specially for the 3% tin sample. On this sample the corrosion process is active until the 10^{th}-12^{th} week (Δt =6) with a growth and dissolution of the patina; afterwards the patina undergoes small changes and can be considered stable.

On the 7% tin sample a patina is formed; it slows down the process due to its barrier properties that are altered during Δt4- Δt6. As indicated in the previous paragraph, during the 8th and 10th weeks rain fell. The precipitation initially partially dissolved the patina formed. At the same time others pollutants in solution drop. A consequent dry cycle energized the corrosion process, according to the many researches exposed in Chapter 1.

The sample with less color damage and less color difference during the exposure turned out to be the 20% tin.

It is worth to note that, similarly to the Ghent tests, the products formed on the samples have different reflectance curves. On the 7% tin sample curve a peak appears in the 475-500 nm region, suggesting an absorption in purple-blue visible spectra. In Rome's tests, also the 20% tin sample produced a peak on its reflectance curve around the 575 nm region (the green visible spectra λ).

Comparing the spectrocolorimetry results obtained in Ghent and in Rome, it seems that corrosion products are similar for the 3% and 7% tin samples, whilst the 20% tin samples curve features a peak (absent in Ghent 20% tin sample) suggesting different corrosion products.

Table 3.4 shows the ΔE of samples exposed in Ghent and in Rome for 5 weeks.

	Ghent	**Rome**
3%	40.26	38.89
7%	24.04	30.82
20%	9.24	15.44

Tab. 3.4: Color difference between the clean alloy and after a 5 week exposure in Ghent and in Rome.

As the table shows, it is clear that the 7% and 20% tin samples exposed in Rome are more corroded than the 7% and 20% tin samples exposed in Ghent. However, the 3% tin sample exposed in Ghent turns out to be more damaged. This is probably because the instable patina (3% in Gent) undergoes a strong corrosion process in the environment with a higher relative humidity (RH) percentage. In the case of more stable patinas the rain does not leach the layer. The 7% and 20% tin samples turn out to be more damaged in Rome, where the environment is more polluted. However, the 3% tin samples are more color damaged in both cities.

Figure 3.10 shows the "color damage scale" of the samples exposed in Ghent and in Rome. The graph shows the color differences undergone after 5 week of exposure to each environment.

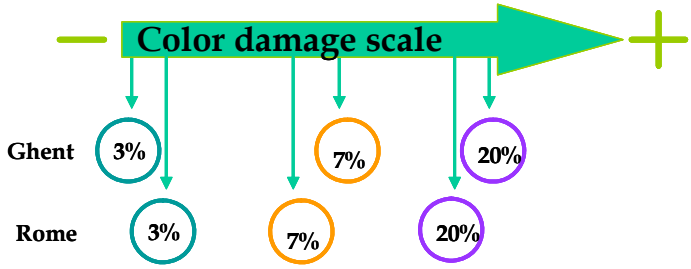

Fig.3.10: The "Color damage scale" for the three alloys exposed in Ghent and in Rome.

References

[41] F.J.R. De Oliveira, D.C.B. Lago, L.F. Senna, L.R.M. De Miranda, E. D'Elia, *" Study of patina formation on bronze speciemens"*, Materials Chemistry and Physics 115 (2009) 761-770;

[42] G.P. Cicileo, M-A Crespo, B.M. Rosales, *"Comparative study of patina formed on statuary alloys by means of electrochemical and surface analysis techniques"*, Corrosion Science 46 (2004) 929-953;

[43] J.R. Macdonald, *"Impedance spectroscopy. Theory, Experimentand Application"*, Edited by Evgenij Barsoukov, Wiley-Interscience 2005;

[44] J.Sandberg, I.O. Wallinder, C. Leygraf, N. Le Bozac, "Corrosion-induced copper runoff from naturally and pre-patinated copper in a marine environment"; Corrosion Science 48 (2006) 4316-4338;

[45] J.H. Payer, G. Ball, B.I. Rickett, H.S. Kim, "Role of transport properties in corrosion products growth", Material science & engineering A198 (1995) 91-102;

[46] W.A. Badway, R.M. El-Sherif, H. Shehata, *"Electrochemical behavior of aluminium bronze in sulfate-chloride media"*, Journal of Applied Electrochemistry (2007) 37:1099-1106;

[47] International Organization for Standardization, ISO 9223: 1992, *"Corrosion of metals and alloys- Corrosivity of the atmospheres- Classification"*, www.iso.org.

4. Urban effects on bronze corrosion: laboratory tests

As mentioned in Chapter 3, the in field exposures were conduced to find a correlation between atmospheric parameters. However, interactions with fluctuating parameters such as temperature, relative humidity, wind speed and gas concentration would be difficult to evaluate all together. In laboratory exposure climatic parameters can be removed, kept constant or accurately measured. The effects of single or combined weather parameters can be investigated.

In this research two kinds of laboratory tests were carried out to understand the corrosion process of metals when these are exposed to long wetness (immersion test) or to frequent wet and dry cycles, always taking into account the influence of tin on bronze corrosion behaviour.

Also in this case the new approach to the interpretation of EIS and colorimetric results was pursued as well as a graphical representation of the different results' contribution.

The two laboratory tests will be compared with each other and with the in field exposure tests results.

4.1 Corrosion tests by immersion

A series of immersion tests were performed with the aim of studying the effects of long and homogeneous wetness on metals' surfaces. Wet and dry cycles were carried out once a week (immersion during 7 days and drying session of 2 hours) for five weeks at environmental temperature. One sample of each alloy (3% of tin, 7% of tin and 20% of tin) was immersed in a synthetic solution of acid rain (composition is reported in paragraph 2.2.2.2 of chapter 2) and in its major acid components: 0.1 M sulphuric acid and 0.1 M nitric acid.

The corrosion evolution was monitored weekly with open circuit potential measurements and electrochemical impedance spectroscopy with a Autolab PGStat 20 instrument in a three electrodes cell: Ag/Ag/Cl (R), Pt (C) and bronze (W) in a solution of 0.1 M of sodium sulfate. The impedance setup was performed from 75 kHz to 1 Hz at 10 mV.

At the end of the five weeks the samples were analyzed with spectrocolorimetry (measuring geometrics d/8° and standard observers 2° & 10°), SEM-EDS (LaB_6 electron source, 40 kV, 40 mA and 10^{-7} mbar) and XRD (40 kV, 40 mA, scanning 2θ from 10° to 80° grade, step width of 0.02° and counting time of 5 seconds per step).

4.1.1 Open circuit potential measurements

The OCP evolution during the five weeks of immersion in the three aggressive solutions is shown in Figure 4.1.

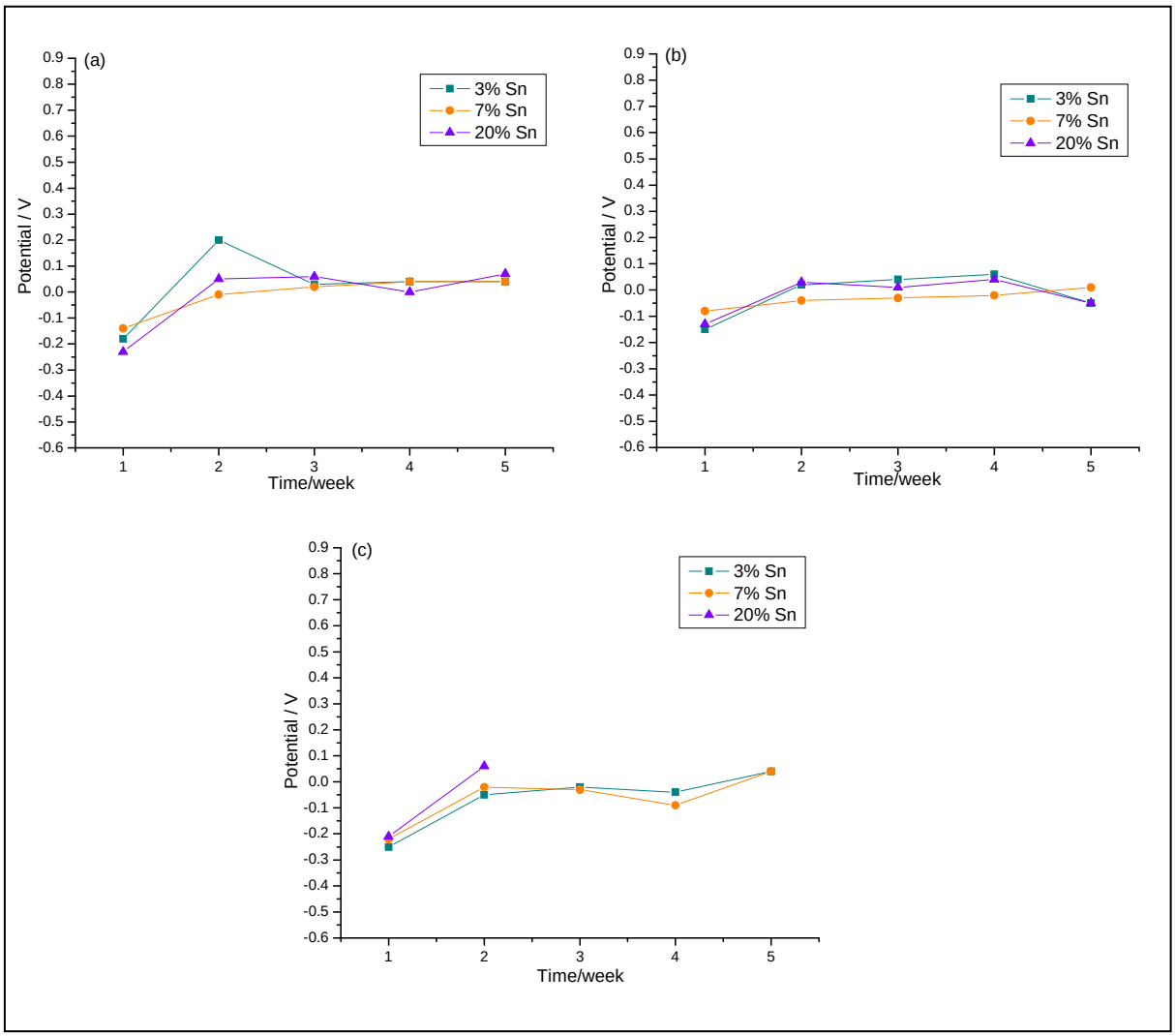

Figure 4.1: : OCP measurements during the five weeks of immersion of 3%, 7% and 20% tin bronzes in: (a) synthetic solution of acid rain; (b) 0.1M sulphuric acid and (c) 0.1M nitric acid.

4.1.1.1 Open circuit potential measurements on bronzes immersed in acid rain solution

The 3% tin sample immersed in the acid rain solution is more oxidized than the other alloys and its patina turns out to be less protective (as the OCP decrease could prove). Cicileo et al. suggested that more stable and protective patina show high and constant potential values [1]. This oxidation is proven by a huge increase towards anodic values (that implies an oxidation process) which diminishes

between the 2nd and the 3rd week due to a partial dissolution of the layer. The potential of the 3% tin sample gets stable afterwards.
The 7% of tin sample undergoes a slow but continuous patina formation as the slight OCP increase towards anodic values demonstrates. Between the 3rd and the 5th week the potential is almost stable, suggesting a protective and stable quality of the layer.
The 20% tin sample immersed in the acid rain solution shows an increase of its potential due to the layer formation in the 1st week. The patina is stable until the 3rd week, then a the potential moves towards cathodic values due to dissolution of the patina which restarts growing until the last week.
Overall results show that the 7% tin sample turns out to be the alloy with the most passive layer in the acid rain solution.

4.1.1.2 Open circuit potential measurements on bronzes immersed in sulphuric acid solution

The 3% and 20% tin samples immersed in sulphuric acid show a very similar open circuit potential evolution. During the first week, a greater increase of the potential evidences a patina formation. This patina is almost stable and protective until the 4th week, when it is partially dissolved from the aggressive solution that penetrates inside the layer.
The 7% tin sample shows a more stable patina also when immersed in the sulphuric acid solution.

4.1.1.3 Open circuit potential measurements on bronzes immersed in nitric acid solution

In the nitric acid immersion, the 3% tin sample forms a patina with an anodic reaction, in two steps during the 1st and 4th week. Between these two steps the potential and patina are stable. The 7% tin sample shows an anodic reaction during the 1st week, a slight decrease of its potential during the 2nd week and a even stronger decrease in the 3rd week. Afterwards the patina forms again. The trends of the OCP curves of 3% and 7% tin samples are however comparable between themselves as well as their potential values that turn out to be really close.
The 20% tin samples could not be analyzed after the 2nd week of immersion in nitric acid because of sample failure. From the beginning of the tests, the 20% tin sample showed a big crack on the surface and the penetration of acid solution corroded and broke it. Therefore, also for other analyses the data for the 20% tin sample immersed in nitric acid could be reported only up to the 2nd week.

4.1.2 Electrochemical Impedance Spectroscopy

4.1.2.1 Electrochemical impedance spectroscopy of bronzes immersed in a synthetic acid rain solution

The impedance spectroscopy results show the different corrosion behaviour of the three alloys (3%, 7%, 20% of tin) immersed in a synthetic acid solution (Figure 4.2).

Analyzing the graph the 3% tin sample shows a fast corrosion process until the 1st week as can be assumed from the smaller Nyquist semicircle. A partial patina dissolution occurs during the 2nd week producing an increase of corrosion reactions during the following week (3rd week). The corrosion process generates a passive layer that reaches its highest R value in the 5th week. These results are coherent with the open circuit potential analysis.

The 7% tin sample undergoes a fast corrosion process in the 1st week. Afterwards the patina slows down the process, as the resistance (R_{tot}) increase and the semi-circle opening up prove.

The 20% tin sample shows a fast corrosion rate between its initial state and the 2nd week. During the 3rd week the patina is almost the same as underlined by the curves similarity and the their overlapping. A partial dissolution of the patina during the 4th week exposes again the surface to the aggressive solution that produces corrosion products.

A smaller surface reactivity is shown on the 20% tin sample where the curves are overlapped to indicate a slower corrosion rate.

Although the higher resistance (that usually implies the passivity of the film) is reached by the 3% tin sample, the more stable and protective layer turns out to be formed on the 7% tin sample, where the phenomenon of patina dissolution is not occurring.

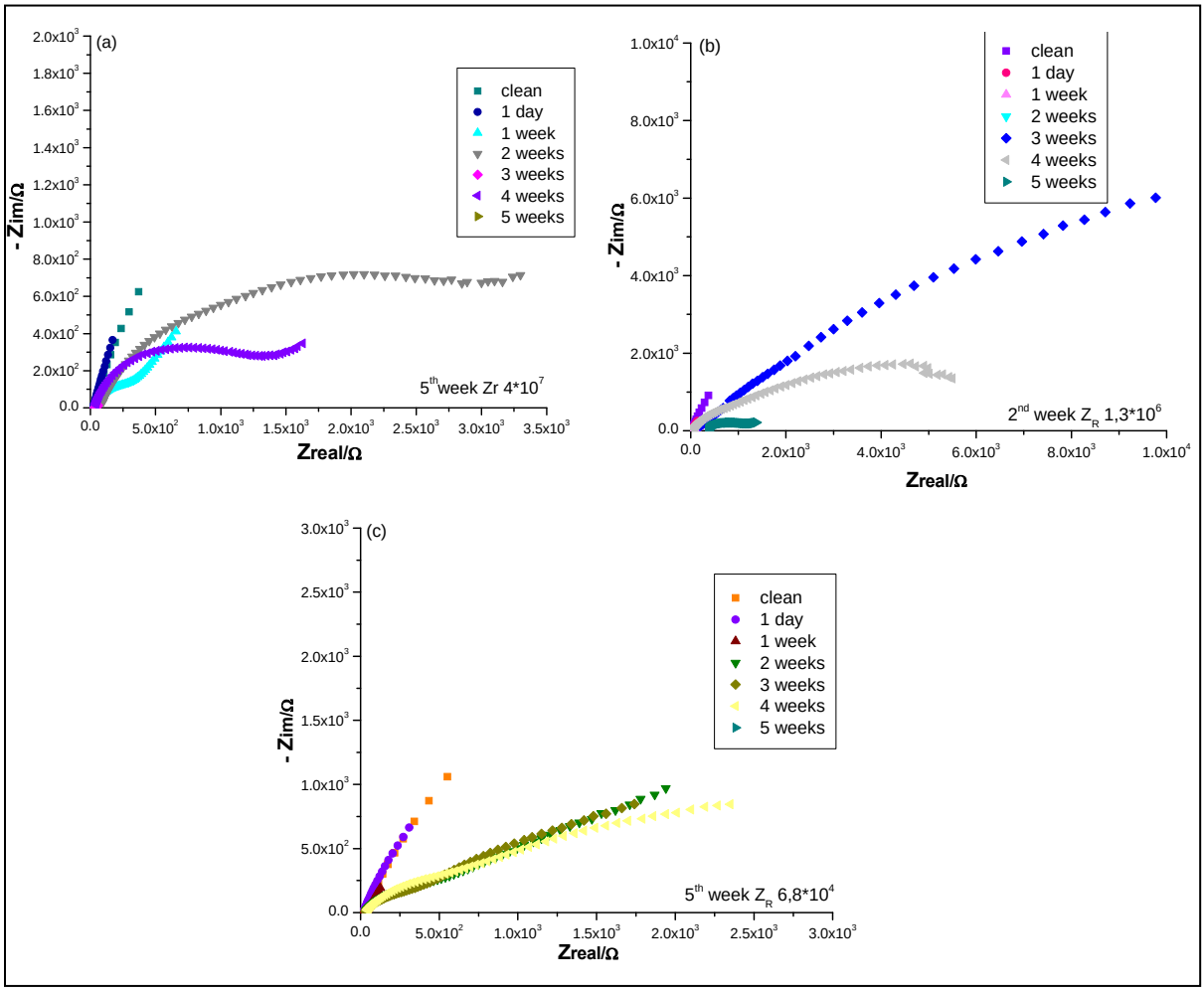

Fig 4.2: EIS results - samples immersed for 5 weeks in a synthetic acid rain solution. (a) 3%, (b) 7% and (c) 20% of tin.

In Appendix 1, Table 2, are reported the equivalent circuits of the samples immersed in the synthetic acid rain solution.

The equivalent circuits of the 3% tin sample reflect the formation and dissolution of the patina. During the 1st week the equivalent circuit evolves from RQ (first day) to RQW. Afterwards the equivalent circuit changes to R(RQ)W, which indicates a higher resistance in the charge transfer due to the patina growth. This patina is porous and rough, as n and W demonstrate.

The presence of the patina, after its partial dissolution, can be implied from the reaction process of the following circuit elements: $R(RC_f)(RQ)W$. The charge transfer capacity (Q) and the Warburg diffusion (W) underline that the reaction is dominated by a charge transfer and a diffusion process. Also the Q index (n=0.66) indicates that the porosity of the film is allowing a diffusion phenomena inside the layer, as also explained in other studies [2-4].

The mechanism of charge transfer continues during and until the 4th week, with an increase of the resistance (from 9.94 Ω of the 3rd week to $1.17*10^3$ Ω of the 4th week) and a decrease of the capacity (from $4.91*10^{-4}$ F of the 3rd week to 6,.$9*10^{-6}$ F of the 4th week) that can be interpreted as the

improvement of the patina's passive properties. During the last week the resistance reaches the value of $4 * 10^7\ \Omega$

The 7% tin sample has different equivalent circuits evolution. During the 1st week the diffusion (W) and charge transfer ($R_{ct}Q_{ct}$) reactions are active on the surface ($R(R_{ct}Q_{ct})W$). In the 2nd week the surface is identified by two circuit mesh: R(RQ)(RQ)W. This explains the protective properties despite the porosity quality (W and n are both present). During the 3rd week the equivalent circuit is composed only by R(RQ), which indicates the dissolution of the outer layer due to its porosity (the n index of the outer layer is at 0.54 and at 0.76 for the n of the inner-layer). However, due to the mechanism of the charge transfer occurring inside the layer, the patina itself grows reducing a bit the pores dimension. In this way the film shows a higher value of resistance that implies higher protective properties than in the previous week.

From that moment on, the patina growth and slows the process, and the circuit goes from (RQ)(RC) (where the process is distinguished from the patina, during the 4th week) to R(RQ)W (during the 5th week).

The patina relative thickness has been evaluated thanks to the film capacity when this circuit element is distinguished from the other.

The relative thickness is a parameter that must be correlated with the Nyquist curves evolution, with the equivalent circuit extrapolation and with the Q, n, and W elements. The relative thickness doesn't explain the patina properties; a thicker layer can be porous and less protective than a thin one.

Relative thickness from the 2nd week equivalent circuit has been calculated for the 3% tin sample. The high value ($8.47*10^5$) can be explained by the porosity of the layer. The n index is at 0,38 and the Warburg diffusion is also present. This interpretation is confirmed by the following process where the patina is partially dissolved, as the OCP, the Nyquist curve and the relative equivalent circuit showed.

During the 4th week the relative thickness for the 7% tin sample reaches the value of $7.29* 10^3\ F^{-1}$. The patina is less thick but more stable than the patina grown on the 3% of tin, as already demonstrated with the OCP and the EIS.

The relative patina thickness of the 20% tin sample was extrapolated from the equivalent circuit of the 2nd and 4th week. In the 2nd week the patinas thickness is at $6,66*10^4\ F^{-1}$ values, whilst in the 4th week it is at $2.23*10^5\ F^{-1}$. The patinas thickness is increasing between the last two weeks, as the analysis above underlined.

In conclusion, the 7% tin sample produces a double layer where the dissolution of the outer film improves the barrier properties of the inner one. The 3% tin sample appears to be the more damaged, with a thick but unstable patina. The 20% tin sample is the less damaged.

4.1.2.2 Electrochemical impedance spectroscopy of bronzes immersed in a sulphuric acid solution

The impedance spectroscopy of the three alloys immersed in 0,1M sulphuric acid is shown in Figure 4.3.

The 3% tin sample underwent a quick corrosion process that formed a patina that however allows the corrosion process progress until the 4th week. Afterwards the patina gets partially leached.

The 7% tin sample shows a progressively decreasing of the corrosion phenomenon due to the film growth, as semi-circle opening up suggests.

The 20% tin sample shows a typical corrosion progress. The patina undergoes a very slight dissolution in the beginning, but immediately reforms afterwards. As the overlapping of the curves shows, the patina properties do not change significantly during the tests duration.

Table 3 of Appendix 1 shows the equivalent circuits and the values of each element for the three alloys immersed in sulphuric acid .

The 3% tin sample changes from RQ (the equivalent circuit of the first day of immersion) to R(RC)(RC)W (the equivalent circuit of the first week). This underlines the rate of the corrosion process in the beginning. However, the patina allows the diffusion process (W). During the 2nd week the patina formation continues but is slower than in the 1st week, as the film and charge transfer resistances sum shows ($R(R_fC_f)(R_{ct}W)$). The resistance increases until the 4th week. Afterwards the partial dissolution exposes again the surface to the aggressive solution.

As mentioned above, the patina formation is more progressive on the 7% tin sample. However, the equivalent circuits outline the different phenomena in act in distinct moments. During the 1st week the corrosion is fast and is represented by the RQ circuit. The "n" index is low (0.43) which demonstrates the porosity of the film. During the 2nd week the film can be distinguished from the charge transfer in the equivalent circuit. Also the diffusion process is occurring in the following equivalent circuit: R(RC)(RQ)W. From the 3rd to the 5th week the patina formation is expressed by the R(RQ) circuit. A diffusion mechanism is occurring only during the 4th week, where the parameters values indicate a decrease of the resistance and an increase of the capacity. This demonstrates the corrosion activity increasing also due to the patina porosity and its partial leaching.

The 20% tin sample shows similar and overlapped curves (Figure 4.3) but, as the equivalent circuit outlines, the phenomena are different during time.

During the 1st week the corrosion rate is high and is correlated to a patina formation: R(RC)(RQ)W. The resistance decreases in the next week from the value of $2.13*10^3$ Ω (R_f+R_{ct}) to $1.69*10^3$ Ω (R_{tot}), due to a slight patina dissolution.

In the 3rd week the patina is already reformed, but its specific resistance is not distinguishable from the charge transfer resistance. The R_{tot} is higher than the resistance sum of the 1st and 2nd week ($2.186*10^3$ Ω).

The patina and resistance grows also during the 4th week, but the porosity level (n=0.66) and Warburg diffusion allow the partial leaching of the film during the last week.

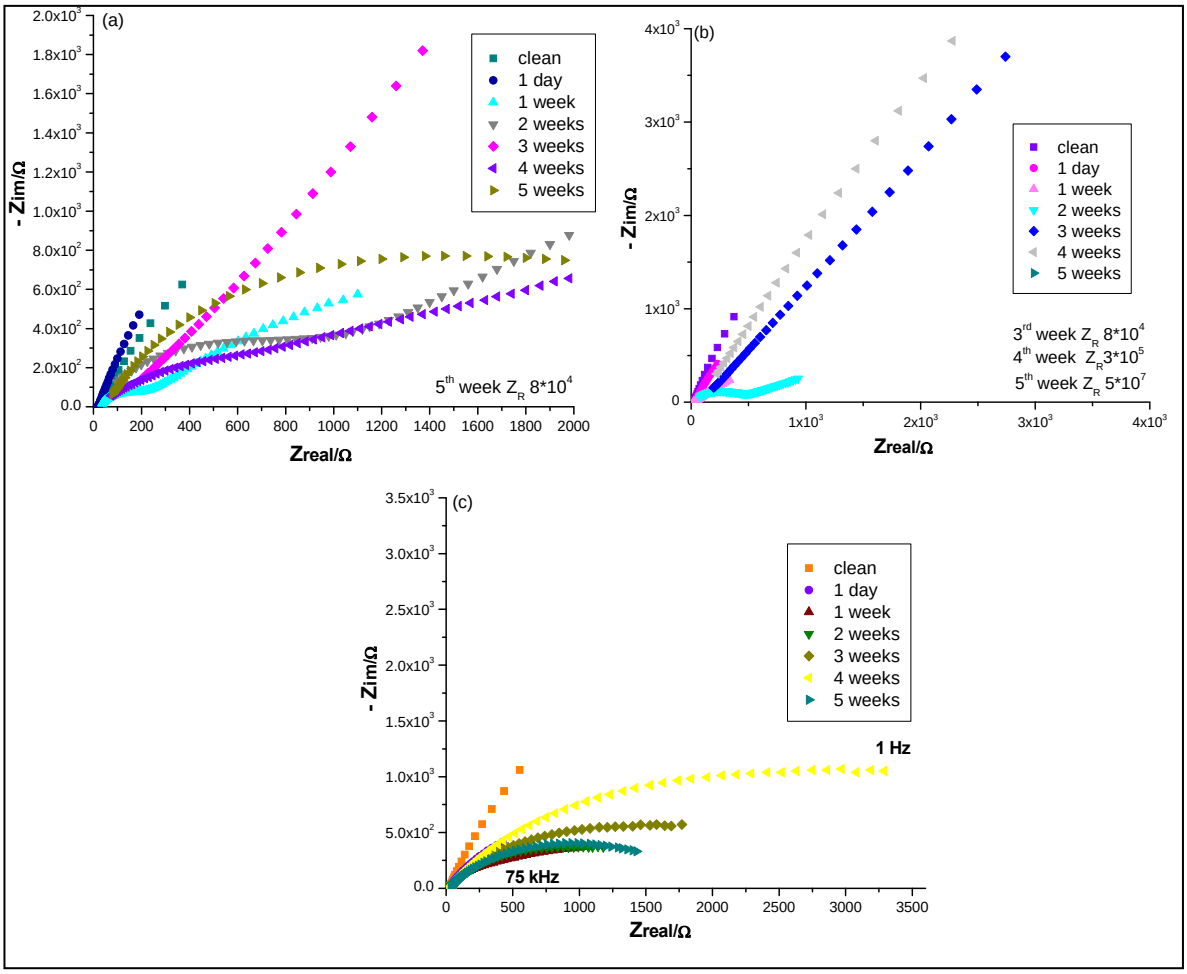

Fig 4.3: EIS results - samples immersed for 5 week in 0.1M sulphuric acid. (a) 3%, (b) 7% and (c) 20% of tin.

For the 3% tin sample, the relative thickness was calculated on the circuit of the 1st, 2nd and 4th week. In the 1st week the value was $2*10^3$ F^{-1}, whilst higher increase were recorded in the 2nd week ($3.4*10^5$ F^{-1}) and in the 4th week ($4.76*10^5$ F^{-1}). The results are comparable with the OCP and EIS interpretation. In the 2nd week the patina relative thickness for the 7% tin sample was higher: $8.3*10^5$ F^{-1}. As for the 20% tin sample, during the first week the thickness was $1.85*10^4$ F^{-1}.

In conclusion, also in this test, a good corrosion behaviour is shown in the 7% tin sample which undergoes a progressive decrease of the corrosion due to the patina formation. The 20% tin sample produces a slighter but less stable patina.

4.1.2.3 Electrochemical impedance spectroscopy of bronzes immersed in a nitric acid solution

The Nyquist graphs of the samples with 3%, 7% and 20% of tin immersed in 0.1M nitric acid for five weeks are shown in Figure 4.4.

As already mentioned, the 20% tin sample could not be analyzed after the 2nd week of immersion in nitric acid due to sample failure. From the beginning of the tests, the 20% tin sample had a relevant crack on its surface which implied the penetration of acid solution that corroded and broke the sample.

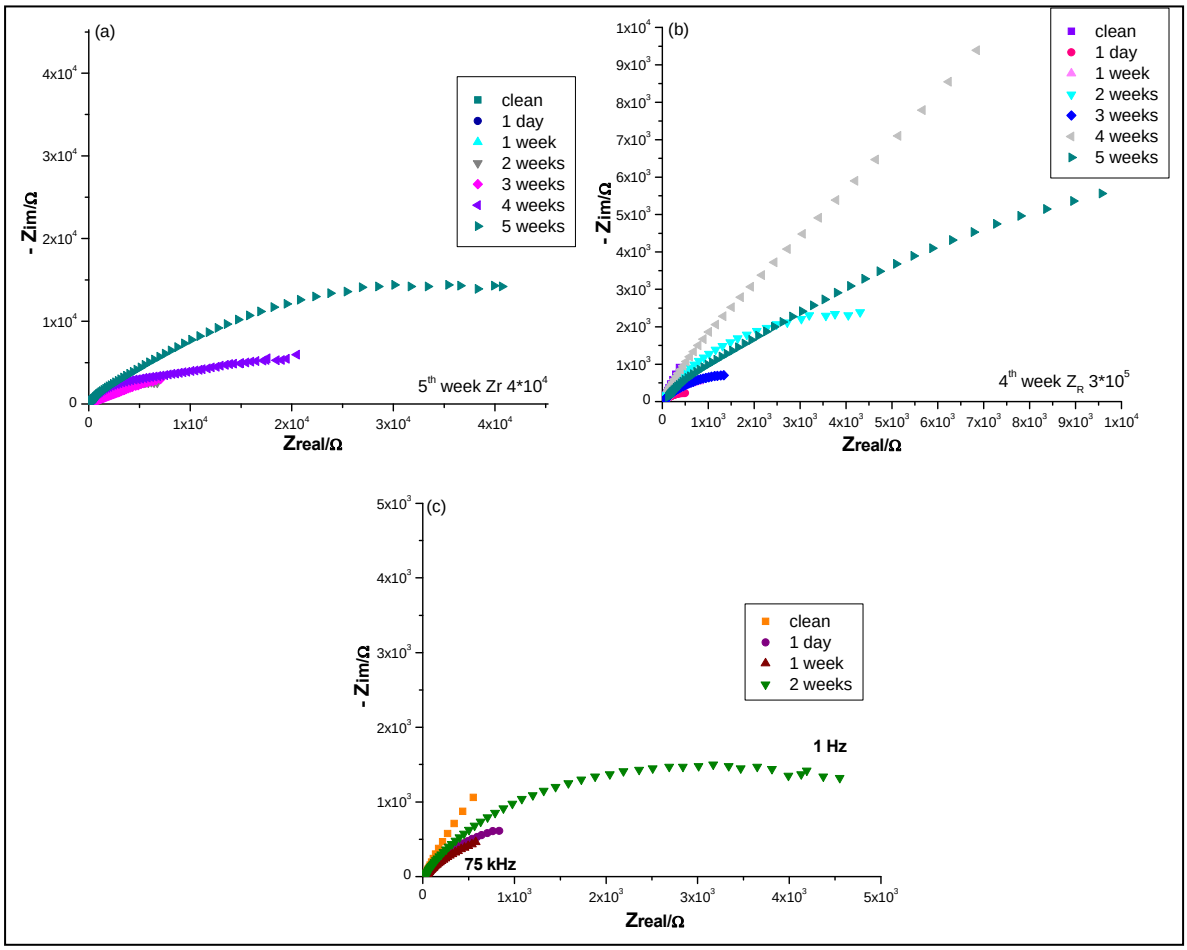

Fig 4.4: EIS results - samples immersed for 5 week in 0.1M nitric acid. (a) 3%, (b) 7% and (c) 20% of tin.

The 3% tin alloy immersed in nitric acid generates a curves overlapping and reaches high resistance values during the 5th week. At the beginning, the corrosion rate is high and slows down afterwards, from the 2nd to the 5th week, as the equivalent circuit demonstrates. On the 7% tin sample the patina formed during the first two weeks is partially removed during the 3rd. The patina restarts its formation process afterwards and the system reaches high resistance values.

The 20% tin sample undergoes a fast corrosion process in the 1st week that slows down in the following weeks.

The equivalent circuits are reported in Appendix 1, Table 4.

The low tin bronze sample has a fast corrosion until the 2nd week where the equivalent circuits for both weeks (1st and 2nd) are R(RQ). The resistance increases and the capacity decreases, which indicates that the patina formation is improving its passive properties even if the layer is porous. During the 3rd this trend is overturned: the resistance decreases and the capacity increases. Also a Warburg diffusion (W) appears (R(RQ)(RQ)W): a charge transfer and diffusion process are in

progress on the surface. These reactions involve a more stable and less porous patina that reaches its highest resistance values in the last week. This analysis is comparable with the OCP monitoring.
During the two weeks of immersion, the 20% tin sample forms a layer that slowed down the corrosion reaction.
The relative thickness of the patina during the 5^{th} week for the 3% tin sample is $1.16*10^{6}\ F^{-1}$. In the 7% tin sample, the patina has a relative thickness of $1*10^{4}\ F^{-1}$. The film growth couldn't be calculated for the following week because the circuit elements weren't distinct.
In this test the patina that appears to be more stable and protective is formed on the 3% tin sample, also compared to the less passive layer of the 7% tin sample.

4.1.3 Spectrocolorimetry

Figure 4.5 shows the reflectance curves for each alloy after five weeks of exposure. Immersed in the acid rain solution the 3% and 7% tin samples form a layer with the presence of green coloured products as the peak in the 500-600 nm region underlines.
The 20% tin sample undergoes only a big reflectance loss, the biggest one compared to the effects of the other environments. This means that the 20% tin sample is more damaged from the acid rain than from the sulphuric and nitric acid. The 3% and 7% tin samples immersed in the sulphuric acid create a patina that has a purple colour and they show a peak on the reflectance curves around the 450 nm. On the 3% tin sample the peak is higher, that because the corrosion products are more consistently formed than in the case of the 7% tin sample. In the case of the 20% tin sample, around 450 nm the curve has a slight increase that indicates the beginning of the formation of purple corrosion product.
The alloys (3% and 7% tin) immersed in nitric acid have a great reduction of reflectance that is particularly relevant on the 3% tin samples.
On the 3% tin sample the biggest reflectance loss is due to the nitric acid, whilst is due to acid rain in the 7% tin sample. This shows the different behaviour of the alloys in different environments. The ΔE values support this interpretation: the higher colour difference for the 3% tin sample is calculated in the case of immersion in sulphuric acid, whilst for the 7% and 20% tin samples the greater ΔE is detected in the case of immersion in acid rain (Table 4.1).
Also the 20% tin sample is more damaged when immersed in the acid rain solution. This is evident when confronting the greater reflectance loss occurring in comparison to the reflectance loss obtained in the case of immersion in sulphuric acid. Also the curve shape is flatter than the other.

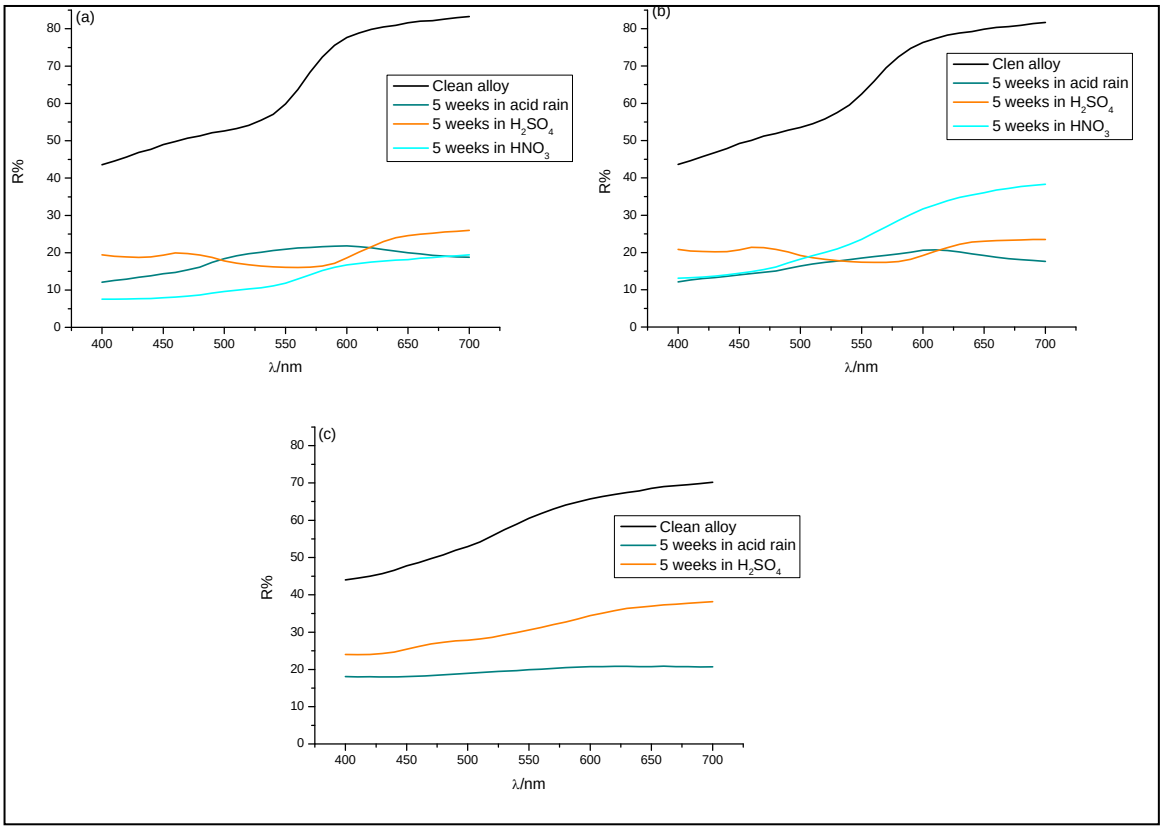

Fig 4.5: Reflectance measurements on (a) 3%, (b) 7% and (c) 20% of tin samples immersed for five weeks in: synthetic acid rain solution, 0.1M sulphuric acid and 0.1M nitric acid.

The colour parameters and the colour differences of each alloy in the different aggressive environments are reported in Table 4.1.

	L^*	a^*	b^*	C^*	h°	ΔE
3%Clean	83.63	10.35	14.17	17.55	53.87	
3% Acid Rain	52.08	-1.55	12.08	12.18	97.31	**33.78**
3% H_2SO_4	49	6.06	-3.35	6.92	59.97	**39.04**
3% HNO_3	42.34	8.13	14.07	16.25	59.97	**41.33**
7%Clean	84.07	8.26	14.63	16.8	60.55	
7% Acid Rain	49.89	1.13	9.43	9.49	83.17	**35.28**
7% H_2SO_4	50.26	4.13	-3.94	5.71	316.33	**38.79**
7% HNO_3	56.59	9.3	19.48	21.59	64.49	**28.47**
20%Clean	81.76	2.99	11.94	12.31	75.96	
20% Acid Rain	51.67	0.82	3.32	3.42	76.2	**30.31**
20% H_2SO_4	62.46	3.63	8.23	8.99	66.21	**19.66**

Tab. 4.1: Cie $L^* a^* b^*$ parameters and ΔE values for the samples with 3%, 7% and 20% of tin, exposed to urban environment and immersed in acid rain solution, 0.1M sulphuric acid and 0.1M nitric acid.

The colour parameters help to distinguish the colour differences that cannot be seen with human eye, as in the case of the patina colour of the 3% and 7% tin samples immersed in sulphuric acid, shown in Figure 4.6. The a* and b* values corresponding to the 3% and 7% tin samples immersed in sulphuric acid are really similar, especially for their blue component. The difference in the two patinas is due to the hue values that are higher for the 7% tin sample. This reaches the purple region of the colour space, whilst the 3% tin sample lies between the purple and red portion of the colour space.

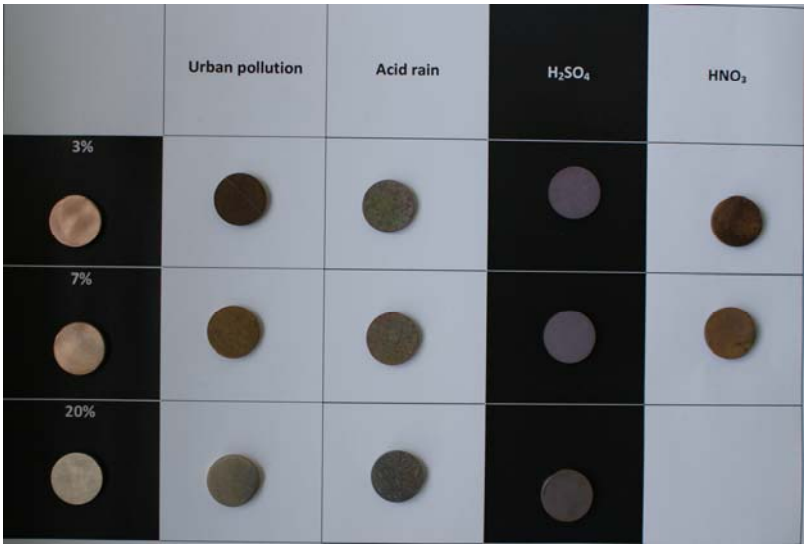

Fig. 4.6: Samples with 3%, 7% and 20% of tin after exposure to urban environment in Ghent (March-April 2010) and after the immersion in the synthetic solution of acid rain, 0.1 M sulphuric acid and 0.1M nitric acid.

The ΔE values show that the 3% tin sample has the largest colour change in each environment, except for the case of the immersion in acid rain, where the 7% tin sample turns out to be the more damaged. The 20% tin sample shows a good corrosion behaviour in every test.

4.1.4 SEM-EDS and X-ray diffraction spectroscopy

Figure 4.7 shows secondary electron images of a 3% tin sample immersed in acid rain.

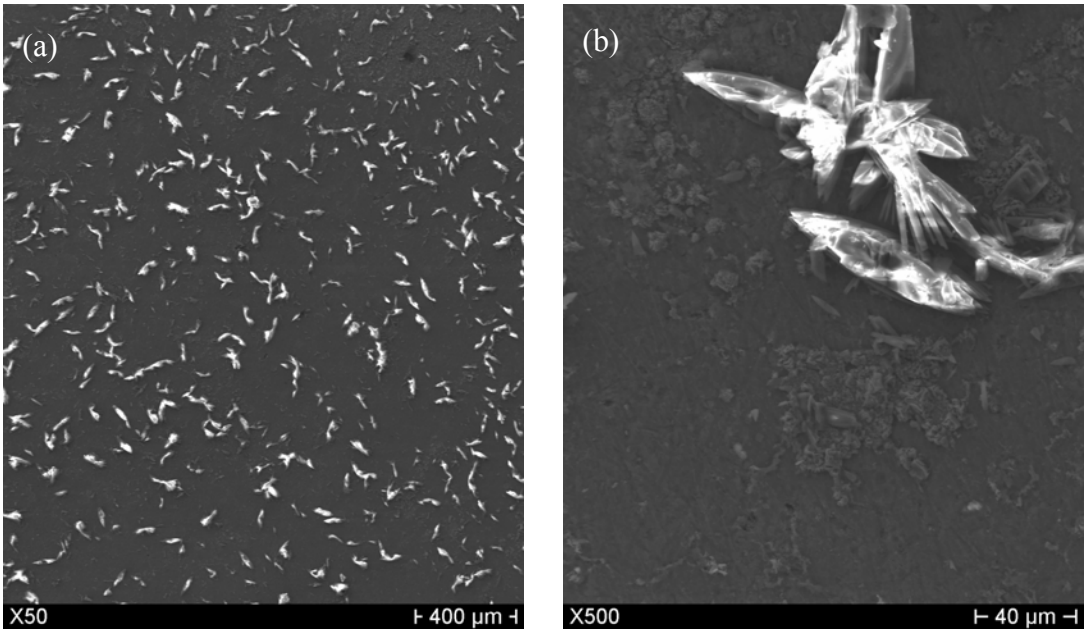

Fig. 4.7: SEM secondary electrons images at x50 and x500 for the 3% tin sample immersed in a synthetic acid rain solution for five weeks.

The white crystals in Figure 4.7 are sulphur compounds. These has grown on a layer of oxides products (Figure 4.8 a). The smaller dark crystals are chloride compounds, as Figure 4.8 b shows.

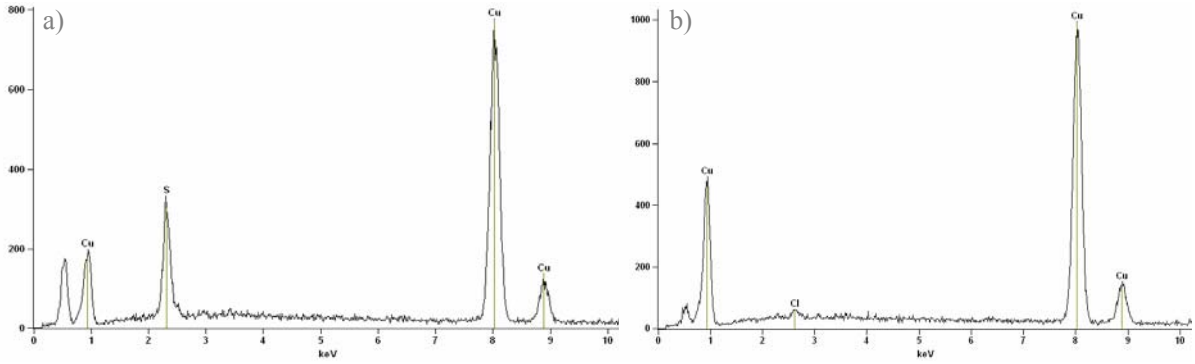

Fig. 4.8: EDS analysis on the a) white crystal and b) gray crystals of the 3% of tin sample immersed in synthetic acid rain solution for five weeks.

The 7% tin sample presents the same patina, whilst the 20% tin sample shows the least damage. On the 20% tin sample, at the same magnification degree of Figure 4.7, the corrosion products are less present (Figure 4.9 a).

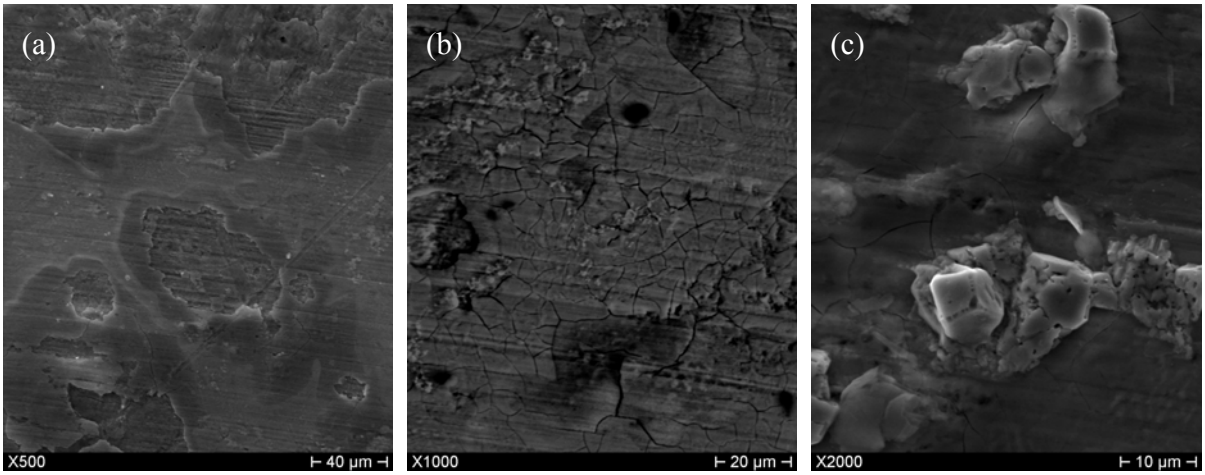

Fig. 4.9: SEM secondary electrons images at (a) x500; (b) x1000 and (c) x2000 for the 20% tin sample immersed in a synthetic acid rain solution for five weeks

Tin and oxygen were found around the cracks, probably indicating the presence of the cassiterite (SnO_2) (Figure 4.10). The crystallographic structure is represented in the section "c" of Figure 4.9.

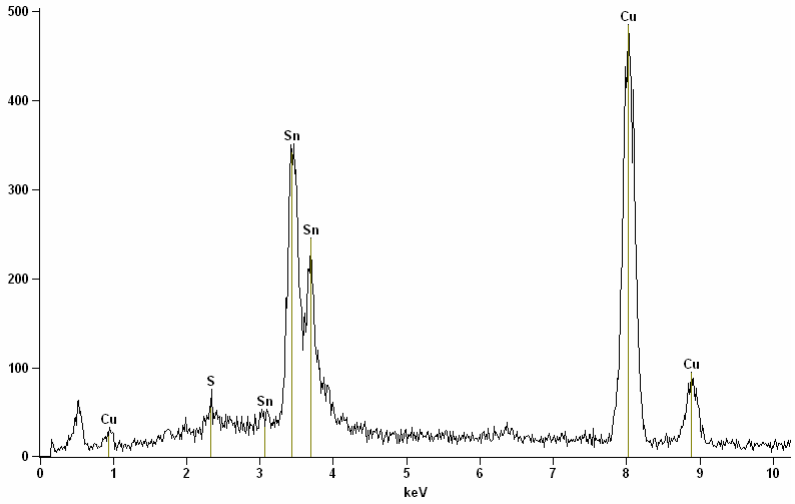

Fig 4.10: EDS analysis around a crack of the 20% tin sample immersed in a synthetic acid rain solution for five weeks.

When immersed in a sulphuric acid solution the patina is completely different. The crystals grow massively and homogeneously on the surface of the alloys, as shown in Figure 4.11. The

elemental composition reveals the presence of copper and oxygen that can be interpreted as the presence of cuprite (Cu2O) and/or tenorite (CuO).

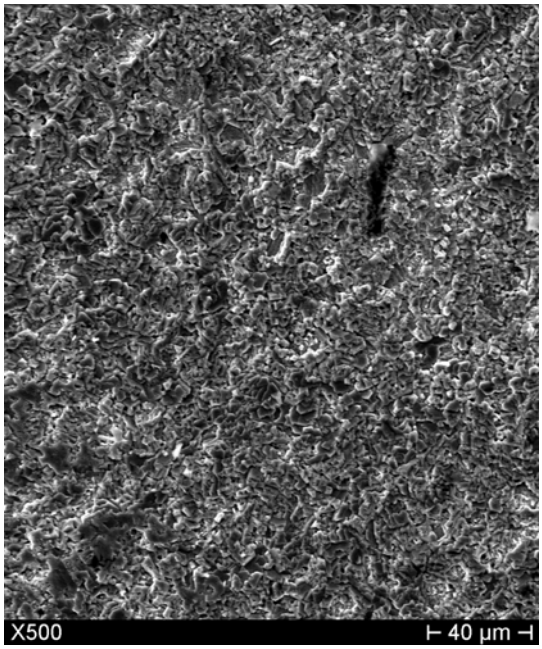

Fig. 4.11: SEM secondary electrons image at x500 for the 3% tin immersed in a sulphuric acid for five weeks.

The XRD measurements were carried out to support the chemical analysis and the interpretation of the EDS results. Figure 4.12 reports the diffractograms of the samples immersed in the synthetic acid rain solution for five weeks.

The patina is formed by oxides such as cuprite (Cu_2O) and cassiterite (SnO_2) and by a sulphur corrosion product known as brochantite ($Cu_4SO_4(OH)_6$). On the 20% tin sample gerhardtite ($Cu_2NO_3(OH)_3$) is also detected.

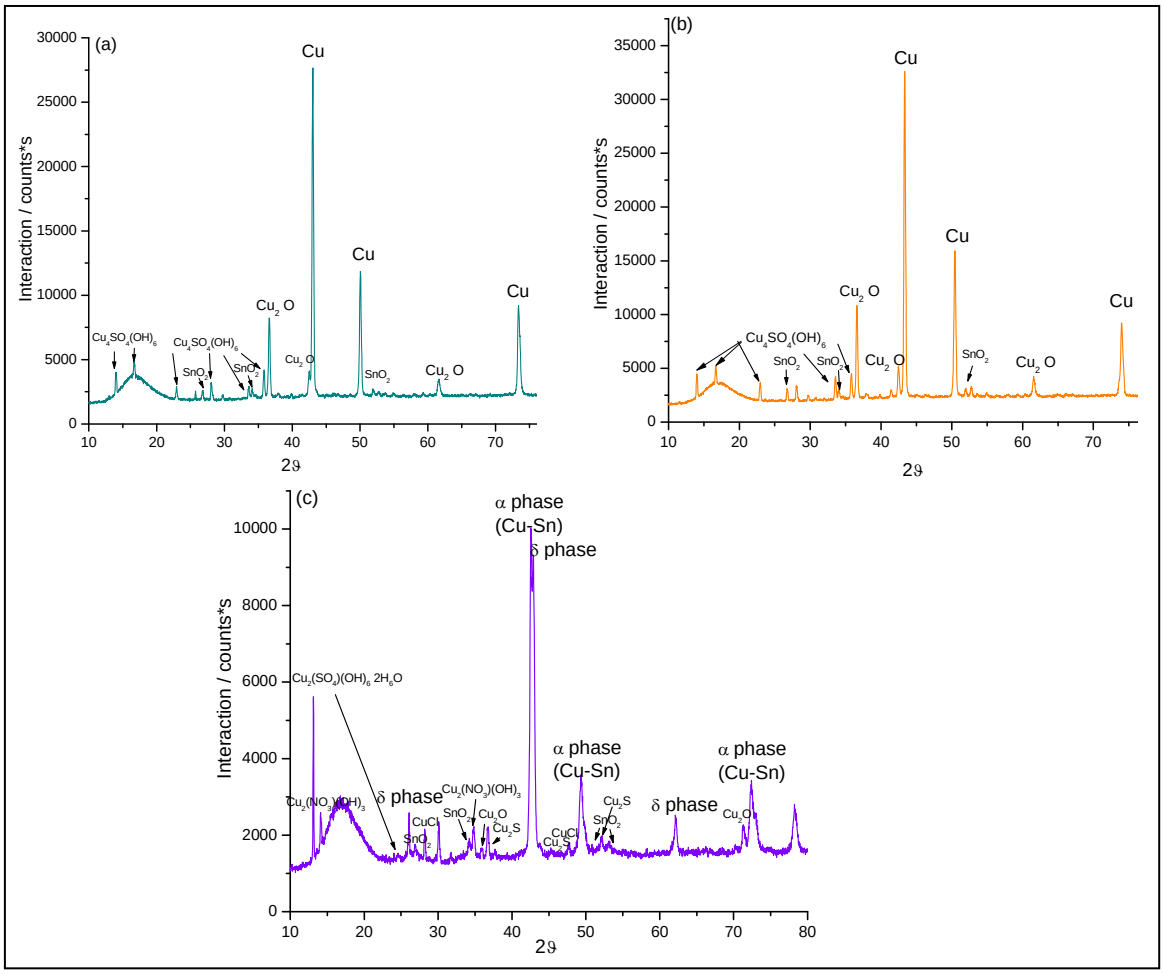

Fig. 4.12: XRD diffractograms of the samples with 3% (a), 7% (b) and 20% (c) of tin immersed for 5 weeks in a synthetic solution of acid rain.

The samples immersed in sulphuric acid for five weeks generate the diffractograms shown in Figure 4.13

The patina composition in all the alloys is simpler than the layer analyzed previously. The presence of cuprite (Cu_2O) and cassiterite (SnO_2) was detected on the three alloys.

Figure 4.14 shows the patina mineral composition of 3% and 7% tin samples immersed in the 0.1 M nitric acid solution for five weeks. Cassiterite (SnO_2) was found on the 3% tin sample, whilst on the 7% tin sample also cuprite (Cu_2O) appears.

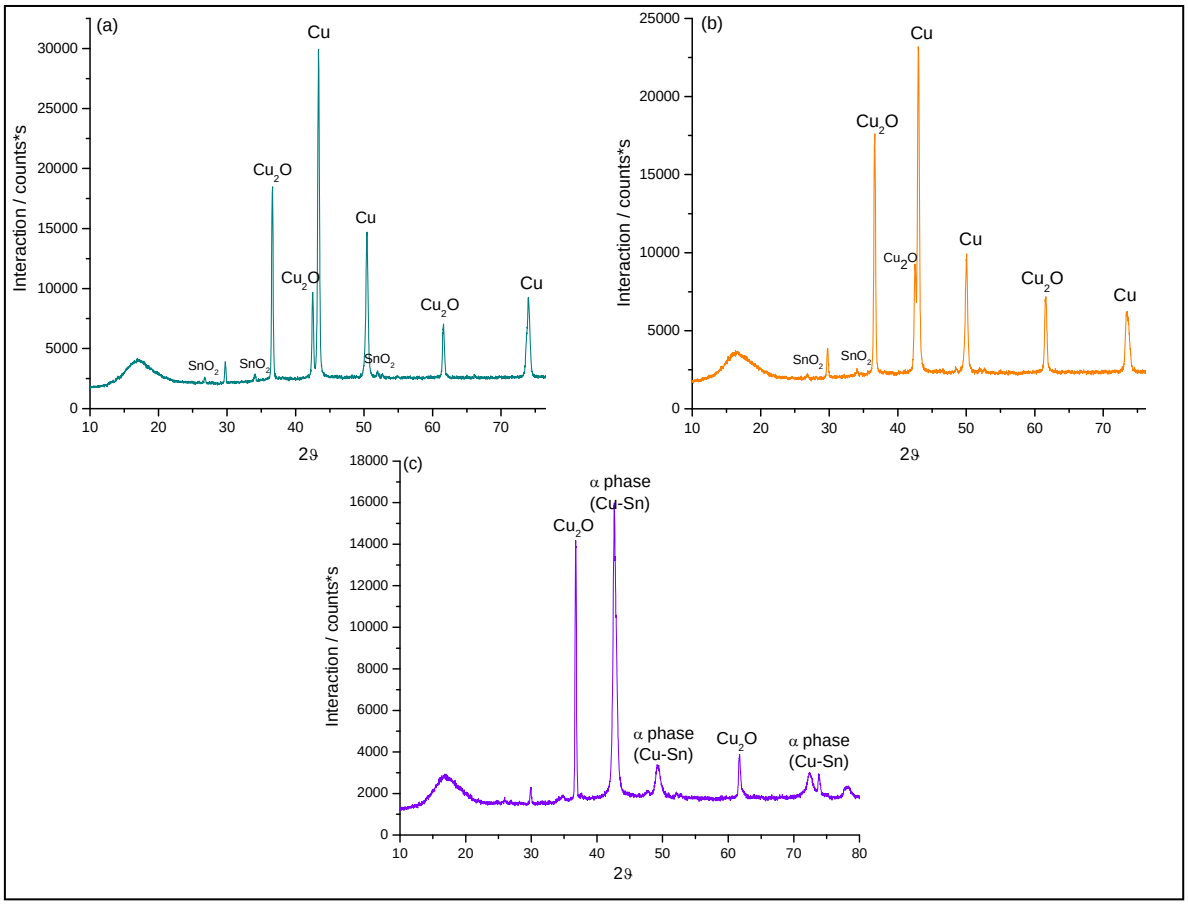

Fig. 4.13: XRD diffractograms of the samples with 3% (a), 7% (b) and 20% (c) of tin immersed for 5 weeks in 0,1 M sulphuric acid.

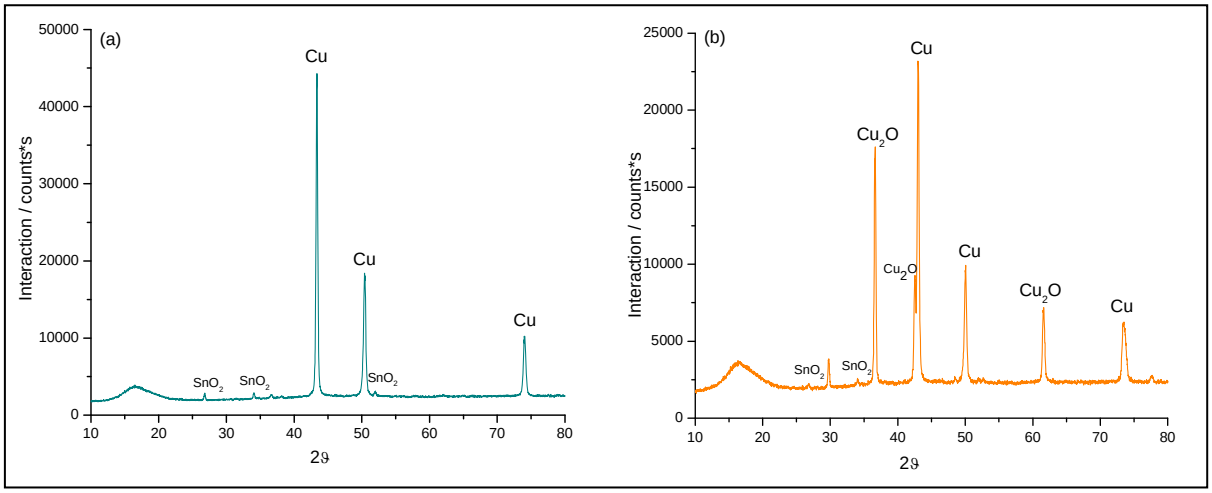

Fig. 4.14: XRD diffractograms of the samples with 3% (a) and 7% (b) of tin immersed for 5 weeks in 0,1 M nitric acid.

4.2 Corrosion test by spraying

With the aim of studying the effects of frequent wet and dry cycles on bronze corrosion behavior, the three bronze alloys were tested in a spray vapor chamber. To simulate the urban environment the samples were vaporized with a synthetic solution of acid rain [5]. Wet and dry cycles were performed six times per day, spraying 0.66 mL of vapor per cycle (following the exposure timing reported in Chapter 2 (paragraph 2.2.2.2)).

Temperature was kept at 25 °C, whilst the relative humidity changes are reported in Figure 2.11 of Chapter 2.

The corrosion evolution was monitored with open circuit potential measurements and electrochemical impedance spectroscopy with a Autolab PGStat 20 instrument in a three electrodes cell: Ag/Ag/Cl (R), Pt (C) and bronze (W) in a solution of 0.1 M of sodium sulfate. The impedance setup was performed from 75 kHz to 1 Hz at 10 mV.

The spectrocolorimetry (measuring geometrics d/8° and standard observers 2° & 10°), SEM-EDS (LaB_6 electron source, 40 kV, 40 mA and 10^{-7} mbar) and XRD (40 kV, 40 mA, scanning 2θ from 10° to 80° grade, step width of 0.02° and counting time of 5 seconds per step).

4.2.1 Open circuit potential measurements

The open circuit potential monitoring of the three alloys exposed to acid rain spray is shown in Figure 4.15.

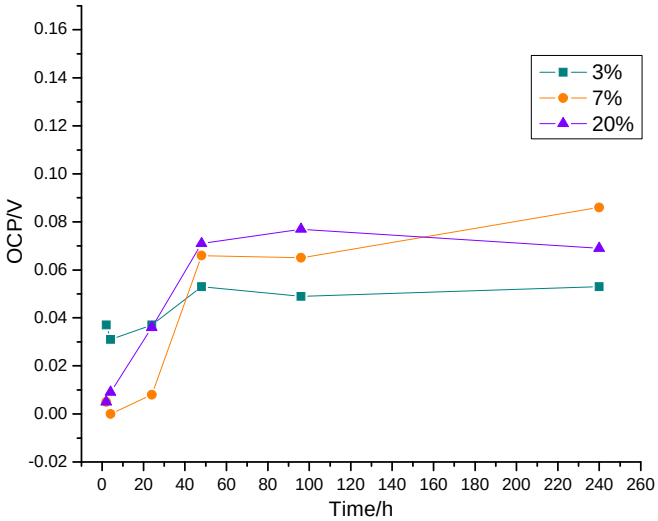

Figure 4.15: OCP measurements of 3%, 7% and 20% tin bronzes sprayed with a synthetic solution of acid rain for 2 hours, 4 hours, 24 hours, 48 hours, 96 hours, 240 hours.

The sample with 3% of tin shows a potential decrease between the 2nd and 4th hour of exposure in the chamber. Afterwards the potential increases towards anodic values due to the formation of corrosion products. The patina undergoes a slight dissolution between the 24th to 48th hour. Afterwards (96th hour) the potential is stable. The potential stability can be interpreted as patina stability.
Since the beginning (2nd hour and on) the 7% tin sample already has a potential increase that gets higher between the 4th to 24th hour. The anodic process of patina formation continues until the 240th hour with the only interruption at around 96th hour. The patina barrier properties improve during all the exposure.
The 20% tin samples show a high corrosion process of the alloy until the 24th hour, when a short time of stability is interrupted by cathodic dissolution of the patina.

4.2.2 Electrochemical impedance spectroscopy

Figure 4.16 shows the Nyquist graphs of the three alloys exposed to acid rain vapour from 0 up to 240 hours.
In this case, the interpretation of the curves and of the equivalent circuits were more difficult compared to the interpretation of graphs obtained with immersion tests. This is due to the overall of different situation occurring on the surface where areas with a thick patina are close to areas without it. Therefore, electrochemical systems are a complex system of electrochemical elements. It was sometimes difficult to distinguish the elements (for example to distinguish the patina's resistance from the charge transfer resistance or to distinguish the film capacity from the C of the charge transfer). It was also difficult to give a linear interpretation of the patina formation during time.
However, a gather of the corrosion behaviour of the surface immersed in the spray chamber was achieved.
On the 3% tin sample the corrosion rate increases until the 4th hour. The semi-circle opening up during the 24th hour shows the passive property of the layer. The layer however undergoes an aggression due to the acid rain vapour during the 48th hour. In the last hours (96-240 hour) the passive patina properties improve reaching highest resistance values at 240th hour, as the huge semi-circle shows.
The 7% tin sample shows a gradual corrosion decrease in the first 4 hours. Between the 24th and 48th hour the patina barrier properties improve, as already demonstrated with OCP measurements. During the 96th hour a closing of the Nyquist curve underlines a restart of some corrosion processes on the metal surface. These processes produce a layer and still go on during the 240th hour.
On the 20% tin sample the corrosion reaction produces a layer that progressively slows down the vapour aggression up until the 48th hour. A new corrosion process restarts on the surface increasing already existing patina.

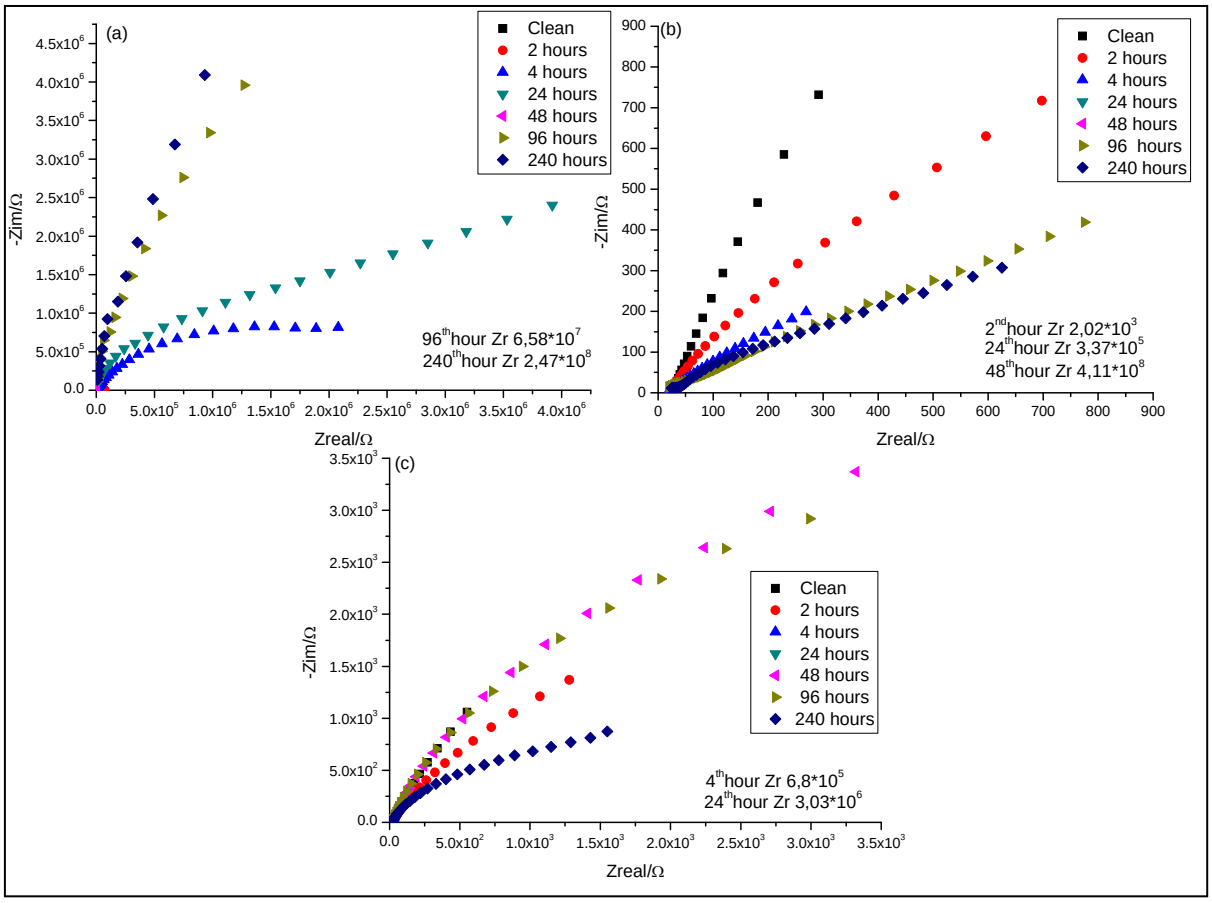

Fig 4.16: EIS results - samples in a chamber sprayed with a synthetic solution of acid rain for 2 hours, 4 hours, 24 hours, 48 hours, 96 hours, 240 hours. (a) 3%, (b) 7% and (c) 20% tin samples.

The equivalent circuits that are better fit to explain this interpretation are reported in Appendix 1, Table 5.

On the 3% tin sample the corrosion process is expressed by the circuit R(RQ)W during the 2nd exposure hour. The circuit of the 4th hour is more complex: R(RQ)(RC)W. In this last circuit, the film with higher resistance value ($9.85*10^5$ Ω instead of the previous 363.64 Ω) along with the lower capacity ($2.89*10^{-9}$ F instead of the previous $5*10^{-4}$ F) allows both phenomena of charge transfer and mass diffusion on the double layer. Those processes have a slight increase during the 24th hour and lead to a R(RQ)W circuit where less elements are detected but the diffusion process are still revealed. In the last hours (96th to 240th hour) the resistance increase occurring (R_{240h}=$7.49*10^8$ Ω) leads to think that a more homogeneous and stable patina formed.

On the 7% tin sample the resistance increases whilst the Warburg diffusion decreases to even disappear during the 24th hour. The corrosion process is therefore leaded by charge transfer (Q). A resistance values increase is detected between 24th to 48th hour of chamber exposure, and turns out to be coherent with the increase of the potential revealed by the OCP measurements. The total resistance reaches $1.92*10^8$ Ω. Afterwards a partial dissolution of the layer reduces the resistance and exposes the surface to the corrosion action up until the 240th hour.

The 20% tin sample shows an equivalent circuit composed by two distinct parts. The film and the charge transfer coexist during exposure. From the 96th hour the Warburg element also appears. The film resistance increases until the 4th hour when it starts decreasing until the 240th hour (R_{2h}=5.60 Ω; R_{4h}=1*10^{6} Ω; R_{48h}= 8.71*10^{3} Ω; R_{96h}=7.24*10^{3} Ω; R_{240h}=8.08*10^{2} Ω).

The patina is formed during the exposure but the passive properties do not improve. The charge transfer is always active.

In conclusion, on the 3% tin sample the passive patina properties improve progressively reaching the highest resistance values at the 240th hour. This alloy is more protected and undergoes fewer aggressions by the solution than the 7% and 20% tin samples.

4.2.3 Spectrocolorimetry

In the laboratory tests, the colour evolution of the three alloys was examined during 10 days. Figure 4.17 shows the reflectance curves as a function of time, while the values of the lightness and colour are reported in the Tables 4.2, 4.3 and 4.4.

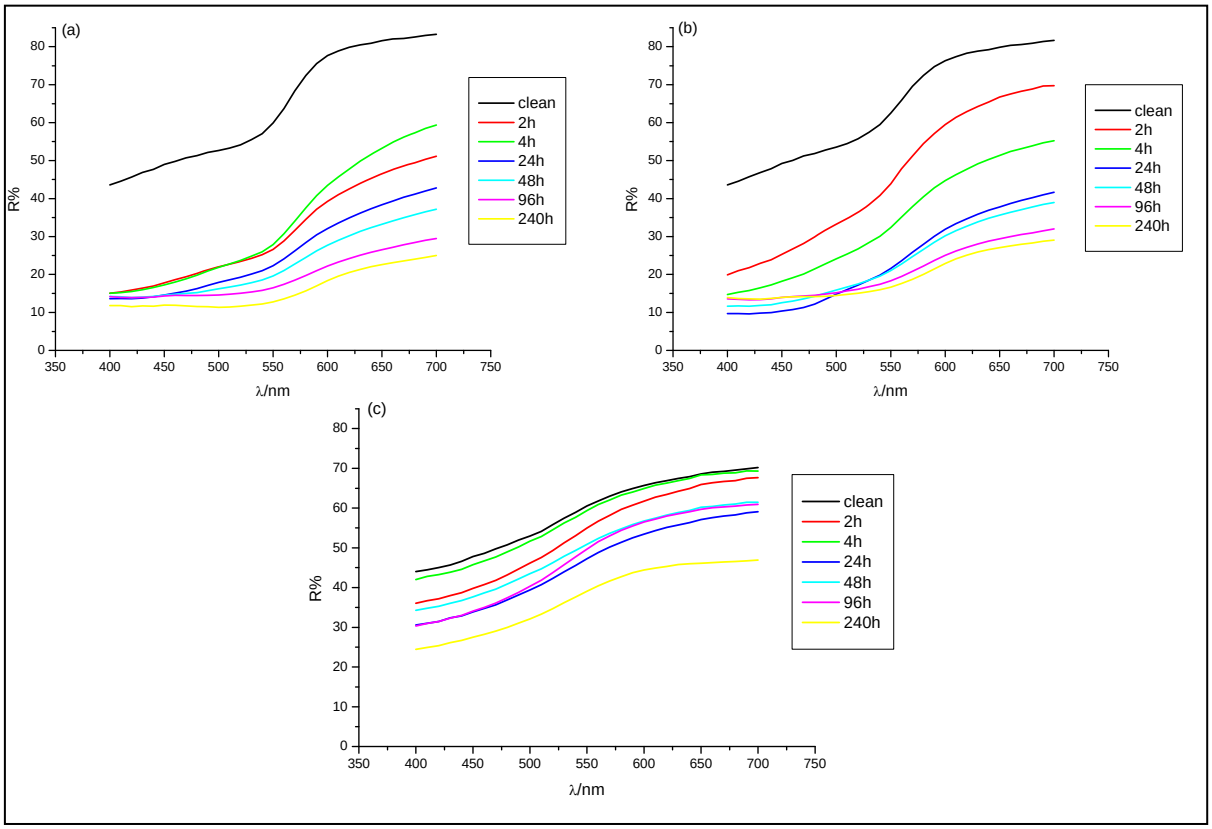

Fig 4.17: Reflectance measurements in chamber on samples sprayed with a synthetic solution of acid rain for 2 hours, 4 hours, 24 hours, 48 hours, 96 hours, 240 hours. (a) 3%, (b) 7% and (c) 20% of tin.

The reflectance curves show a similar trend compared to the urban environment trend (Chapter 3, paragraph 3.1.2): a relatively large difference between no chamber exposure and two hours of chamber

exposure for the 3% and 7% tin samples and only a small variation for the 20% tin sample were detected. The corrosion occurs faster for the first two alloys and is more slowly for the 20% tin sample. In all three samples the corrosion gets an accentuation in the first hours. It is worth noting that the reflectance loss for the 3% and 20% tin sample is bigger after 2 hours of exposure than after 4. This is probably due to a inhomogenity of the patina and to its instability in this first phases of the process.

In the case of the 3% tin sample the reflectance decrease is significant and fast in the first hours. A progressive reflectance decrease is detected afterwards. The corrosion process is slowed down by the patina formed on the surface. The colour parameters a^* and b^* are in the positive region. The red ratio (a^*) has values increasing until the 4th hour and decreasing from the 4th hour until the 96th hour. However, the values are almost stable around 10. Also the yellow component increases until the 24th hour to decrease until the last hour of exposure.

The red and yellow values combined with the lightness and chroma decrease describe the evolution towards a dark red-brown colour. The ΔE value underlines the colour change process occurring with the formation of corrosion products. The ΔE value is correlated to the corrosion rate and to the patina properties. At the beginning the colour difference is significant (22): the corrosion starts quickly producing a film which changes in colour. Between the 2nd and the 4th hour the corrosion process slows down (4.95). The patina grows faster in the 4th -24th and 48th -96th time lapses. The patina is unstable and undergoes smaller changes also in the remaining hours of exposure. The patina does not protect the surface from the environment aggression and is partially dissolved and then built again during exposure to acid rain vapour as the ΔE values and the interpretation above given demonstrated.

	L^*	a^*	b^*	C^*	h°	ΔE
0h	83.63	10.35	14.17	17.55	53.87	**22.78**
2h	61.06	12.38	19.73	23.3	57.89	**4.95**
4h	62.66	15.25	23.44	27.96	56.94	**8.83**
24h	56.26	11.54	18.61	21.89	58.2	**5.53**
48h	53.26	11.07	13.98	17.83	51.63	**7.32**
96h	49.31	9.39	8.05	12.37	40.58	**5.22**
240h	44.57	10.98	6.53	12.78	30.76	

Tab. 4.2: CIEL* a* b* parameters and ΔE values for the 3% tin samples exposed to acid rain vapour.

The 7% tin sample shows a^* values continuingly decreasing, and shows an increase only during the 24th hour. The yellow component is dominant until the 24th hour and decreases to 9.33. The colour saturation (C^*) shows a fluctuating situation of alternate increasing and decreasing of values. Also in this case a significant lightness decrease occurs during exposure, significantly influencing the colour of the patina. The biggest differences in colour are detected in the first two hours and between the 2nd and 24th hour, as a^*, b^* and C^* values already indicated. The periods of patina stability are between the

24th and 48th hour (where the ΔE is 2.35) and between the 96th – 240th hour (where the is 3.57) according with the EIS analysis.

	L*	a*	b*	C*	h°	ΔE
0h	84.07	8.26	14.63	16.8	60.55	**16.32**
2h	73.31	11.3	26.52	28.83	66.92	**8.56**
4h	64.85	11.21	25.18	27.56	66.01	**10.19**
24h	54.92	12.6	27.04	29.83	65.02	**2.83**
48h	54.48	11.43	20.56	23.53	60.93	**4.53**
96h	51.38	9.79	12.4	15.8	51.71	**3.57**
240h	49.55	9.88	9.33	13.59	43.34	

Tab. 4.3: CIEL* a* b* parameters and ΔE values for the 7% tin samples exposed to acid rain vapour.

The smaller difference in colour (ΔE) occurring in the 7% tin sample at the beginning of the test (compared to the 3% tin sample behavior) can be explained with a slower reaction of the alloy. Afterwards the 3% tin sample is less damaged by the acid vapours (until the 24th hour). After the 24th hour the patina formed on the 7% tin sample turns out to be a bit more stable than the 3% tin sample. The 20% tin sample undergoes less colour changes. The biggest decrease in values is detected for the lightness. The red and yellow ratio discontinuity increases. The h* is almost stable around the value of 75, whilst the chroma is more fluctuating. The 20% tin sample ΔE are smaller then the 3% and 7 % tin samples ΔE, which indicate a greater stability of the colour patina.

	L*	**a***	**b***	**C***	**h°**	**ΔE**
0h	81.76	2.99	11.94	12.31	75.96	**4.99**
2h	78.71	4.35	15.65	16.25	74.46	**3.78**
4h	81.17	3.21	13	13.39	76.11	**7.56**
24h	74.09	4.42	15.38	16.01	73.97	**2.63**
48h	76.36	3.74	14.23	14.71	75.27	**3.05**
96h	75.45	4.64	17.4	18.01	75.08	**7.36**
240h	68.48	4.1	15.09	15.63	74.81	

Tab. 4.4: CIEL* a* b* parameters and ΔE values for 20% tin samples exposed to acid rain vapour.

Comparing the ΔE values evolution, the 3% and 7% tin samples show a non linear corrosion process. The 3% turns out to have a stable patina between the 2nd-24th hour, whilst in the same time frame the 7% tin sample is more damaged. Afterwards the situation is the opposite, even if the difference between the two alloys color behaviour is less marked. The 20% tin sample is the less changed as also the ΔE between the color of the natural alloy and the color at the end of the test highlights.

4.2.4 SEM-EDS and X-ray diffraction spectroscopy

Figure 4.18 shows the SEM images taken for the 3%, 7% and 20% tin sample after 240 hours of chamber exposure to acid rain vapour.

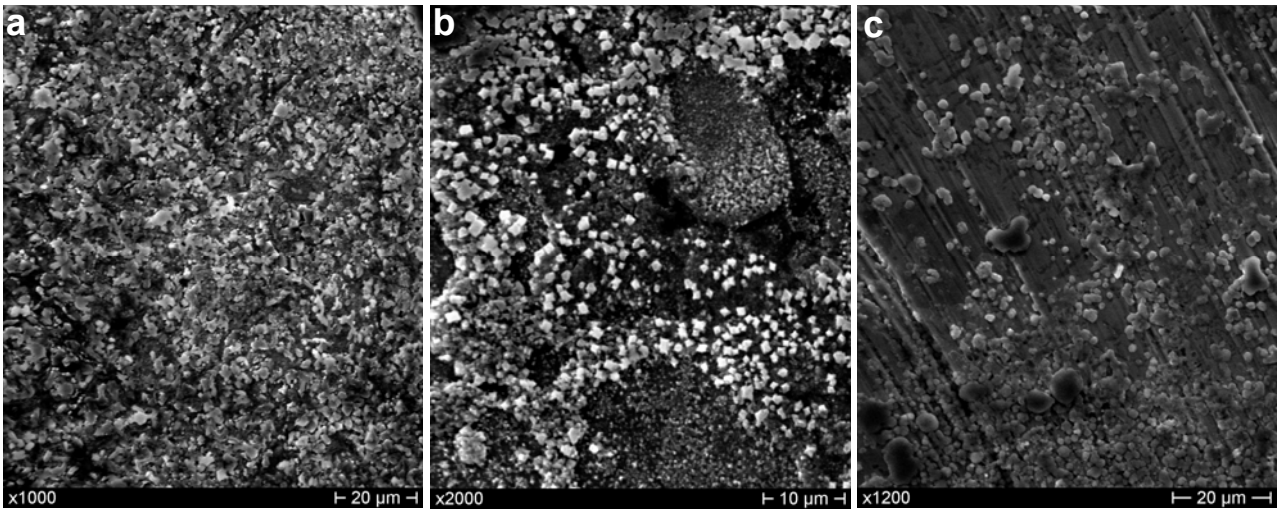

Fig. 4.18: SEM secondary electrons images of a) 3%, b) 7% and c) 20% tin samples after 240 hours of exposure to acid rain vapour.

The 20% tin samples surface is less covered by corrosion products as image "c" of the Figure 4.18 shows. Also the morphologies are different: on the 3% tin sample the crystals shape is less defined than in the 7% tin samples patina where some almost perfectly cubic crystals are detected. The slight patina formed on the 20% tin sample is more "granular".

The elementary patina composition in specific points of the surface was characterized with the use of the EDS.

In the following figures (4.19, 4.20 and 4.21) the SEM images are reported together with and the corresponding chemical analysis for the three samples (tables: 4.5, 4.6, 4.7, 4.8, 4.9, 4.10 and 4.11). They demonstrate the different corrosion product morphologies, the different distribution of the corrosion products and the overall different corrosion of the three alloys

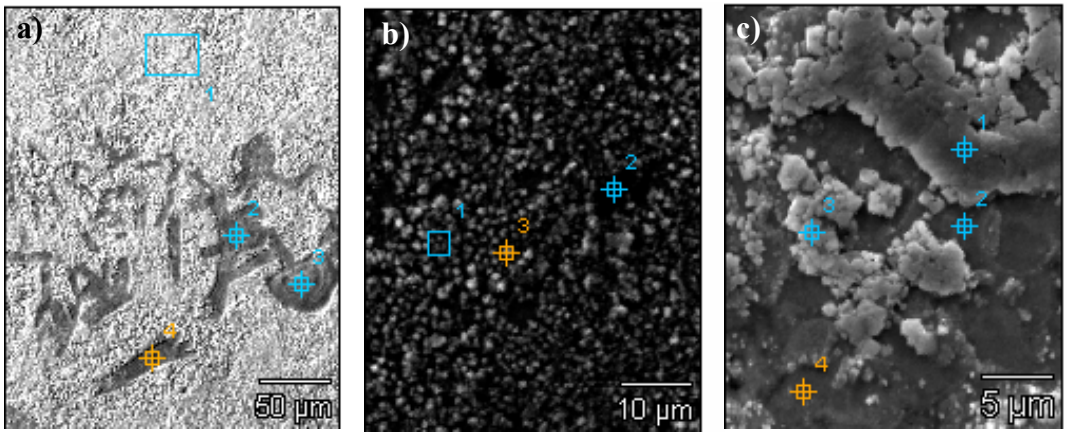

Fig. 4.19: SEM secondary electrons images of 3% tin sample at a) x400, b) x2000 and c) x4000 exposed to acid rain vapour in the chamber for 240 hours.

The points highlighted on the images have been analysed with EDS. The elementary composition (in weight %)of the points in figure 4.19 "a" are reported in Table 4.5.

	Cu	Sn	S	Ni	Zn
3%240h pt1	96.61	3.05	0.34		
3%240h pt2	88.03	0.67	7.38	1.48	2.43
3%240h pt3	87.62	4.99	5.77	1.62	
3%240h pt4	77.51	0.00	14.08	3.27	5.13

Tab.4.5: Elementary composition in weight % of the points indicated on image "a" of figure 4.19.

As can be understood from the table above, the darker part in image "a" is composed of sulfur, copper and tin. Tin decreases when sulphur increases. We can therefore assume that sulphur is combined with copper. The crystal composition of the 3% tin sample (Figure 4-19 b) is shown in Table 4.6.

	Cu	S
3%240h pt1	100.00	
3%240h pt2	98.36	1.64
3%240h pt3	98.22	1.78

Tab.4.6: Elementary composition in weight % of the points indicated on image "b" of figure 4.19.

Table 4.6 indicates the presence sulphur in the patina, but the main corrosion product is probably a copper oxide that can be detected by EDS. Oxygen cannot be quantify with EDS used in that research. Table 4.7 refers to Image "c" of Figure 4.19. The high magnification allows seeing the inner layer of the patina where low concentration of sulphur is always detected. In this case the high concentration of copper and low concentration of tin can be attributed to copper oxide presence.

	Cu	Sn	S
3%240h pt1	98.96	0.81	0.23
3%240h pt2	98.67	1.24	0.09
3%240h pt3	99.89	0.00	0.11
3%240h pt4	95.40	4.35	0.24

Tab.4.7: Elementary composition in weight % of the points indicated on image "c" of figure 4.14.

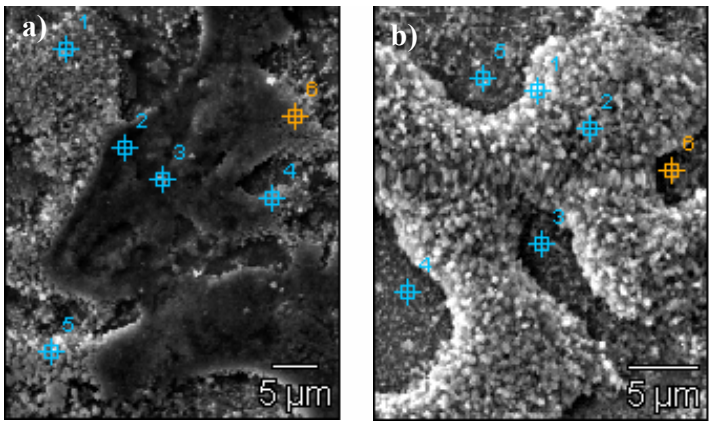

Fig. 4.20: SEM secondary electrons images of 7% tin sample at a) x2500 and b) x4000 exposed to the acid rain vapour in the chamber for 240 hours.

The sulphur is not detected on the 7% tin sample surface (image "a" of figure 4.20 Table 4.8), while it was detected in the case of the 3% tin sample. Table 4.8 reports the weight percentage of copper and tin measured with EDS.

	Cu	Sn
7%240h(3)_pt1	96.72	3.28
7%240h(3)_pt2	96.76	3.24
7%240h(3)_pt3	93.84	6.16
7%240h(3)_pt4	93.59	6.41
7%240h(3)_pt5	96.13	3.87
7%240h(3)_pt6	95.83	4.17

Tab.4.8: Elementary composition in weight % of the points indicated on image "a" of figure 4.20.

At higher magnifications, traces of sulphur are detected. Also in this case the main corrosion products are oxides of alloy components. Table 4.9 reports the weight percentage composition of the points analyzed.

	Cu	Sn	S
7%240h(3)_pt1	83.04	9.12	0.48
7%240h(3)_pt2	99.49	0.16	0.35
7%240h(3)_pt3	90.85	8.41	0.74
7%240h(3)_pt4	86.84	12.29	0.87
7%240h(3)_pt5	90.12	9.31	0.57
7%240h(3)_pt6	95.35	4.54	0.11

Tab.4.9: Elementary composition in weight % of the points indicated on image "b" of figure 4.20.

Figure 4.21 shows the images of the 20% tin sample exposed for 240 hours in acid rain vapour.

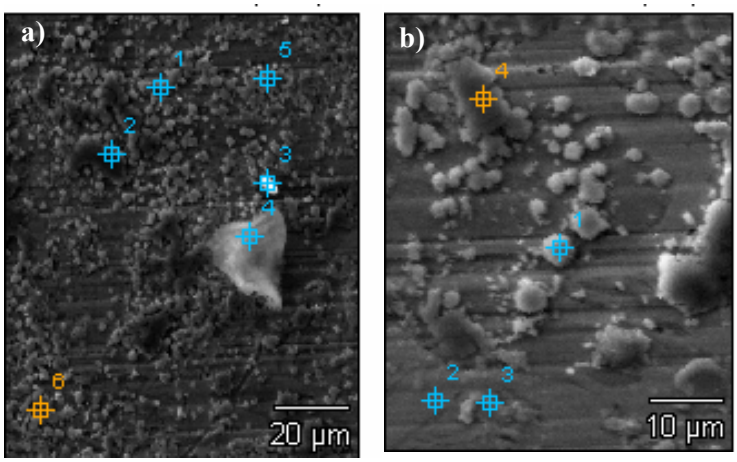

Fig. 4.21: SEM secondary electrons images of 20% of tin sample at a) x1000 and b) x2000 exposed to the acid rain vapour in the chamber for 240 hours.

Table 4.10 shows the weight percentage of the elements detected in the points indicated in the image "a" of figure 4.21.

The interesting new evidence is the presence of some chloride on three of the six points analyzed. Chloride was not detected on other alloys exposed to the same environment and conditions. Also sulphur content is quite high and increases when the weight percentage of tin decreases.

	Cu	Sn	S	Cl
20%240h_pt1	74.35	21.38	4.28	
20%240h_pt2	77.74	12.62	9.64	
20%240h_pt3	69.41	20.07	0.72	2.39
20%240h_pt4	65.10	31.35	1.25	2.30
20%240h_pt5	87.70	6.90	4.42	0.98
20%240h_pt6	69.62	23.86	6.51	

Tab. 4.10: Elementary composition in weight % of the points indicated on image "a" of figure 4.21.

At higher magnifications no chloride crystals were found. Only some sulphur was detected, as Table 4.11 shows.

	Cu	Sn	S
20%240h_pt1	79.91	11.71	8.38
20%240h_pt2	66.40	33.60	
20%240h_pt3	71.93	27.19	0.88
20%240h_pt4	83.11	9.72	7.17

Tab. 4.11: Elementary composition in weight % of the points indicated on image "b" of figure 4.21.

In order to support the qualitative analysis of EDS and to identify the composition of the corrosion products XRD analysis was performed on the samples after the 240th hour of exposure.

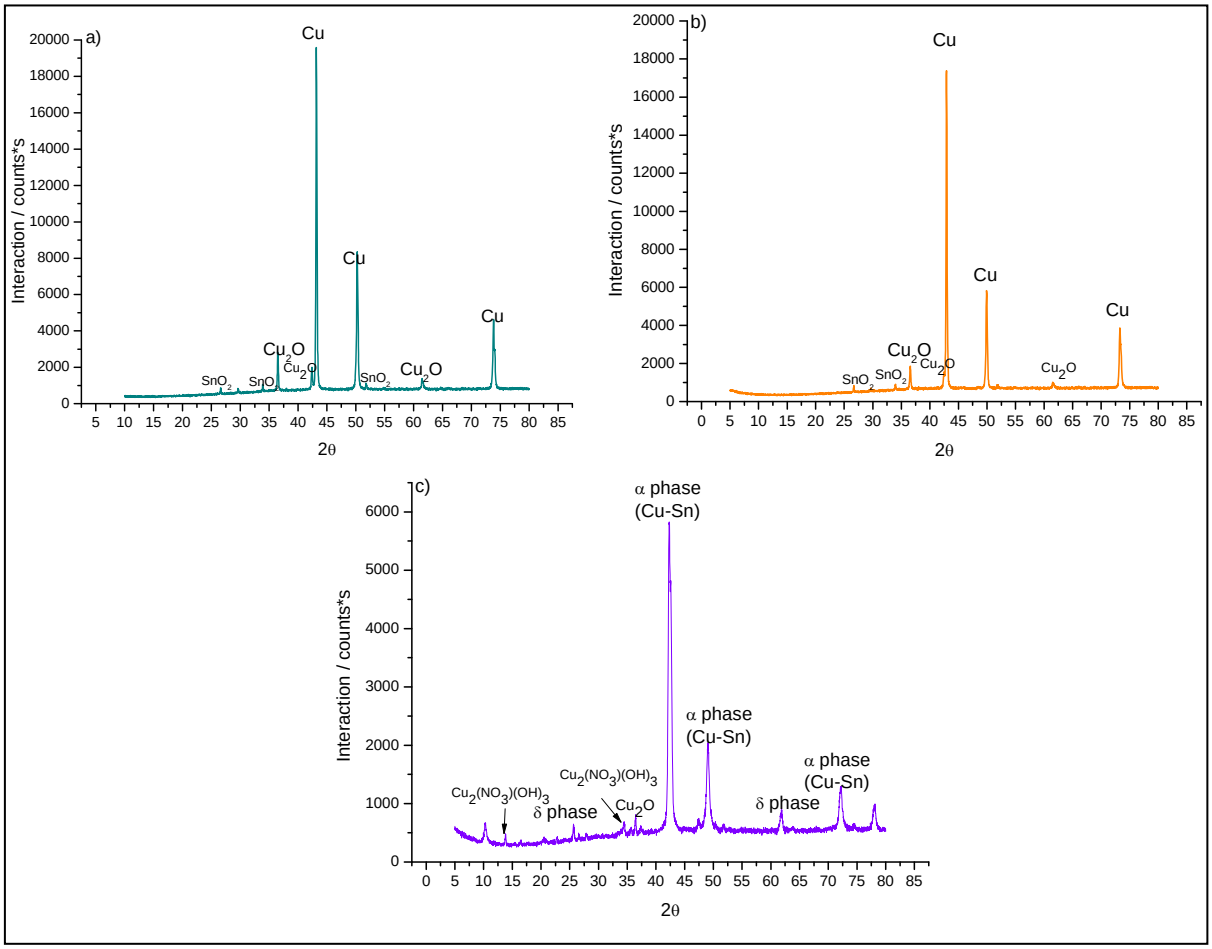

Fig. 4.22: XRD diffractograms of the samples with 3% (a), 7% (b) and 20% (c) of tin exposed for 240 hours to acid rain vapour.

XRD detected cuprite (Cu_2O) and cassiterite (SnO_2) presence on the 3% and 7% tin samples. In neither the 3% and 7% diffractrograms sulfur compounds appeared. It was detected with EDS in both 3% and 7% tin samples. The EDS detected low content of sulphur that was under the limit of XRD

detection. This data indicates that some sulphur compound is in its first phase of formation on 3% and 7% tin samples. On the 20% tin sample, cuprite (Cu_2O) is present along with some gherardite crystal ($Cu_2(NO_3)(OH)_3$.

4.3 Conclusions

The results obtained with immersion tests (paragraph 4.1) and with spray tests (paragraph 4.2) proved a more progressive corrosion process of the first test and a complexity and inhomogeneity of the patina of the second one. Also in this case the three alloys showed different corrosion behaviors.
The results of the immersion and spray tests will be compared both singularly and crossed.
The laboratory tests (immersion test or spray test) and the *in field* exposition results (carried out in Ghent and in Rome) will be also compared to associate laboratory tests to the corresponding urban environments.

4.3.1 Laboratory urban environments results: a comparison

4.3.1.1 Immersion tests

The open circuit potential measurements on the samples immersed in a synthetic solution of acid rain show how the patina stability improves from the 3% tin content to 20% and 7% tin content. This last alloy seems to have the best corrosion behavior of all. Immersed in sulfuric acid the 3% and 20% tin samples show a similar patina growth. The most protective layer turns out to form on the 7% tin sample. The open circuit potential evolution of the 3% and 7% tin samples immersed in nitric acid seems similar. A slightly more stable patina is revealed on the 3% tin sample (Figure 4.23).
The electrochemical impedance spectroscopy, coherently with the OCP measurements, detects a protective patina on the 7% tin sample immersed in acid rain. EIS shows a thick layer often dissolved on the 3% tin sample immersed in acid rain. Corrosion is less aggressive on the 20% tin sample, but the patina formed is less passive than the 7% tin sample patina.
A similar interpretation can be applied in the case of sulphuric acid immersion. The 3% tin sample is more damaged, followed by the 20% and the 7% tin samples. Each of these last two samples reveal different but “good” corrosion behaviors.
On the other hand, when immersed in nitric acid, the 7% tin sample’s patina turns out to be less stable: it is frequently partially dissolved. In the case of the 3% tin sample, more damage occurs but a more stable patina is produced compared to the case of the 7% tin sample. This result is in accordance with the OCP measurements above mentioned (Figure4.23).

The colorimetric measurements show that each alloy immersed in acid rain undergoes a relevant color change. The scale of damage is 7%, 3% and 20% tin content. The first two alloys produce a layer that changes the color of natural alloys, more than the patina formed on the 20% tin sample which is the less attacked.

The 3% tin sample immersed in sulfuric acid shows a bigger difference in terms of patina color. The fact that the patina is less stable, as we understood before, doesn't mean that it is not present on the surface. The 7% tin sample changes less its surface color, followed by the 20% tin sample.

The 3% tin sample immersed in nitric acid (as we saw with OCP and EIS) produces a layer that corresponds to a bigger ΔE compared to the 7% ΔE (Figure 4.23).

Figure 4.23. graphically illustrates the comparisons.

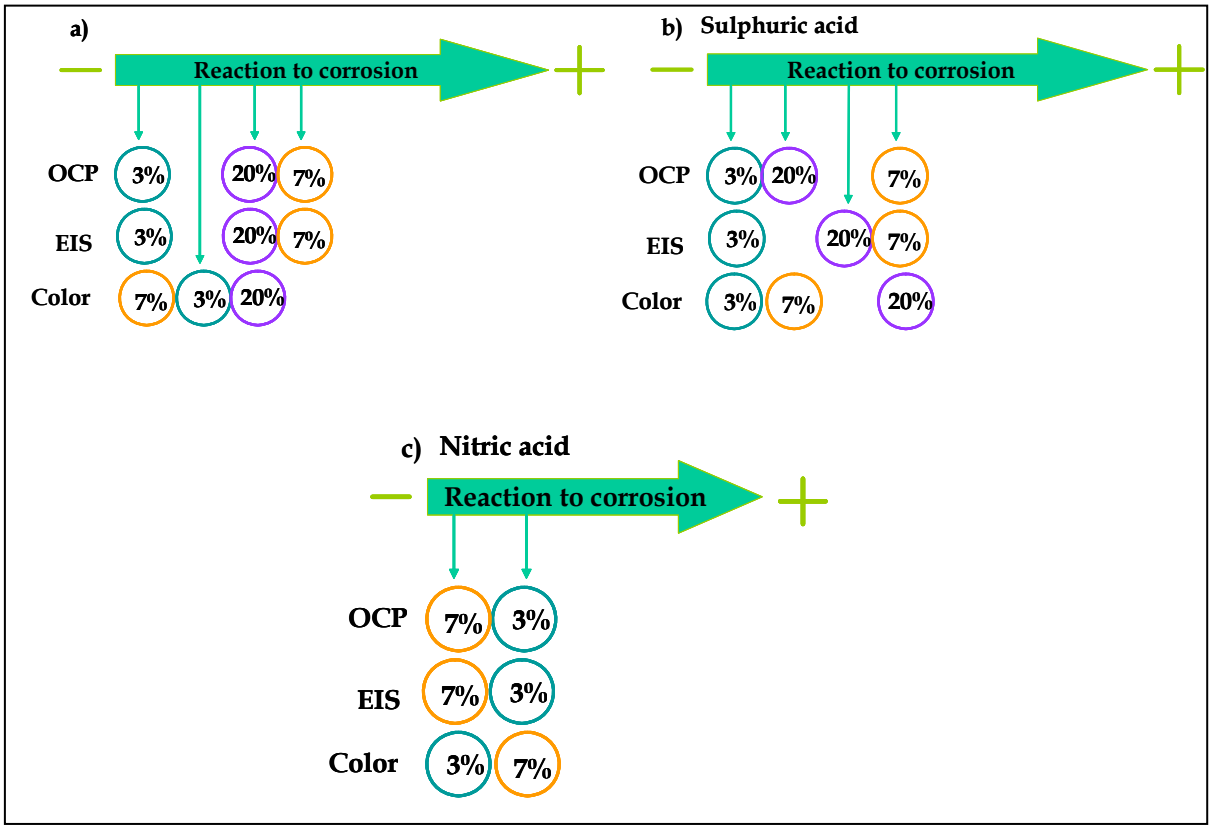

Fig. 4.23: The "Damage scale" for the three alloys immersed for 5 weeks in a) acid rain, b) sulphuric acid and c) nitric acid.

Considering the color difference, we can assume that the more aggressive solution for the 3% tin alloy turns out to be the nitric acid, followed by sulphuric acid and acid rain. In the case of the 7% tin sample the most aggressive solution is the sulphuric acid, followed by acid rain and nitric acid. The 20% tin sample undergoes more damage caused from acid rain exposure.

4.3.1.2 Spray test

In the chamber where acid rain was sprayed, the corrosion behavior of the alloys was different.

With OCP measurements we found that the more instable patina grows on the 7% and 20% tin samples. This results were confirmed by electrochemical impedance spectroscopy. The EIS confirmed that on the 7 % tin sample the patina is instable and frequently dissolved. Also the 3% tin sample patina is partially dissolved during the exposure but the effects are less relevant. The 20% tin sample has an intermediate behavior (between the 7% and the 3% tin samples), due to its least reaction with the environment. However the patina is less protective than the 3% tin sample patina.

Color measurement support this electrochemical data interpretation: the 3% tin sample shows more color changes due to more developed patina (compared to the 7% and 20% tin sample patinas).

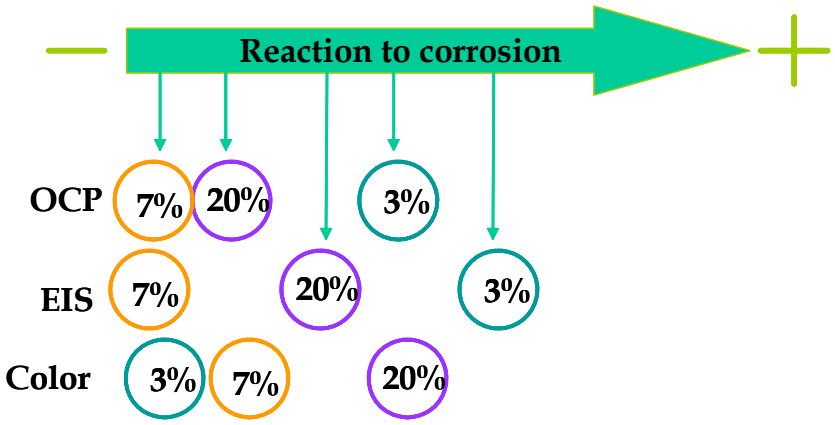

Fig. 4.24: The "Damage scale" for the three alloys sprayed with acid rain for 240 hours.

Analyzing the graph in Figure 4.25, it is clear that the patinas formed on the three samples are less stable during the test, also compared to the patina formed in the immersion test. The color difference variation is due to the patina growth and/or dissolution but also to the inhomogenity of the layers.

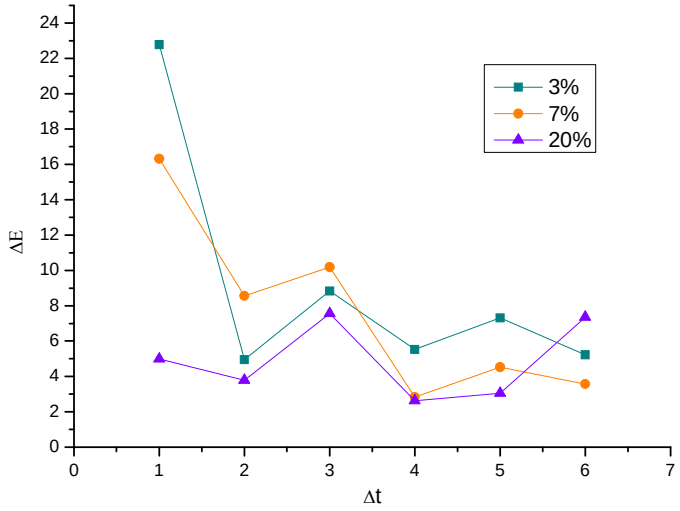

Fig. 4.25: Color differences during exposure of the three alloys to acid rain vapor.

4.3.1.3 Immersion test vs spray test

A comparison can be done between the immersion tests in acid rain and the spray tests considering that the immersion test took 5 weeks whilst spray test almost 2. However the biggest color changes occurring at the beginning of exposure time (as shown in the previous paragraphs) and the spray test is stronger than the immersion.

In the immersion test the 3% tin sample shows a more instable patina, whilst in the 7% tin sample features a thick stable layer showing up. The opposite happens during the spray test: the 7% tin sample shows a more instable patina, whilst in the 3% tin sample features a thick stable layer showing up.

.

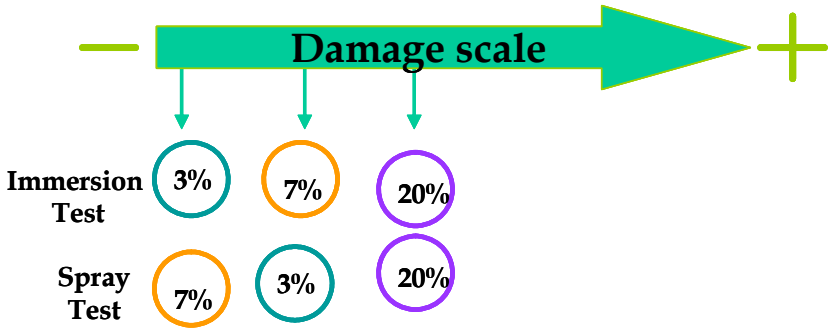

Fig. 4.26: The "Damage scale" for the three alloys immersed and sprayed with synthetic acid rain.

Table 4.12 shows the ΔE of the alloys immersed and sprayed with acid rain. As already clarified, to better barrier properties of the patina can correspond smaller color changes: in the immersion test the more color damaged is the 7% tin sample, followed by the 3% and 20% tin samples. In the spray test the bigger color change is undergone by the 3% tin sample.

	Immersion Test	**Spray test**
3%	33.78	39.80
7%	35.28	34.96
20%	30.31	13.69

Tab. 4.12: Color difference between the clean alloy and after 5 week in acid rain and after 240 hours in acid rain vapor

The spray test took 240 hours but the color difference values are similar to the ΔE resulting from the immersion test. A lower color difference is detected on the samples exposed to immersion test, but the minor exposure time must be considered. The shorter wet and dry cycles are more aggressive than the longer wet and dry cycles.

4.3.2 Natural urban environments vs laboratory urban environments

The natural environment analysis results (Chapter 3) have been compared with the analysis results of the laboratory tests in order to find a the correspondence of tin influence on bronze corrosion behavior between in field exposure and laboratory tests.

As saw for the 3% tin sample patina is particularly instable when facing high concentrations of water (as in Ghent and in immersion tests) that leaches the layer, whilst the 7% tin sample is more damaged from major pollutant provision in wet and dry cycles (as in Rome and in spray tests).

Table 4.13 shows the sequences of the three alloys (from the more damaged to the less damaged) for each technique and environment.

Urban				
	Natural		**Laboratory**	
Techiques	**Rome**	**Gent**	**Immersion**	**Spray**
OCP	/	3%-20%~7%	3%-20%~7%	7%~20%-3%
EIS	/	3%-20%~7%	3%-20%~7%	7%-20%-3%
Color	3%-7%-20%	3%-7%-20%	7%~3%-20%	3%-7%-20%

Tab. 4.13: Comparison of alloys damage scale for each technique in natural and laboratory environments.

The Ghent results are comparable with the laboratory immersion test. The alloys damage scale is similar in almost all analysis. A little difference can be observed in color measurements between "Ghent" and "Immersion" results. However, the figures divided by the symbol "~" means that there is small difference in terms of damage between the alloys. Therefore results are comparable also for the color and diffractograms.

The Rome's environment can be correlated to the laboratory spray test, the instability of the patina detected with the EIS for the laboratory test is comparable with the instability revealed analyzing the color changes during the exposure in Rome as well as the ΔE damage scale. This underlines that Rome's environment is characterized by more repeated wet and dry cycles. On the other hand, the corrosion in Ghent is dominated by long wet period and can therefore be appropriately correlated to the immersion test.

References

[48] G.P. Cicileo, M-A Crespo, B.M. Rosales, *"Comparative study of patina formed on statuary alloys by means of electrochemical and surface analysis techniques"*, Corrosion Science 46 (2004) 929-953;

[49] J.Sandberg, I.O. Wallinder, C. Leygraf, N. Le Bozac, "Corrosion-induced copper runoff from naturally and pre-patinated copper in a marine environment"; Corrosion Science 48 (2006) 4316-4338;

[50] J.H. Payer, G. Ball, B.I. Rickett, H.S. Kim, "Role of transport properties in corrosion products growth", Material science & engineering A198 (1995) 91-102;

[51] W.A. Badway, R.M. El-Sherif, H. Shehata, *"Electrochemical behavior of aluminium bronze in sulfate-chloride media"*, Journal of Applied Electrochemistry (2007) 37:1099-1106;

[52] C. Chiavari, A. Colledan, A. Frignani, G. Brunoro, *"Corrosion evaluation of traditional and new bronzes for artistic castings"*, Materials Chemistry and Physics 95 (2006) 252-259;

5. Corrosion in a marine environment

As already mentioned in Chapter 3 the in field exposure of the samples was conducted in order to find a connection between atmospheric parameters and corrosion rate of bronze alloys and in order to understand the corrosion process in marine environment (in this case). On the other hand, the laboratory test was carried out to investigate the effects of single or combined weather parameters.

5.1 Marine environment effects on bronze corrosion: field exposure

The three alloys tested (3%, 7%, 20% tin samples) were exposed to a marine environment in Fiumicino City (Rome, Italy) from January to May 2011. The samples were positioned following the ISO 9223 standard [1].

The samples were analyzed monthly with spectrocolorimetry (measuring geometrics d/8° and standard observers 2° & 10°), and after a month with SEM-EDS (LaB_6 electron source, 40 kV, 40 mA and 10^{-7} mbar).

▪ 5.1.1 Spectrocolorimetry

Colorimetric measurements were carried out once a month during a four months period. Figure 5.1 shows the reflectance curves of the 3% tin sample exposed to the natural marine environment.

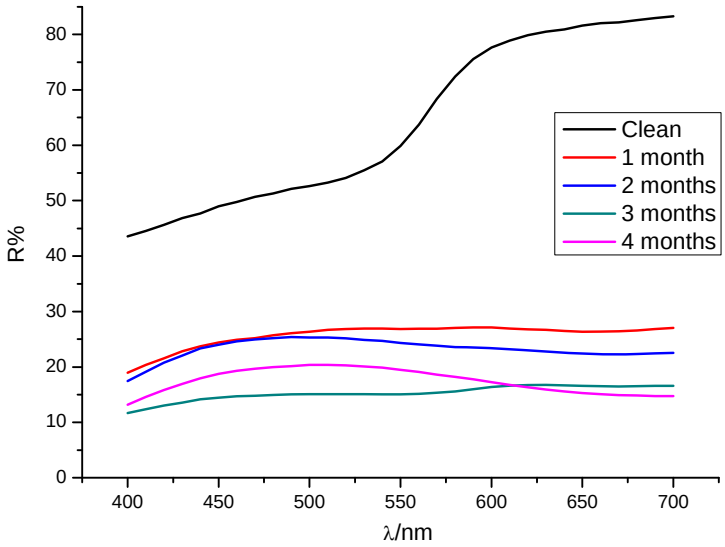

Fig. 5.1: Reflectance curves of 3% tin sample exposed to marine environment in Fiumicino from January to May 2011.

The reflectance decreases over time and this is due to the corrosion progress occurring during the four months of exposure. An inversion of the reflectance trend can be observed between the 3rd and 4th month, and this can be explained by the partial dissolution of the patina. The typical peak (450-475 nm) that appears since the first month of exposure disappears from the curve during the 3rd month, when a thin dark film covers the green products previously formed. In other words, the flattening of the curve explains the grey coloured surface.

The dissolution of the patina mentioned above occurred between the 3rd and 4th month, dissolving the dark layer and releasing again the green corrosion products. These corrosion products are detectable by the peak in the region of 450-475 nm.

Table 5.1 shows the colour parameters for the 3% tin sample.

	L^*	a^*	b^*	C^*	h
clean	83.63	10.35	14.17	17.55	53.87
1 month	58.59	-1.49	4.16	4.42	109.75
2 months	56.3	-3.1	0.95	3.24	162.99
3 months	46.2	1.13	2.69	2.92	67.14
4 months	50.58	-5.8	0.93	5.87	170.91

Tab 5.1: Cie $L^* a^* b^*$ parameters of the 3% tin samples exposed to marine environment in Fiumicino from January to May 2011.

The lightness decreases in the first month and continues dropping at a slower rate afterwards (towards 50.58). A lightness increase occurs only in the 3rd month, due to the partial dissolution of the patina mentioned above. The a^* values are positioned in the green section of the red-green axis. During the 4th month the green component reaches higher negative values (-5.8). This is also underlined by the difference in the hue values: starting from 53.87 (in the red area) to set at 170.91 (in the green area). In the beginning (1st month – 3rd month) the color saturation (C*) decreases and subsequently shows an increase in the last measurement. The a*, the hue and the C* indicate an enhancement of the green corrosion products.

Figure 5.2 illustrates the 7% tin sample reflectance curves.

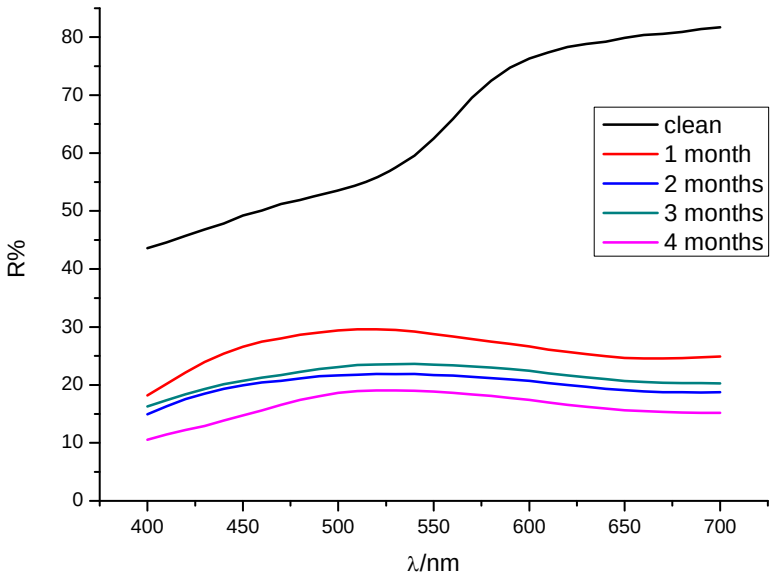

Fig. 5.2: Reflectance curves of 7% tin samples exposed to marine environment in Fiumicino from January to May 2011.

Here also the reflectance decreases with time. The greatest reflectance loss occurs during the first month. Afterwards the corrosion slows down, especially between the 2nd and 3rd month. The corrosion again grows faster between the 3rd and the 4th month, as the reflectance loss demonstrates. A partial dissolution of the patina occurs between the 2nd and 3rd month, as the higher reflectance values of the 3rd month reveal. Since the beginning of the test a peak appears in the region of 450-547 nm. This peak slightly weakens and moves towards higher wavelength values, to increase again afterwards (4th month). This reveals the formation of green products on the surface: products that are almost stable between the 2nd and 3rd month and continue growing during the 4th month. However, the peak for the 7% tin sample is higher than the 3% tin sample peak. Table 5.2 shows the colour parameters.

	L^*	a^*	b^*	C^*	h
clean	84.07	8.26	14.63	16.8	60.55
1 month	59.99	-5.24	3.01	6.05	150.09
2 months	53.23	-3.4	2.86	4.45	139.93
3 months	54.97	-3.59	4.13	5.47	131.02
4 months	49.62	-5.84	7.04	9.15	129.65

Tab 5.2: Cie $L^* a^* b^*$ parameters of the 7% tin samples exposed to marine environment in Fiumicino from January to May 2011.

As Table 5.2 shows, the lightness decreases following the reflectance tendency. The green component (a^*) increases non-linearly but reaches the negative value of -5.84. This value is comparable to the 3% green component value mentioned above. The b^* values move back and forth tending towards lower values. So does the chroma that moves towards the grey region. Also in this case the hue shows a

relevant increase of values, even if less accentuated than in the case of the 3% tin sample. The hue is closer to the green region (h=129) than in the case of the 3% tin sample (h=170, green-blue region). The 20% tin sample reflectance and colour behaviour are reported in Figure 5.3 and Table 5.3.

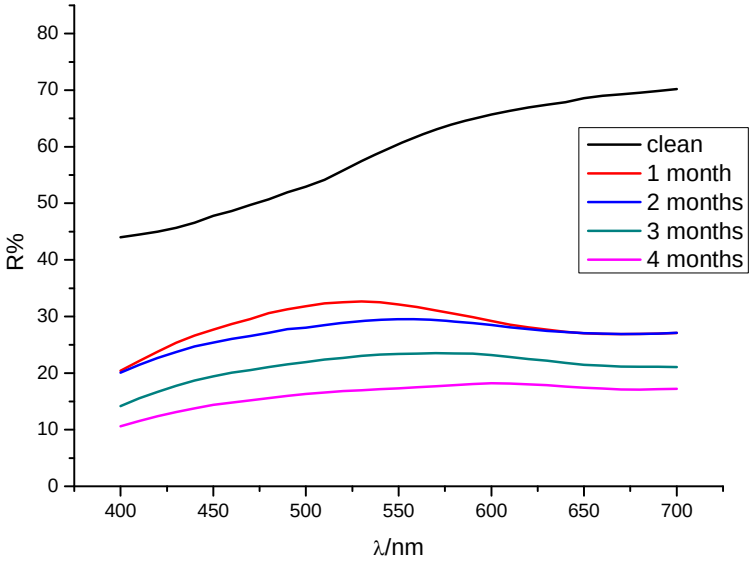

Fig. 5.3: Reflectance curves of 20% tin samples exposed to marine environment in Fiumicino from January to May 2011.

The reflectance loss is similar to the loss observed in the 3% and 7% tin alloys. Since the beginning of the test a peak in the 475-500 nm region is observed. The peak progressively decreases, indicating less green products formation. The flattening of the curve explains the grey coloured surface.

	L^*	a^*	b^*	C^*	h
clean	81.76	2.99	11.94	12.31	75.96
1 month	62.45	-6.01	4.94	7.78	140.58
2 months	60.47	-2.86	5.3	6.02	118.32
3 months	54.83	-2.42	6.47	6.91	110.54
4 months	48.48	-0.62	6.61	6.63	95.33

Tab 5.3: Cie $L^* a^* b^*$ parameters of the 20% tin samples exposed to marine environment in Fiumicino from January to May 2011.

The lightness decreases during the 1st month and stays stable during the 2nd month. Between month 1 and 2 the corrosion process is quite slow. This is due to the formation of a green products layer that protects the surface from the environment. The a* value decreases, due to green products coverage. The hue is lower than in the 3% and 7% tin samples and is located in the green-yellow part of the hue colour space.

The grey corrosion products were revealed in the 3% tin samples, during the 3rd month of exposure (in the case of the 20% tin sample the grey corrosion products appeared only during the 4th month). We therefore assumed that the 3% corrosion process was in a more advanced state compared to the 20% corrosion process. However, the grey corrosion products of the 3% tin samples were partially dissolved during the 4th month, allowing the green corrosion products formation. On the other hand, the grey products were not observed at all in the 7% tin samples.

Figure 5.4. shows the colour difference of the three alloys exposed to a marine environment for 4 months.

The ΔE value shows the corrosion dynamics: fast in the first month and slow afterwards. However, for every alloy and for different moments, the ΔE value increases again due to a restarting of the corrosion process. The addition of a new layer on the samples surface results in a new colour of the patina. The phenomenon can be explained with a partial dissolution of the patina (due to the leaching of the rain) and to the consequently less protected surface attacked by the environment.

Differently than in the case of urban environment exposure, the 3% and 7% tin sample exposed to marine environment show a similar corrosion behaviour, if compared to one another. Also the 20% tin sample turns out to be more damaged compared to its exposure to urban environment.

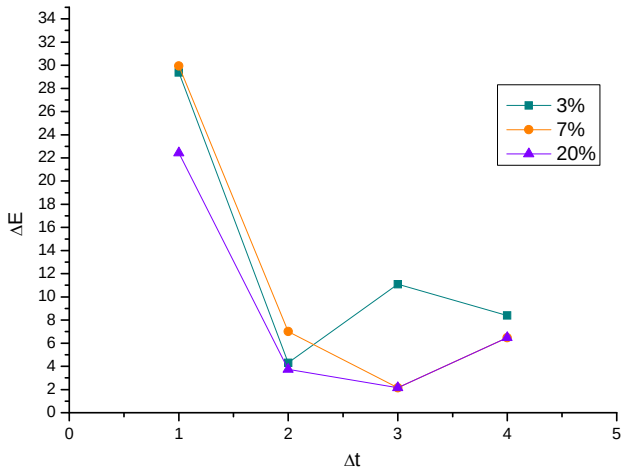

Months	3%	7%	20%
0-1	29.37	29.95	22.42
1-2	4.31	7.01	3.74
2-3	11.09	2.16	2.16
3-4	8.38	6.49	6.49

Fig. 5.4: Colour difference graph and table of the three alloy exposed to marine environment in Fiumicino from January to June 2011.

5.1.2 SEM

As already pointed out, the corrosion due to exposure in a marine environment is very fast: a thick green patina is rapidly formed in the 1st month of exposure, as the optical microscopy images show (Figure 5.5).

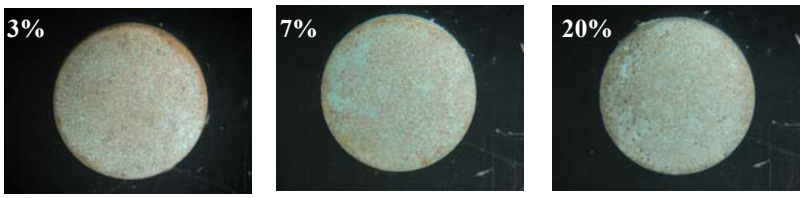

Fig. 5.5: Optical images of the 3%, 7% and 20% tin samples exposed to marine environment for 1 month in January 2011.

Figure 5.6 shows secondary electrons images of different magnification for 3% and 7% tin samples after 1 month of exposure. The patina on the samples is similar: powdery, thick and crystalline. At higher magnification the surface of the patina reveals multiple cracks and some sort of "scales".

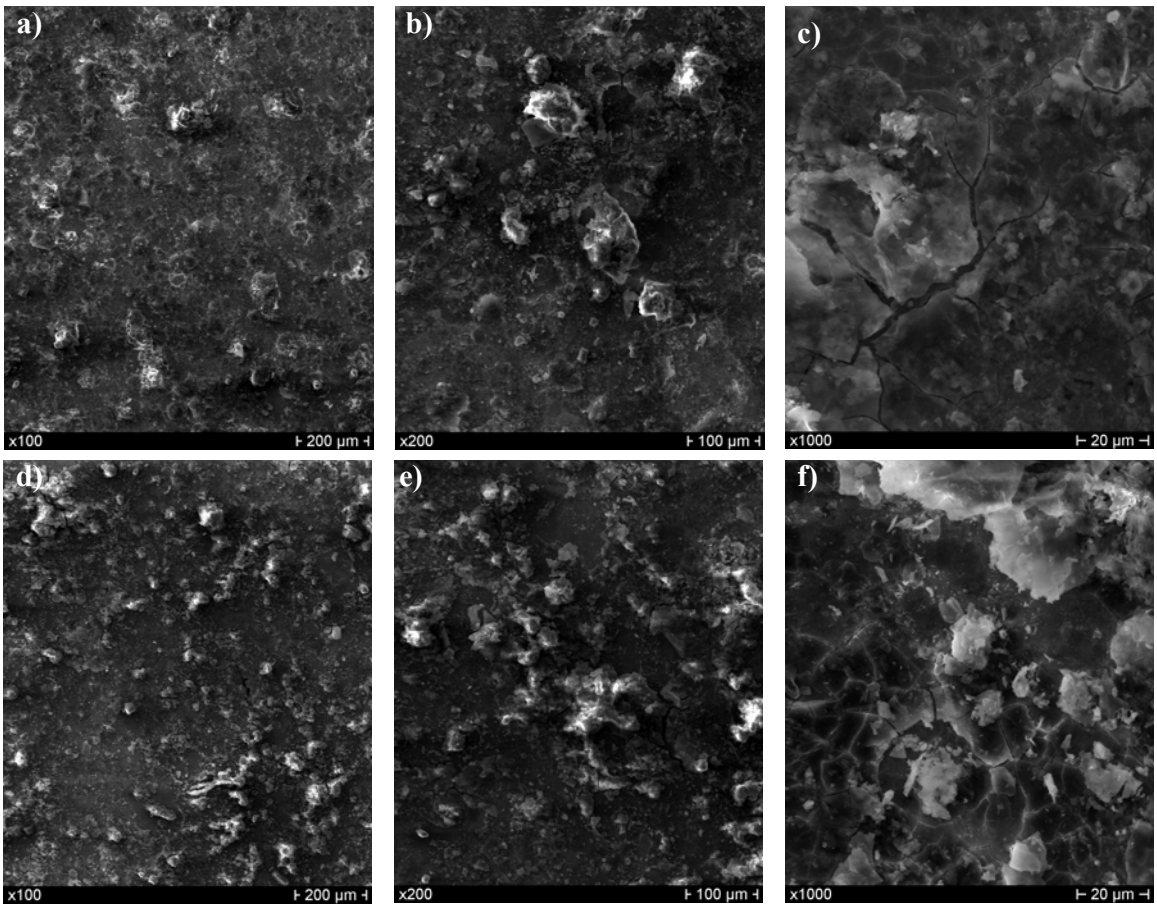

Fig. 5.6: SEM secondary electrons images at different magnification of the 3%tin sample: a) x 100, b) x200 and c) x 1000 and 7% tin sample: d)x 100, e) x 200 and f)x 1000 after 1 month of exposure to marine environment.

The “scales” are positioned on a layer composed of granular products, as can be observed at higher magnification (Figure 5.7).

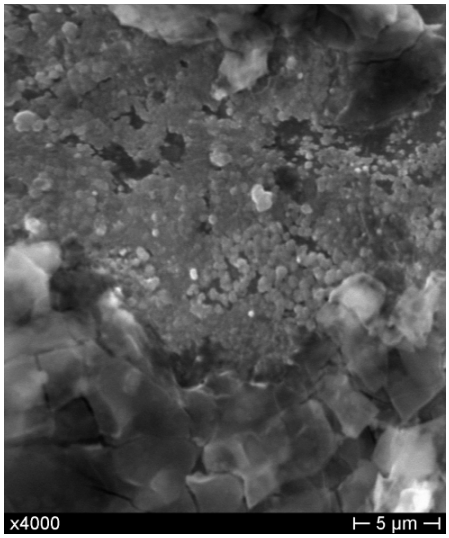

Fig. 5.7: SEM secondary electrons image (x4000) of the 7% tin sample after 1 month of exposure to marine environment.

5.2 Marine environment effects on bronze corrosion: laboratory tests

To simulate the marine environment the samples were vaporized with a synthetic solution of sea water [2]. Wet and dry cycles were performed six times per day, spraying 0.66 mL of vapor per cycle (following the exposure timing reported in Chapter 2 (paragraph 2.2.2.2).
Temperature was kept at 25 °C, whilst the relative humidity changes are reported in Figure 2.11 of Chapter 2.
The corrosion evolution was monitored with spectrocolorimetry (measuring geometrics d/8° and standard observers 2° & 10°), SEM-EDS (LaB_6 electron source, 40 kV, 40 mA and 10^{-7} mbar) and XRD (40 kV, 40 mA, scanning 2θ from 10° to 80° grade, step width of 0.02° and counting time of 5 seconds per step).

5.2.1 Spectrocolorimetry

In laboratory tests, the color evolution of the three alloys was examined. The samples were exposed to sea water vapour for the duration of 2, 4, 24, 48, 96 and 240 hours. Figure 5.8 shows the reflectance curves.

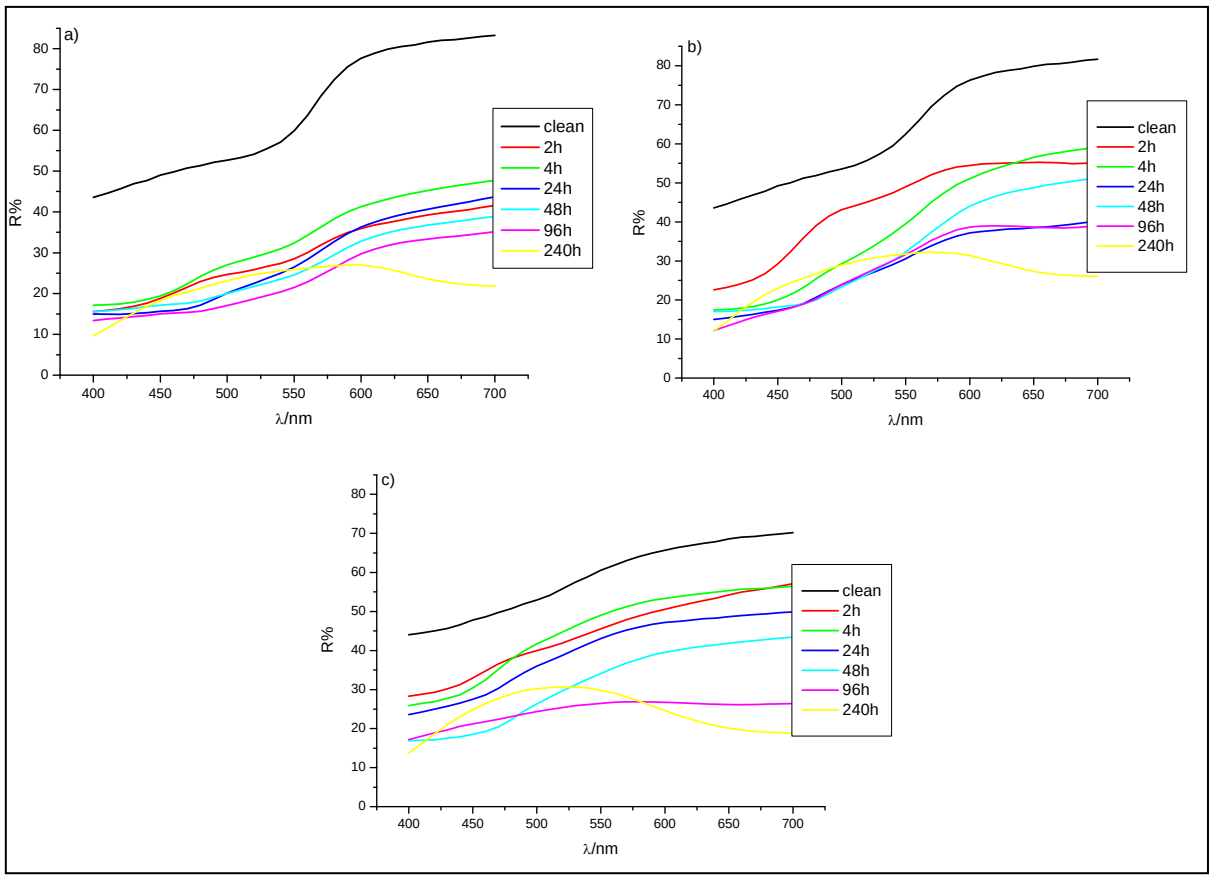

Fig. 5.8: Reflectance measurements on samples sprayed with a synthetic solution of sea water for 2 hours, 4 hours, 24 hours, 48 hours, 96 hours, 240 hours. (a) 3%, (b) 7% and (c) 20% of tin samples

The reflectance decreases similarly to the case of reflectance in the natural marine environment tests. An increase on the reflectance is observed during the 4th hour. Afterwards the value drops continuously. The biggest reflectance loss occurs in the 1st hour, due to the fast corrosion which produces a layer that continues growing and that influences progressively less the reflectance properties. During the 2nd and 4th hour the curves indicate two peaks in the region of 475-500 nm and 575-600 nm. These λ are respectively to the blue and green-yellow regions of the visible spectra. The peaks decrease as time goes by. The 96th hour curve flattens due to the grey coloured products on the surface. These grey products subsequently disappear during the last hours. In the 240th hour curve a relevant peak is observed in the 450-600 nm region. A more complex patina with a large absorption region of visible colour spectrum forms.

During the 2nd hour of exposure of the 7% tin sample the two peaks appear in the curve. In the following hours the blue component disappears and the green peak decreases. During the 24th hour of exposure a large peak appears in the 425-600 nm region. This peak turns out to be higher than the 3% tin sample peak exposed to the same environment. The corrosion products are similar but demonstrate stronger absorption qualities.

During the 2nd hour of exposure of the 20% tin sample a slight curve peak is observed in the 475 nm region. Between the 4th and the 48th hour of exposure, the curve features a relevant peak on the 475-

600 nm region. During the last hours of exposure this peak moves towards the 425-575 nm region. On the 20% tin alloy the patina colour composition and its evolution differs from the other alloys (3% and 7% tin samples), nevertheless the final results are the same in all three cases.

	L^*	a^*	b^*	C^*	h°
0h	83.63	10.35	14.17	17.55	53.87
2h	61.33	5.7	17.55	18.45	72.01
4h	64.52	6.41	21.19	22.14	73.16
24h	59.58	10.06	21.81	24.01	65.23
48h	57.86	9.04	15.99	18.37	60.53
96h	54.84	10.08	15.77	18.71	57.42
240h	57.16	-2.74	12.93	13.22	101.95

Tab. 5.4: Cie $L^* a^* b^*$ parameters for the 3% tin samples exposed to sea water vapour for 2 hours, 4 hours, 24 hours, 48 hours, 96 hours and 240 hours.

Table 5.4 shows the colour parameters of the 3% tin samples. Here the lightness decreases slightly towards 57.16. The increase of the value during the 240th hour (from 54.84 of the 96th hour of exposure) means that the corrosion process is in act and it produces a new layer with different colour characteristics. This can be understood from the reflectance curves and from the a^* value behaviour (a* shifts to negative values only in the last measurement). The b^* value doesn't undergo strong changes: it increases during the 4th and 24th hour of exposure and then comes back to the initial value. The same happens for the chroma: during the 4th and 24th hour of exposure the patina is characterized by an important contribution of products with yellow component. This component disappears afterwards, covered by other products. The hue undergoes a great evolution moving towards the green part of the colour space.

Table 5.5 shows the colour values of the 7% tin patina.

	L^*	a^*	b^*	C^*	h°
0h	84.07	8.26	14.63	16.8	60.55
2h	75.11	-0.1	22	22	90.27
4h	69.5	8.48	28.34	29.58	73.34
24h	62.08	4.87	21.72	22.26	77.37
48h	64.41	10.99	24.44	26.8	65.8
96h	62.81	4.71	23.94	24.4	78.87
240h	62.07	-4.68	12.41	13.26	110.67

Tab. 5.5: Cie $L^* a^* b^*$ parameters for the 7% tin samples exposed to sea water vapour for 2 hours, 4 hours, 24 hours, 48 hours, 96 hours and 240 hours.

The lightness parameter decrease is related to the corrosion evolution. The process, that slows down due to the creation of a patina, increases again in the 48th hour of exposure, causing a partial dissolution of the layer. Afterwards the patina grows continuously. The a^* values go back and forth to finally reach high negative values (which demonstrate an intense green products presence) during the last hours of exposure. The b^* is almost stable from 2nd to 96th hour of exposure, with high values (in the yellow region of the axis). The patina colour is therefore due to the a^* values. In the beginning of the tests the chroma contributes to the saturation of the colour but decreases. Also in this case, during the 240th hour, the hue moves towards the green region. This means that the patina grows discontinuously with different elements contribution that changes the colour of the surface. The evolution towards a green coloured patina occurs mainly during in the last measurements.

Table 5.6 shows colour parameters of the 20% tin sample. Also in this case the non-linear decrease of a^* and b^* values implies a patina formation characterized by the contribution of different layers each of which typical of a specific phase of the corrosion process. In the last measurement of the 20% tin sample, the a^* reaches lower values compared to the other alloys: the green component reaches 10.97. Differently from a^* and b^* values, the lightness decreases continuously suggesting that the corrosion process is active. The initial and the final value of the chroma is almost identical, but changes during the different phases of the test. The hue reflects the a^* values dynamic and reaches the green area in the colour space graph.

	L^*	**a^***	**b^***	**C^***	**h°**
0h	81.76	2.99	11.94	12.31	75.96
2h	73.13	2.56	14.67	14.89	80.08
4h	74.76	0.53	20.11	20.12	88.48
24h	70.86	1.48	18.37	18.43	85.4
48h	64.46	3.59	23.03	23.31	81.15
96h	57.87	-1.39	8.01	8.13	99.86
240h	59.87	-10.74	5.39	12.02	153.34

Tab. 5.6: Cie $L^* a^* b^*$ parameters for the 20% tin samples exposed to sea water vapour for 2 hours, 4 hours, 24 hours, 48 hours, 96 hours and 240 hours.

Figure 5.9 represents the colour difference of the alloys.

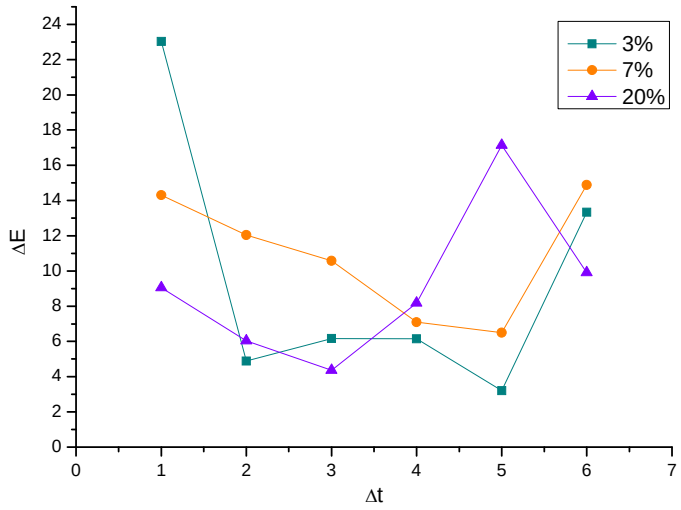

Hours	3%	7%	20%
0-2	23.02	14.30	9.06
2-4	4.89	12.05	6.03
4-24	6.17	10.58	4.37
24-48	6.15	7.09	8.19
48-96	3.20	6.50	17.14
96-240	13.34	14.89	9.91

Fig. 5.9: Colour difference graph and table of the three alloys exposed to sea water vapour for 2 hours, 4 hours, 24 hours, 48 hours, 96 hours and 240 hours.

The graph and the table show that the major changes in colour occur during the first hours of the tests. The most stable patina is formed on the 7% tin sample characterized by a slight evolution of the colour until the 240th hour of the exposure, when the patina shows a relevant change due to the re-activation of the corrosion process. This new corrosion activation generates new products on the surface. The 3% tin sample appears to be more damaged in the initial phases of the corrosion process if compared to the other alloys. However the patina stays stable until the 96th hour of exposure. Afterwards a new layer is formed. Also in the case of the 20% tin sample, an enhancement of the corrosion process occurs in the last hours of exposure. Differently from the case of urban environment tests, the less damaged alloy turns out to be the 7% tin sample.

5.2.2 SEM-EDS and X-ray diffraction spectroscopy

Figure 5.19 shows secondary electrons images of the 3% tin sample exposed for 48 hours to sea water vapour. The surface appears to be covered by a powdery patina that features a nucleation area where the crystal grows. At higher magnification the crystals show their “cubic faces”. In both areas (the cubic crystals area and the flat surface on which they lie) EDS detects the presence of chloride combined with copper (as will be further explained later). Small concentrations of sulphur are detected in the less crystalline part (image “a”).

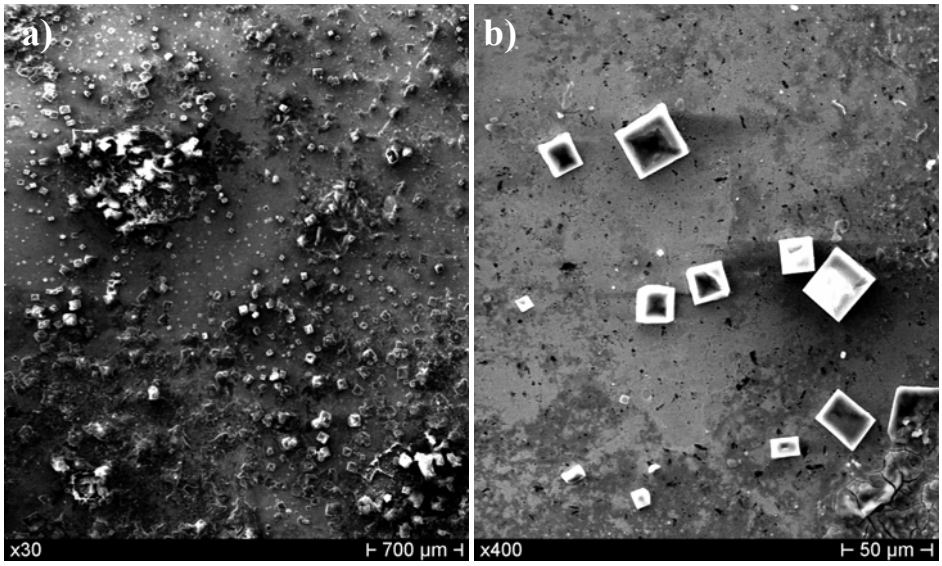

Fig 5.10: SEM secondary electrons images at a) x30 and b)x400 of 3% tin sample exposed to sea water vapor for 48 hours.

As time of exposure increases, the patina grows and gets thicker thanks to the generation of corrosion products with different morphologies, as shown in Figure 5.11.

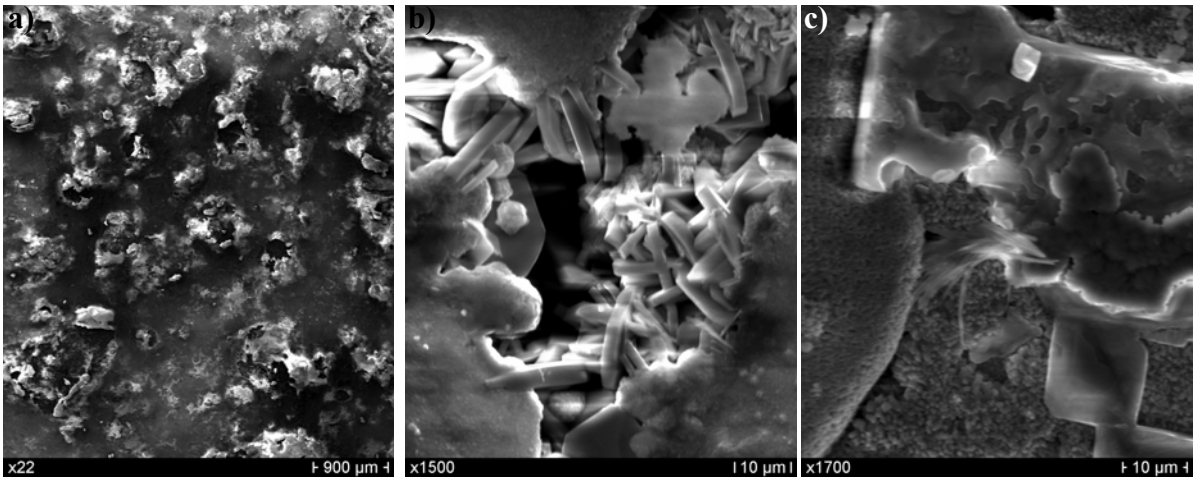

Fig 5.11: SEM secondary electrons images at a) x22, b)x1500 and c) x1700 of 3% tin sample exposed to sea water vapor for 48 hours.

EDS analysis of the surface (Figure 5.11 a) reveals the presence of chloride and copper (as also evident in Figure 5.12).

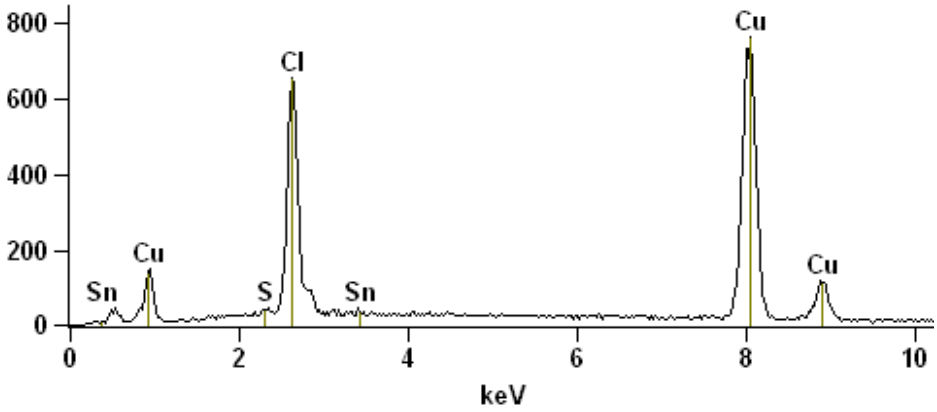

Fig. 5.12: EDS analysis on the patina of the 3% tin sample formed after 48 hours of exposure to sea water vapor. Image 5.11 d.

At higher magnification (image "b") the crystals shape is prismatic with a typical orientation. Also in this case the EDS detects high concentration of chlorides combined with copper and oxygen (Figure 5.13).

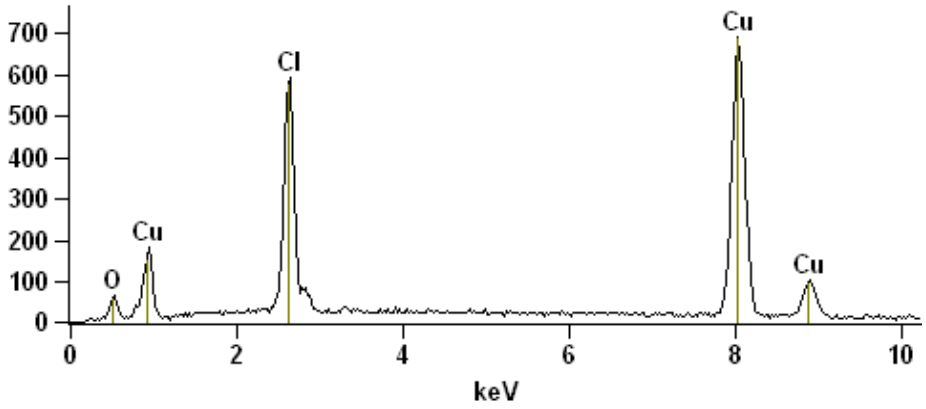

Fig. 5.13: EDS analysis on the patina of the 3% tin sample formed after 48 hours of exposure to sea water vapor. Image 5.11 b.

Image "c" shows different morphologies of corrosion products of the 3% tin sample. Copper and chloride are detected everywhere in the different corrosion morphologies. The composition of the cubic crystals in image "c" is shown in Figure 5.14.

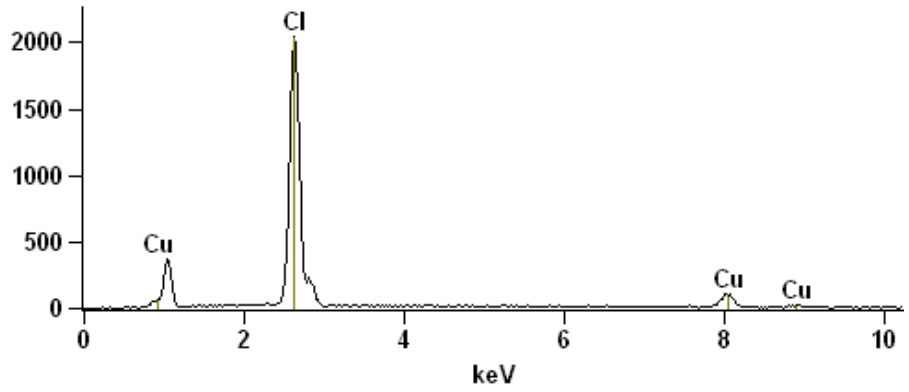

Fig. 5.14: EDS analysis on the patina of the 7% tin sample formed after 48 hours of exposure to sea water vapor. Image 5.11 c.

After 48 hours of exposure of the 7% tin sample, some peculiar shapes are detected on the surface, as shown in Figure 5.15.

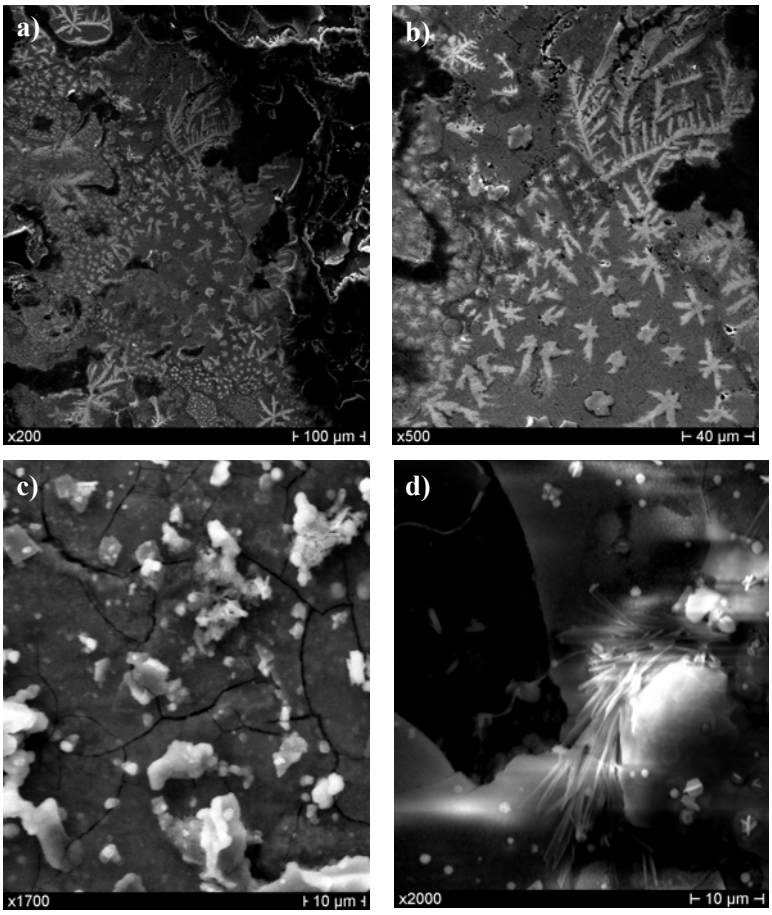

Fig 5.15: SEM secondary electron images at a) x200, b)x500 of 7% tin sample exposed for 48 hours to sea water vapor; c) x1700 and d) x2000 of 7% tin sample exposed to sea water vapor for 240 hours.

Images “a” and “b” show a characteristic corrosion morphology that wasn’t noticed in the case of the 3% tin sample. Also the 20% tin sample reveals a dendritic morphology on its surface after a 48 hours exposure to sea water vapor. On both alloys surfaces exposed to marine spray for 240 hours these crystals disappear. EDS was also performed on the surface represented in Figure 5.15 d: the white crystal “globes” along with the flat surface underneath (also shown in Figure 5.15 c) is composed of chloride, copper and tin. The “filamentary” crystals (identifiable in the center of Figure 5.15 d) are composed of sulfur and copper. The EDS analysis results are reported in Figure 5.16.

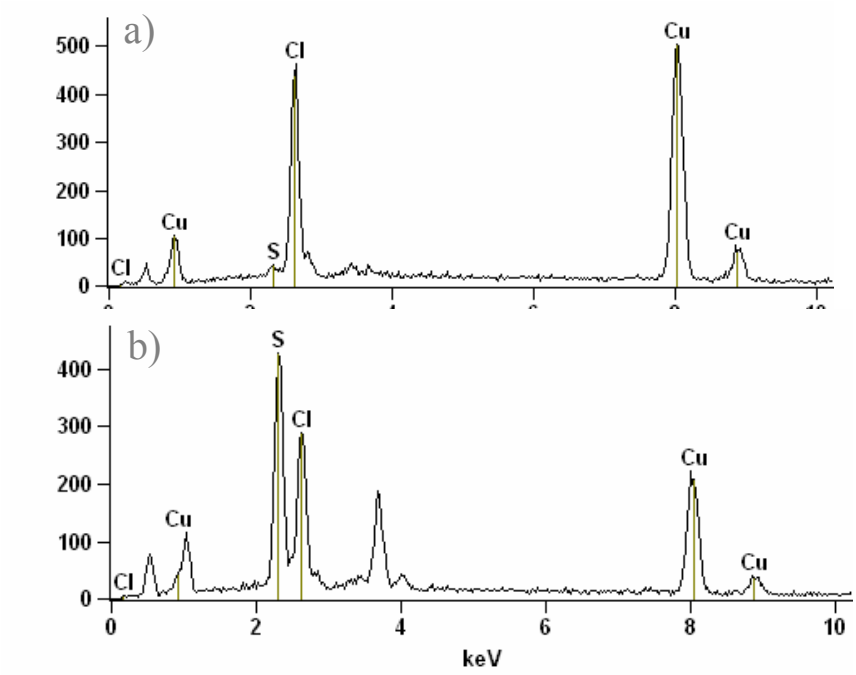

Fig. 5.16: EDS analysis on the patina of the 7% tin sample formed after 48 hours of exposure to sea water vapor. EDS carried out on the a) white crystal “globes” and on the b) “filamentary” crystals of the Image 5.15 d.

XRD was performed in order to complete a qualitative analysis on samples exposed for 240 hours to sea water spray. Figure 5.12 shows the relative diffractograms.

On the 3% tin samples XRD detected the presence of two oxides: cuprite (CuO_2) and cassiterite (SnO_2). No chloride was found. On the 7% tin sample XRD also detected atacamite ($Cu_2Cl(OH)_3$) (a chloride compound). Atacamite was detected also on the 20% tin sample along with covellite (CuS). However, the absence of the chloride on the 3% tin sample XRD analysis does not support the EDS and visual analysis conclusions. This is probably due to the film chloride inhomogeneity, to the copper oxide high concentration, and to the specifics of the XRD instrument that doesn’t work at slant angles.

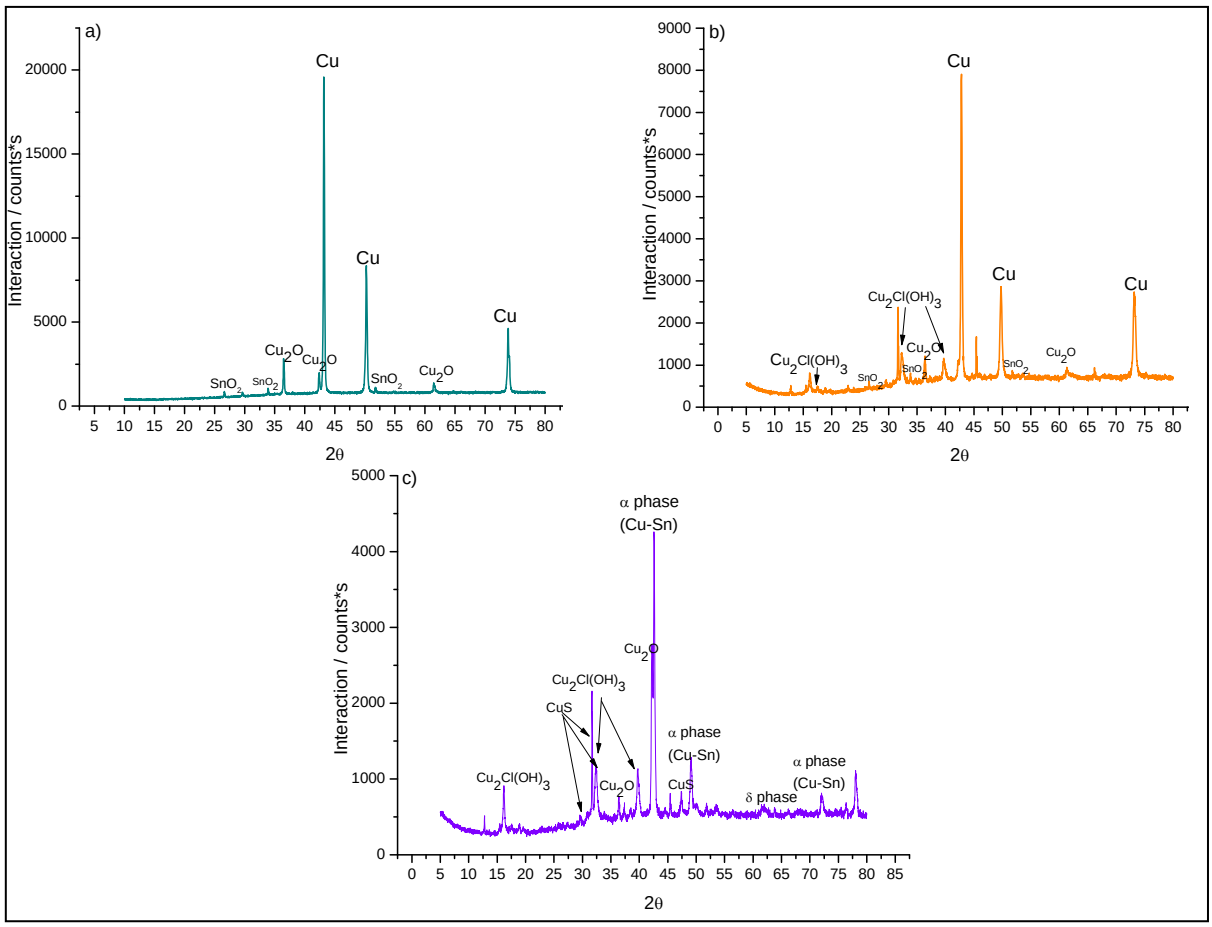

Fig.5.12: XRD diffractograms of the 3% (a), 7% (b) and 20% (c) tin samples exposed to sea water vapour for 240 hours.

5.2.3 Mass gain

The samples were weighted before and after the exposure to sea water vapor in order to calculate the mass gained with the corrosion products. This measurement can be used as an index of corrosion aggression of the alloys.

Table 5.7 shows the weight difference between clean samples and samples after chamber exposure.

	Δw 3% mg	**Δw 7% mg**	**Δw 20% mg**
2 hours	0.5	0.2	0.1
4 hours	0.2	0.4	/
24 hours	0.4	0.7	0.4
48 hours	0.8	0.5	0.2
96 hours	0.4	0.9	0.5
240 hours	0.25	0.19	0.23

Table 5.7: weight difference between the clean alloy and after their exposure to sea water vapor.

Weight values depend on the patina leaching phenomena but also on the alloys elements loss during the tests. However, summing up the results, the mass gained after exposure turns out be almost the same for the three different alloys. The higher value is observed for the 3% tin sample, followed by the 20% and 7% tin samples. This result supports the colorimetric results. The 7% tin sample shows a higher increase in weight from the 4^{th} to the 96^{th} hour. Afterwards this increase gets lower compared to weight increase of other alloys.

5.3 Conclusions

The results obtained with the in field exposure (paragraph 4.1) and with spray tests (paragraph 5.2) proved a more intense aggressiveness of marine environment compared to the urban environment. All the alloys tests showed a strong corrosion progress with little differences between the corrosion products in each specific sample.

In this paragraph the results obtained by the different techniques will be compared to extrapolate more information about the bronze alloys conservation state in natural and artificial environments.

A comparison between the *in field* exposure and the laboratory tests will be provided.

The samples exposed for 4 months in a natural marine environment show a different corrosion process.

In this environment the difference of damage on the three samples is less clear.

The 3%, 7% and 20% tin samples have the same reflectance percentage loss, (as shown in the reflectance curves) but different absorption in the 450-550 nm region were registered. A higher peak is detected on the 20% tin sample curve, followed by the 7% and 3% tin samples curves. In the 20% tin sample the corrosion products have a higher green component compared to the other alloys.

The color differences are very similar (as shown in Table 5.8).

	Natural marine environment	**Laboratory marine environment**
3%	39.09	29.55
7%	37.98	25.61
20%	33.89	26.65

Tab. 5.8: Color difference between the clean alloy, after 4 months of exposure to natural environment and after 240 hours to sea water spray.

However, the more damaged turns out to be the 3% tin sample followed by the 7% and 20% tin samples.

In the laboratory test the 7% tin sample shows a better corrosion behavior than the 20% tin sample but the difference between the two samples is really small.

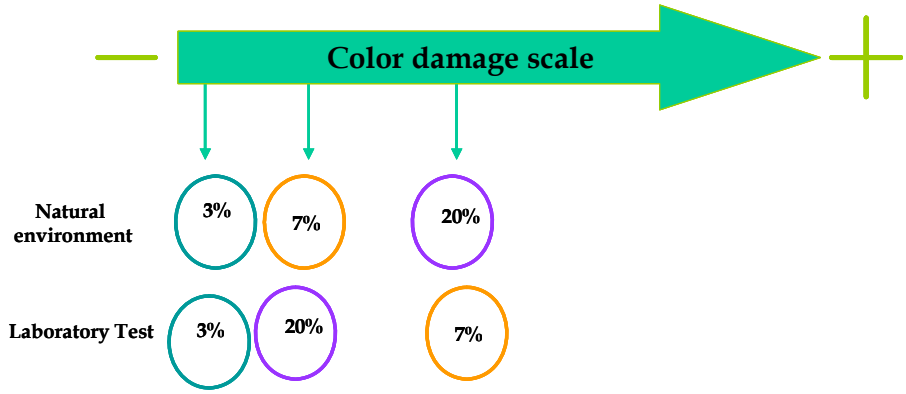

Fig. 5.13: The "Color damage scale" for the three alloys exposed to natural and laboratory test.

References

[53] International Organization for Standardization, ISO 9223: 1992, "Corrosion of metals and alloys- Corrosivity of the atmospheres- Classification", www.iso.org.

[54] A. Granic, H. O. Curkovic, E. Stupnisek – Lisac, M. Kharshan, AFurman, *"Bronze protection in artificial seawater"*, The Electrochemical Society 902, 1712 (2009), 35-48.

6. EIS and spectrocolorimetry: new approaches to improve the use of these techniques in the field cultural heritage

One of the aims of the research was to suggest a new approach to the interpretation of data obtained from a set of techniques used in diagnostics and conservation of cultural heritage.
As shown in the previous chapters, a tight correlation between electrochemical spectroscopy impedance parameters and corrosion indexes was pursued as well as with the colorimetric parameters. Also an illustration of graphical results was introduced to summarize and simplify the process description.
In this chapter, EIS and spectrocolorimetry was studied, tested and re-interpreted to improve its application to diagnostic of cultural heritage.
Regarding the EIS, this aspect has been considered by studying a measurement arrange that could result less invasive as possible. Moreover, the reproducibility and sensibility of the measurements on complex cases of corrosion was evaluated.
The re-interpretation of the spectrocolorimetry was suggested by a new data elaboration to identify corrosion products.

6.1 Electrochemical impedance spectroscopy applied to cultural heritage diagnostic: precautions and innovative use of the results

Although the processes of electrochemical corrosion of metals are well known, the application of electrochemical analytical techniques in conservation and diagnostic of cultural heritage is still difficult. Only in recent years the electrochemical analysis have become frequently used, highlighting the importance of taking specific precautions in order to result not invasive for the artefacts.
A preliminary research was done to find the best conditions in which electrochemical measurements can be performed [1].
Two common electrolytes used in the Electrochemical impedance were tested to evaluate the aggressiveness towards copper and its alloys. Figure 6.1. shows impedance measurements.

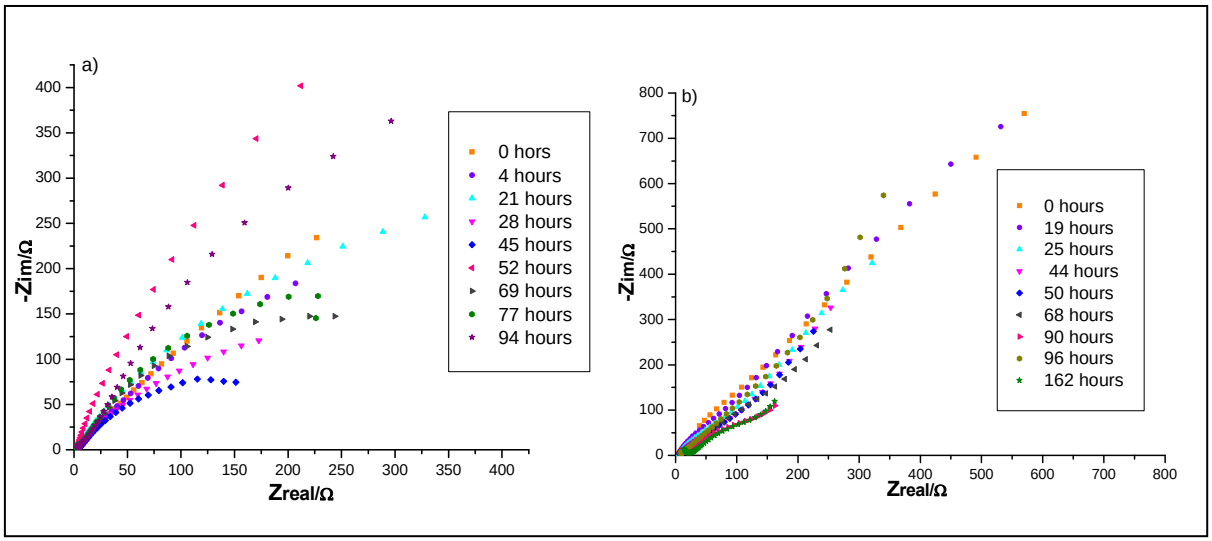

Fig. 6.1: EIS of stability test of copper immersed in a solution a) NaCl 1M and b) Na_2SO_4 1M [1].

A copper electrode was immersed in sodium chloride for six days and EIS was carried out twice a day (Figure 6.1 a).

As shown, the curves close to indicate a patina formation. At the 52nd hour the film is dissolved as well as the patina formed until the 77th hour.

The EIS results on copper immersed in sodium sulphate during 7 days are shown in Figure 6.1 b. As can be seen, the curves are overlapped especially during the first five measurements. Only after 68 hours the curve is closed and continues and enhances as time goes by, indicating a patina formation. The immersion time is higher compared to the previous test, even if the results show a less powerful aggression: the copper turns out to be less damaged from sodium sulphate than from sodium chloride. This is why it is better to use sodium sulphate as an electrolyte when working with cultural heritage artefacts [1].

Another important aspect which needs to be investigated is the sensibility of the electrochemical impedance spectroscopy in order to detect the smallest corrosion evolution.

Understanding the sensibility of the EIS is also important to identify the influence of surface characteristics on results and to underline the correct context of application for diagnosis. The sensibility explains what kind of questions can be answered by EIS and what diagnostic problem can be encountered.

A preliminary test on the measurements reproducibility was also performed.

Figure 6.2 shows a selection of EIS graphs of some samples analyzed in this work. Each graph reports the lasts two curves of a EIS consecutively performed on the samples in order to show the reproducibility of the results.

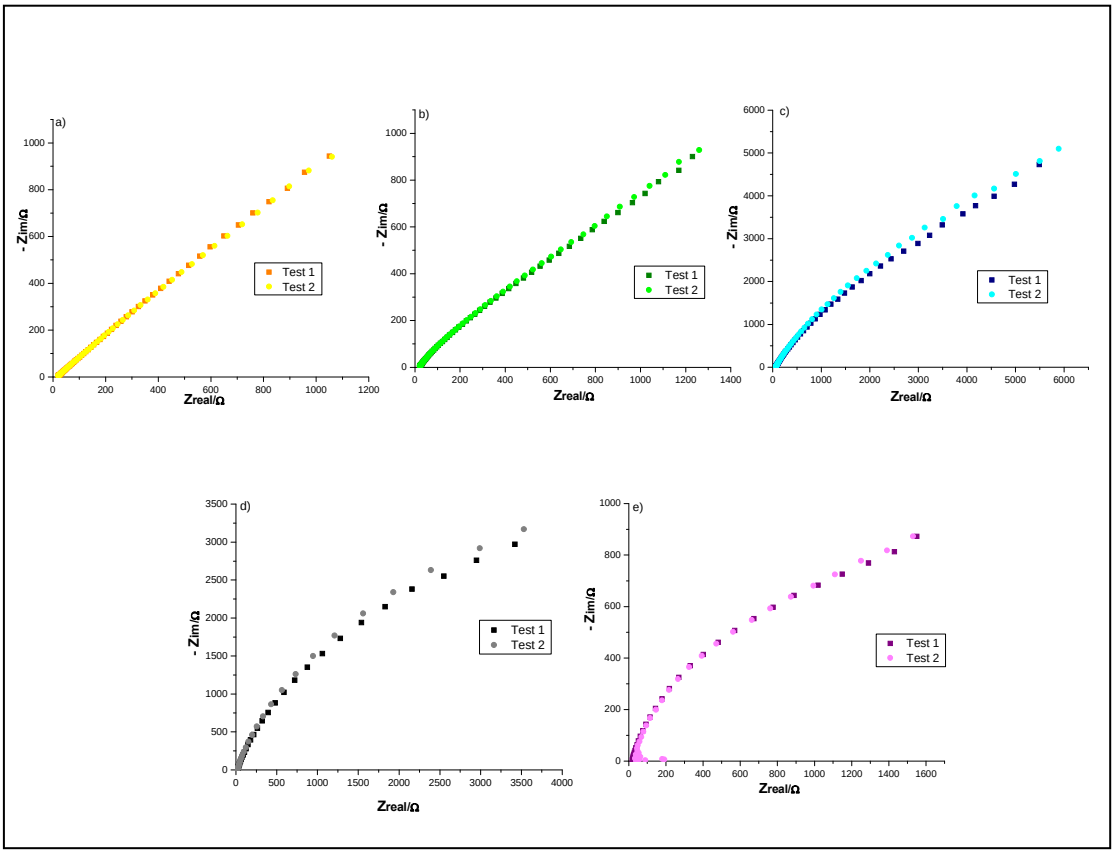

Fig. 6.2: EIS of reproducibility measurements test done on samples a) 3% of tin b) 7% of tin and c) 20% of tin exposed in Ghent; d) 20% of tin exposed for 96 hours to acid rain vapour and e) 20% of tin exposed for 240 hours to acid rain vapour.

As shown in Figure 6.2, the consecutive measurements give the same spectra, suggesting that results are reproducible. However, if the measurements are repeated after a few days the results change. The samples exposed to the different corrosion tests were analyzed with EIS and afterwards preserved in a no-oxygen chamber for some days before repeating the measurement.

The chamber with RH%, temperature and oxygen concentration monitored is an inert environment where it is possible to conserve the samples.

Figure 6.3 shows two examples of EIS carried on the same sample after a corrosion test and after some days in a no-oxygen chamber.

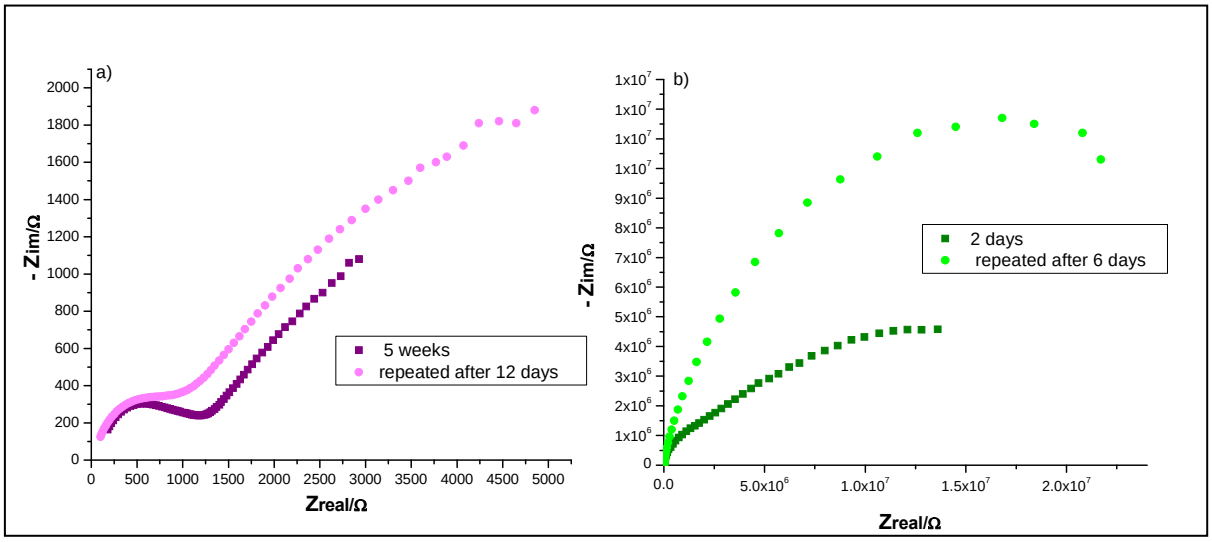

Fig. 6.3: EIS done immediately after and after some days of corrosion test of 3% tin sample in a) sulphuric acid and b) acid rain vapour.

The graphs show that, even if the sample was preserved in a specific inert environment, the surface undergoes some changes that were not identified with other analysis techniques. This difference can be detected by the electrochemical impedance that is sensitive to the smallest surface evolutions.

For this quality the EIS is particularly appropriate to analyse the phases of corrosion processes and to underline the difference between two surfaces or two patinas. Moreover, the patina property's differences can be precisely (and singularly) calculated and quantified from the circuit equivalent elements: porosity (n and W)[2], resistance to corrosion (R), thickness ($1/C_f$)[3], reactivity (Q and W[2]), as mentioned in previous chapters.

These positive aspects are combined with the difficulty of comparing two single measurements (and their parameters) due to the strong affection of the results of surface morphology and the high sensibility of the technique. To make a tight comparison we would need samples treated similarly, preserved in the same identical manner and analyzed almost in the same time. Nevertheless, a comparison of patina evolution can be done with a more generic explanation. Also the values of the porosity, thickness etc. of two cases can be compared in terms of their evolution during time and not necessarily in a tight/strict value comparison. This is the case of cultural heritage artefacts where surfaces are different and the patina formation is influenced by many and multiple factors.

In order to facilitate the interpretation and translation in equivalent circuits of the Nyquist curves in complex real cases, corrosion processes analyzed in this research are collected with others EIS studies performed with the same goal [1]. This is done to build a corrosion impedance cases that could improve EIS use in the field of conservation sciences. Such a cases collection, indeed, could be consulted to support the interpretation of the corrosion phenomenon in similar environmental conditions, to help in the elaboration of the graphs and to explain/describe the corrosion of specific materials in specific environments.

These information could be of a great support to conservation scientists, archaeologists and restorers, whenever a large number of cases is collected.

6.2 Spectrocolorimetry applied to cultural heritage diagnostic: innovative use of the results

In this research an innovative use of spectrocolorimetry is attempted, not only in order to characterize the patina color but also to describe the corrosion evolution (as shown in the previous chapters). Colorimetric parameters were associated to specific corrosion indexes. The correct relationships between colour parameters and corrosion description was evaluated comparing the colorimetry interpretations/results with the interpretations/results obtained with other techniques.

More in detail, the reflectance curves and the lightness (L^*) were used to explain the patina formation and its growth. These parameters can distinguish small differences and can therefore highlight small patina evolution. The a^*, b^* and hue were correlated to the quality composition of the patina. Different values of these parameters on a same sample can mean different kinds of products formation. The colour difference (ΔE) was used to describe the corrosion rate: relevant ΔE values indicate a great color change associated to fast corrosion that produces a patina with a colour that differs from the surface colour previously analyzed. The ΔE is also an index of color damage (color difference from the natural alloy's color). The variation of the ΔE during time can be used to estimate the patina's evolution and stability. The color difference, indeed, can be correlated to the patina formation or to the patina dissolution. The dissolution process occurring on the film is an indicator of instability or poor passivity property of the patina.

In this work, in order to attempt improving spectrocolorimetry use in the analysis of metallic artefacts, a new data elaboration to identify the corrosion products was envisaged.

Few researches were carried out in this direction: an example is Franceschi [4] that used spectrocolorimetry to determine the copper content in quasi-binary bronzes and brasses.

To pursue this general aim, many colorimetries of many corrosion products analyzed singularly and/or combined need to be appropriately collected.

In this research an attempt to make a first step to reach this goal was done: spectrocolorimetry measurements combined with XRD analysis were collected and studied to find color parameters characteristics as fingerprints of corrosion products.

To extrapolate this information we suggest the possible transformation of the graphs and data from the λ to the energy's domain (Figure 6.4 "a" e "b"). This conversion is possible using the following equation:

$$E = h \times c / \lambda$$

where:

h is the Plank costant (6.626×10^{-34} Js – 4.1357×10^{-15} eV);

c is the light speed (300.000 km/s – 3×10^{8} m/s).

By deriving the reflectance curve in relation to the energy (obtained with the equation above), the adsorption edge of the patina can be obtained [5] (Figure 6.4 c).

The position of the adsorption edge can be used to try finding a correlation with the corrosion products as well as the values of the area above that curve. By integrating that function, the energy reflected from the patinas when radiated from the spectrophotometer radiation is obtained.

Figure 6.4 shows the above described steps.

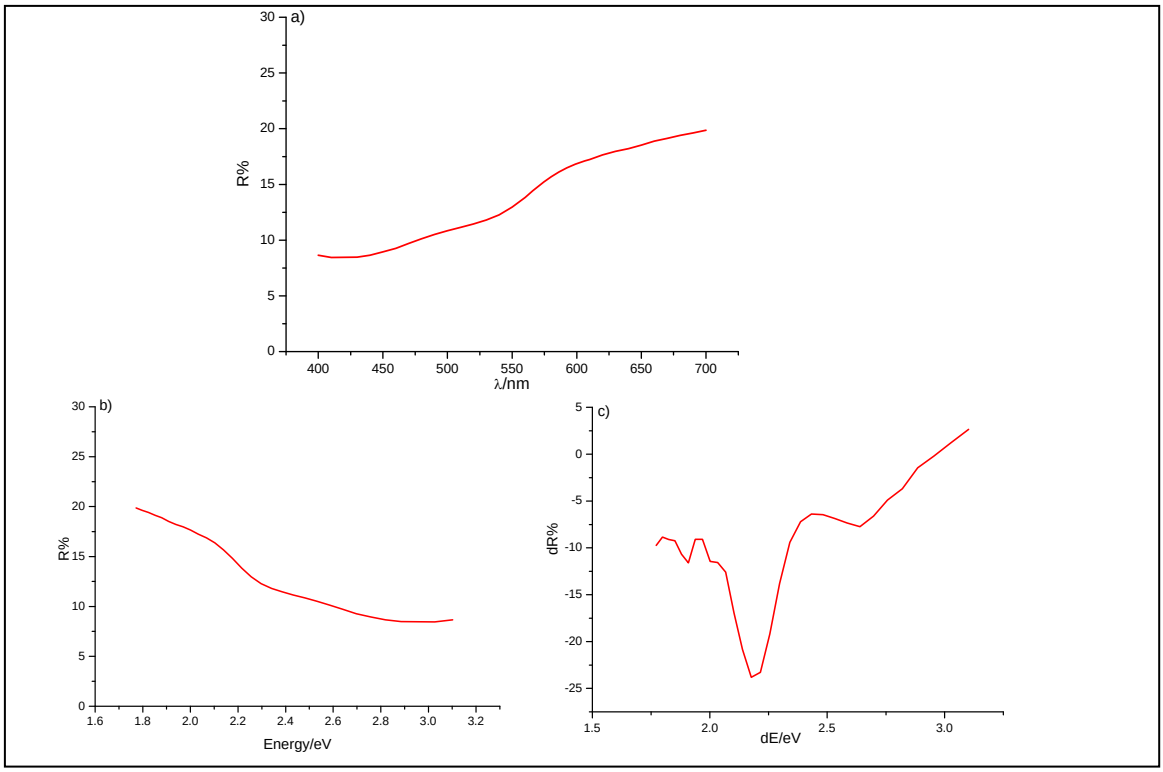

Fig. 6.4: Reflectance curve in a) R%/λ, b) R%/E and c) dR%/dE with the adsorption edge.

A correlation between the adsorption edge's position and/or energy with its specific corrosion product is in progress. However, Appendix III shows a table with the indication of the samples tested, the corrosion products found, the adsorption's edges position and the energy reflected.

References

[55] L.Gianni: "*Synthesis and characterization of new electrolyte systems for the study of electrochemical process of copper and its alloys"*, Masters degree Thesis and published on XXII National Congress of Italian Chemical Society (2009) Congress atcs,;

[56] J. Sandberg, I.O. Wallinder, C. Leygraf, N. Le Bozec, "Corrosion induced copper runoff from naturally and pre-patinated copper in marine environment", Corrosion Science 48 (2006) 4316-4338;

[57] W.A. Badawy, R.M. El-Sherif, H. Shehata, *"Electrochemical behavior of alluminium bronze in sulfate-chloride media"*, Journal Applied Electrochemistry (2007) 37:1099-1106;

[58] E. Franceschini, *"Synthese de dix ans de recherces sur la premiere metalurgie en Ligurie (1988-1998)"*, in: A. Guarino (Ed), Proceedings of second international congress on science and technology for the safeguard of cultural heritage in the Mediterranean basin, Paris, 5-9 July 19999, Elsevier, 2000, pp.521-525;

[59] T. Shiraishi, Y. Takuma, E. Miura, Y. Tanaka, K. Hisatsune, *"Factors affecting the optical properties of Pd-free Au-Pt based alloys"*, Journal of Material Science, Materials in Medicine 14 (2003).

7. Conclusions

By studying the influence of tin on bronze corrosion we have seen that the behavior of a specific alloy is similar in each environment where a sample is exposed. There are exceptions, but the general interpretation that corrosion behavior improves when the tin content increases in an alloy is confirmed. In the two urban environments taken into account in this research, the 3% tin samples turned out to be the most damaged compared to the 7% and 20% tin samples. It is worth noting that the 7% tin sample, that is more attacked than the 20% tin sample, generates a patina with some good "barrier" properties. This explains why – occasionally –the 7% tin sample was referred to as the sample with the more effective anti-corrosion behavior.

In laboratory tests the results are different only when the samples are immersed in nitric acid or sprayed with synthetic acid rain: the 7% tin sample showed a more instable patina, whilst in the 3% tin sample a thick stable layer showed up.

With the laboratory tests of immersion in acid solutions, we highlighted the different aggressiveness of solutions for the three alloys immersed. The 3% tin sample turned out to be more damaged from the immersion in nitric acid, a bit less from the sulphuric acid and even less from the acid rain. The 7% tin sample appeared to be more attacked from the sulphuric acid and acid rain rather than from nitric acid, while the 20% tin sample appeared more damaged by the immersion in the acid rain solution.

As saw for the 3% tin sample, the patina is particularly unstable when facing high levels of water (as in Ghent and in immersion tests) that leaches the layer. The 7% tin sample is more damaged from high concentration of pollutants in wet and dry cycles (as in Rome and in spray tests). These corrosion behavior of the alloys allow to correlate the accelerated aging test of immersion to Ghent tests and the spray chamber tests to Rome tests.

In the marine environment the corrosion is quite fast, stronger than in urban environment, and damages the three alloys almost in the same way.

The research was also aimed to improve the EIS and CIE L^* a^* b^* techniques results interpretation on the field of cultural heritage conservation sciences. In this framework, a tight correlation between electrochemical spectroscopy impedance parameters and corrosion indexes was found and a new approach to the use and interpretation of spectrocolorimetry results was established. Moreover, a graphical results illustration was introduced in order to summarize and simplify the results interpretation. The "Damage scale" is a clear tool thought to be consulted by professionals of different disciplines to plan a restoration or conservation activity and to set up an emergency restoration scale knowing the conservative state of artefacts.

Regarding the EIS, improvements to the technique's application to increase its use in the field of cultural heritage diagnosis was considered by studying the less invasiveness of the measurements. By

testing the aggressiveness of the electrolytic solutions frequently used in EIS measurements, we found that the sodium sulphate is the less dangerous for the bronze.

By testing the sensibility of the electrochemical impedance spectroscopy was understood that the technique could be read in macroscopic terms (to explain the corrosion evolution) as well as in microscopic terms (to determinate the patina evolution, properties and reactivity by the equivalent circuits).

The cases analyzed were collected to build a EIS impedance cases. The interpretations of equivalent circuits and corrosion models were collected to build a collection with the aim of simplifying the understanding of the EIS results and to widespread its use in cultural heritage diagnostics.

The impedance collection can be consulted to support the interpretation of the corrosion phenomenon in similar environmental conditions, to help in the elaboration of the graphs, in their translation in equivalent circuits and to explain/describe the corrosion of specific materials in a specific environment. These information could be of support to a conservation scientists that approaches the EIS, to the archaeologist that can have an immediate vision of the conservation state of an object and to the restorers that can know what physical and chemical properties has the patina formed before removing it.

A new relationship between colorimetric and corrosion parameters was found. These relationships results are useful to describe the patina formation (R% and L^*), the patina quality-composition (a^*, b^*, C^* and hue), the corrosion rate and the damage (ΔE). These parameters showed to be really sensitive to small changes and are therefore particularly appropriate to distinguish even small differences of the corrosion processes.

In an attempt to determine a patina's composition with spectrocolorimetry, a first step was done testing a procedure that must be applied and further tested to find color parameters characteristics as fingerprints of corrosion products.

Appendix I: Equivalent Circuit of EIS

Table 1: Ghent field exposition from March 2010 to April 2010																		
	3%Sn						7%Sn						20%Sn					
Time	R_1	R_2	C_1	n	C_2	n	R_1	R_2	C_1	n	Q_2	n	R_1	R_2	C_1	n	C_2	n
Clean	26.22		$3.65 *10^{-4}$	0.73	/	/	24.5	/	$2.28 *10^{-4}$	0.80	/	/	22.93	$15.78 *10^{3}$	$2 *10^{-4}$	0.76	/	/
	R(RQ)						R(RQ)						R(RQ)					
1 week	23.36	$2.18 *10^{3}$	$1.83 *10^{-4}$	0.69	/	/	23.08	$2.24 *10^{3}$	$2.9 *10^{-4}$	0.73	/	/	16.82	$2.13 *10^{3}$	$1.7 *10^{-4}$	0.74	W 26.04	/
	R(RQ)						R(RQ.						R(RQ)W					
2 weeks	16.19	/	$2.79 *10^{-4}$	0.49	/	/	17.48	282.8	$1.51 * 10^{-4}$	0.67	W 2291	/	59,72	$15.03 *10^{3}$	$2.68 * 10^{-5}$	0.67	/	/
	RQ						R(RQ)W						R(RC)					
3 weeks	1.53	1.046	$3.75 *10^{-4}$	0.95	$4.11 *10^{-4}$	/	151.33	$5.599 *10^{3}$	$1.99 *10^{-8}$	W 8.05 $*10^{4}$	/	/	28,77	$12.60 *10^{3}$	$0.21 *10^{-4}$	/	/	/
	R(RQC)						R(RC)W						R(RQ)					
4 weeks	45.96	905.8	$9,11 *10^{-6}$	R 463.87	$5.32 *10^{-5}$	W $3.33 *10^{3}$	415.32	$9.74 *10^{3}$	$4.150 *10^{-9}$	W $8.68 *10^{5}$	/	/		$7,.2 *10^{6}$	$1,.6 *10^{-7}$	0.38		
	R(RC)(RQ)W						R(RC)W						RQ					
5 weeks	141.5	$11.63 *10^{3}$	$6.10 *10^{-5}$	0.58	/	/	37.63	$8.72 *10^{3}$	$3.44 *10^{-5}$	0.60	/	/	129,2	$33.30 *10^{3}$	$4.31 *10^{-5}$	0.53	/	/
	R(RQ)						R(RQ)						R(RQ)					

Capacitance are expressed in F
Resistance are expressed in Ohm
R_1 = Electrolite resistance
R_2 = Charge transfer resistance or film resistance
Q = CPE
n = CPE index
C= Film capacity
W= Warburg

Table 2: Samples immersed in synthetic acid rain solution																		
Time	**3%Sn**						**7%Sn**						**20%Sn**					
	R_1	R_2	C_1	n	C_2	n	R_1	R_2	C_1	n	C_2	n	R_1	R_2	C_1	n	C_2	n
Clean	26.22		$3.65 *10^{-4}$	0.73	/	/	24.5	/	$2.28 *10^{-4}$	0.80	/	/	22.93	$15.78*10^{3}$	$2 * 10^{-4}$	0.76	/	/
	RQ						RQ						R(RQ)					
1 day	22.94	/	$5.04 *10^{-4}$	0.78	W 37,88	/	23.88	/	$9.3 * 10^{-4}$	0.74	/	/	17.10	/	$3.23 * 10^{-4}$	0.78	/	/
	RQW						RQ						RQ					
1 week	21.1	433.8	$9.4 * 10^{-5}$	0.56	$W 1*10^{-5}$		18.02	27.25	$5.04 *10^{-4}$	0.41	W 621.5	/	20.78	/	$1.58 * 10^{-3}$	1	/	/
	R(RQ)W						R(RQ)W						RQ					
2 weeks	70.7	823	$11.8 *10^{-6}$	$1.57 *10^{3}$	$5.3 *10^{-5}$	0.38	0,01	$7.49 *10^{5}$	$1.33 *10^{-7}$ n= 0,76	R $5.16 *10^{5}$	$8.36 *10^{-8}$ n= 0.54	W $2.88 *10^{5}$	17.85	52.56	$1.33 * 10^{-4}$ n= 0.43	R 157.7	C $1.50 *10^{-6}$	/
	R(RC)(RQ)W						R(RQ)(RQ)W						R(RQ)(RC)					
3 weeks	34.38	9.94	$4.91 *10^{-4}$	O.81	W 3471	/	88.2	$32.7 *10^{3}$	$5.66 *10^{-6}$	0.53	/	/	10.76	$0.510 *10^{3}$	$1.04 * 10^{-4}$	R $7.78 *10^{3}$	$2.4 *10^{-4}$	0.46
	R(RQ)W						R(RQ)						R(RQ)(RQ)					
4 weeks	28.10	$1.175 *10^{3}$	$6.59 *10^{-6}$	0.66	W 1057	/	$3.80 *10^{3}$	$2.35 *10^{3}$	$7.24 *10^{-6}$	0,56	$13.75 *10^{3}$	/	20.65	$1.34 *10^{3}$	$2.01 *10^{-5}$	0.56	R = 1.35	C = $44.8* 10^{-6}$
	R(RQ)W						(RQ)(RC)						R(RQ)(RC)					
5 weeks	20.62	$1.46 *10^{3}$	$0.12 *10^{-4}$	0.60	/	/	351.9	844.8	$1.93 *10^{-5}$	0.59	W 556.6	/	$8.82*10^{3}$	$1.06 *10^{3}$	$4.45 *10^{-5}$	0,.4	R $1.02 *10^{5}$	/
	R(RQ)						R(RQ)W						R(RQ)R					

Capacitance are expressed in F
Resistance are expressed in Ohm
R_1 = Electrolite resistance
R_2 = Charge transfer resistance or film resistance
Q = CPE
n = CPE index
C= Film capacity
W= Warburg

Table 3: Samples immersed in 0,1M H_2SO_4																		
	3%Sn						7%Sn						20%Sn					
Time	R_1	R_2	C_1	n	C_2	n	R_1	R_2	C_1	n	C_2	n	R_1	R_2	C_1	n	C_2	n
Clean	26.22	/	3.65 $*10^{-4}$	0.73	/	/	24.5	/	2.28 $*10^{-4}$	0.80	/	/	22.93	15.7 $*10^{3}$	2 $*10^{-4}$	0.76	/	/
	RQ						RQ						R(RQ)					
1 day	19.75	/	4.6 $*10^{-4}$	0.79	/	/	31.7	/	5.7 $*10^{-4}$	0,73	/	/	24.81	2.15 $*10^{3}$	4.1 $*10^{-4}$	0.67		
	RQ						RQ						R(RQ)					
1 week	36.84	2.121 $*10^{3}$	C 5 $*10^{-4}$	R 119.2	C 1.77 $*10^{-7}$	W 3.57 $*10^{3}$	24,44	/	1.19 $*10^{-3}$	0.42	/	/	24.74	733.4	C 1.42 $*10^{-5}$	R 1.40 $*10^{3}$	6.68 $*10^{-5}$	W 851.3
	R(RC)(RC)W						RQ						R(RC)(RQ)W					
2 weeks	75	0.58 $*10^{3}$	C 29.7 $*10^{-6}$	R 6.71 $*10^{3}$	W 0.7 $*10^{-4}$	/	12.41	79.9	C 123 $*10^{-6}$	R 0.50 $*10^{3}$	6.30 * 10^{-4} n=0.45	W = 0.86 $*10^{3}$	17.38	1.69 $*10^{3}$	1.02 $*10^{-4}$	0.54	/	/
	R(RC)(RW)						R(RC)(RQ)W						R(RQ)					
3 weeks	132	131 $*10^{5}$	1.75 $*10^{-6}$	0.63	/	/	102	1.52 $*10^{5}$	1.75 $*10^{-6}$	0.62	/	/	23.63	2.18 $*10^{3}$	5.01 $*10^{-5}$	0.60	/	/
	R(RQ)						R(RQ)						R(RQ)					
4 weeks	1415	557.2	2,22 $*10^{-5}$	0.46	C 8.88 $*10^{-6}$	W 1.89 $*10^{3}$	32.43	2.84 $*10^{3}$	1.61 $*10^{-5}$	0.65	W 2.24 $*10^{3}$	/	29.1	2.44 $*10^{3}$	1.92 * 10^{-5}	0.66	W 0.32 * 10^{-3}	/
	(RQ)(RC)W						R(RQ)W						R(RQ)W					
5 weeks	33.56	2.71 $*10^{3}$	2.16 $*10^{-6}$	0.66	W 3.12 $*10^{3}$	/	1.68 $*10^{5}$	2.28 $*10^{7}$	4.02 $*10^{-12}$				28.8	1.67 $*10^{3}$	5.42 * 10^{-5}	0.57	/	/
	R(RQ)W						R(RQ)						R(RQ)					

Capacitance are expressed in F
Resistance are expressed in Ohm
R_1 = Electrolite resistance
R_2 = Charge transfer resistance or film resistance
Q = CPE
n = CPE index
C= Film capacity
W= Warburg

Table 4: Samples immersed in 0,1M HNO_3																		
	3%Sn						7%Sn						20%Sn					
Time	R_1	R_2	C_1	n	C_2	n	R_1	R_2	C_1	n	C_2	n	R_1	R_2	C_1	n	C_2	n
Clean	26.22	/	3.65 $*10^{-4}$	0.73	/	/	24.5	/	2.28* 10^{-4}	0.80	/	/	22.93	15.78 $*10^{3}$	2 $*10^{-4}$	0.7	/	/
	RQ						RQ						R(RQ)					
1 day	27.81	4.32 $*10^{3}$	1.93 $*10^{-3}$	0.68	/	/	24.81	/	3,39 $*10^{-5}$	0.78	R 960.8	W 2.04 $*10^{3}$	20.35	1.98 $*10^{3}$	1.64 $*10^{-4}$	0.6	/	/
	R(RQ)						R(Q[RW])						R(RQ)					
1 week	20.32	3.13 $*10^{3}$	1.83 $*10^{-4}$	0.76	/	/	26.29	1.32 $*10^{3}$	C 1.01 $*10^{-4}$	R 144.1	C 1.2 $*10^{-4}$	/	18.25	118.7	C 4.82 $*10^{-4}$	W 1.1 $*10^{3}$	/	/
	R(RQ)						R(RC)(RC)W						R(RC)W					
2 weeks	34.84	10.5 $*10^{3}$	1.90 $*10^{-5}$	0.59	/	/	25.91	7.51 $*10^{3}$	2.71 $*10^{-5}$	0.71	/	/	26.92	5.03 $*10^{3}$	1.18 $*10^{-5}$	0.6	/	/
	R(RQ)						R(RQ)						R(RQ)					
3 weeks	24.96	7.72 $*10^{3}$	3.6 $*10^{-5}$	R 1.21 $*10^{3}$	6.61 $*10^{-6}$	W = 0.25 $*10^{-3}$	3.,50	2.28 $*10^{3}$	8.9 $*10^{-5}$	0.62	/	/						
	R(RQ)(RQ)W						R(RQ)						BROKEN					
4 weeks	6.48 $*10^{3}$	36.3 $*10^{3}$	2.89 $*10^{-7}$	0.72	2 $*10^{-5}$	0.36	9.29 $*10^{5}$	/	5.47 $*10^{-7}$	0.65	/	/						
	(RQ)(RQ)						(RQ)						BROKEN					
5 weeks	43.9 $*10^{3}$	/	8.67 $*10^{-7}$	W 1.37 $*10^{5}$	/	/	27.19 $*10^{3}$	/	4.88 $*10^{-5}$	/	/	/						
	(RC)W						(RQ)						BROKEN					

Capacitance are expressed in F
Resistance are expressed in Ohm
R_1 = Electrolite resistance
R_2 = Charge transfer resistance or film resistance
Q = CPE
n = CPE index
C= Film capacity
W= Warburg

Table 5: Samples sprayed with synthetic acid rain																		
Time	**3%Sn**						**7%Sn**						**20%Sn**					
	R_1	**R_2**	**C_1**	**n**	**C_2**	**n**	**R_1**	**R_2**	**C_1**	**n**	**C_2**	**n**	**R_1**	**R_2**	**C_1**	**n**	**C_2**	**n**
Clean	26.22		$3.65*10^{-4}$	0.73	/	/	24.5	/	$2.28*10^{-4}$	0.80	/	/	22.93	$15.78*10^{3}$	$2*10^{-4}$	0.76	/	/
	RQ						RQ						R(RQ)					
2 hours	22.61	363.64	$5*10^{-4}$	0.44	W 925.3	/	18.76	31.33	$3.87*10^{-4}$	R $1.99*10^{3}$	$3.60*10^{-4}$	W $6.48*10^{3}$	13.31	5.60	$1.58*10^{-4}$	R $1.24*10^{3}$	$9.92*10^{-6}$	W $1.16*10^{3}$
	R(RQ)W						R(RQ)(RC)W						R(RQ)(RC)W					
4 hours	844.42	$9.86*10^{5}$	$2.09*10^{-9}$	R $9.32*10^{5}$	C $8.75*10^{-9}$	W $1.12*10^{6}$	18.57	191.59	$5.04*10^{-4}$	R 120.9	$2.83*10^{-5}$	W 702.4	623.4	$1*10^{6}$	$7.31*10^{-9}$	R $3.01*10^{5}$	$1.58*10^{-8}$	0.81
	R(RQ)(RC)W						R(RQ)(RC)W						R(RC)(RQ)					
24 hours	839.4	$7.75*10^{5}$	$2.1*10^{-8}$	R $2.94*10^{-13}$	$4.16*10^{-7}$	W $7.96*10^{6}$	146.5	$1*10^{6}$	$2.83*10^{-8}$	R $3.64*10^{5}$	$4.25*10^{-8}$	0.77	$6.24*10^{6}$	/	$1.21*10^{-9}$	0.6	/	/
	R(RQ)(RQ)W						R(RC)(RQ)						RQ					
48 hours	22.61	363.64	$5*10^{-4}$	0.44	W 925	/	$1.08*10^{6}$	$1.92*10^{8}$	$4.33*10^{-11}$	0.9	/	/	$2.18*10^{-13}$	$8.71*10^{3}$	$3.19*10^{-5}$	0.79	R 20.4	$1.34*10^{-8}$
	R(RQ)W						R(RQ)						R(RQ)(RC)					
96 hours	$7.8*10^{4}$	$5.33*10^{7}$	$2*10^{-10}$	0.89	/	/	2.85	$5.73*10^{3}$	$5*10^{-4}$	R 13.59	$6.42*10^{-7}$	/	15.07	$7.24*10^{3}$	$2.06*10^{-5}$	R 996	$1.96*10^{-5}$	W $1*10^{3}$
	R(RQ)						R(RQ)(RC)						R(RC)(RC)W					
240 hours	$5.21*10^{5}$	$7.49*10^{4}$	$3.65*10^{-10}$	0.70	/	/	17.09	$1.77*10^{3}$	$4.4*10^{-4}$	0.41	/	/	20.15	808	$7.82*10^{-5}$	R 518	$9.78*10^{-5}$	W $3.55*10^{3}$
	R(RQ)						R(RQ)						R(RC)(RC)W					

Capacitance are expressed in F
Resistance are expressed in Ohm
R_1 = Electrolite resistance
R_2 = Charge transfer resistance or film resistance
Q = CPE
n = CPE index
C= Film capacity
W= Warburg

Appendix II: XRD mineral diffraction

Bronze corrosion products				
Mineralogical name	**Chemical formula**		**2θ**	**Miller indexes [h k l]**
Cassiterite	SnO_2		26.59	[1 1 0]
			33.87	[101]
			50.77	[2 1 1]
Cuprite	Cu_2O		36.42	[1 1 1]
			42.30	[2 0 0]
			61.36	[2 2 0]
Brochantite	$Cu_4SO_4(OH)_6$		13.88	[2 0 0]
			16.54	[2 1 0]
			22.79	[3 1 0] – [2 2 0]
			27.96	[4 0 0] – [1 3 0]
			35.61	[0 2 2]
Gerhardite	$Cu_2(NO_3)(OH)_3$	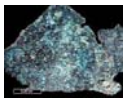	12.8	[0 2 2]
			34.94	[2 0 2]
			25.80	[0 4 0]
Nantokite	CuCl		28.5	[1 1 1]
			47.44	[2 2 0]
			56.46	[3 1 1]
Atacamite	$Cu_2Cl(OH)_3$	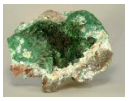	16.19	[0 1 1]
			31.66	[1 1 2]
			39.94	[2 0 2]
Covellite	CuS		31.78	[1 0 3]
			47.93	[1 1 0]
			32.85	[0 0 6]

Appendix III: Chart of the samples tested, the corrosion products found, the adsorption's edges position and the energy reflected

	Corrosion products	Adsorption edge position (eV)	Energy reflected (eV)
Ghent field exposition from March 2010 to April 2010			
3%	SnO_2	1.90; 2.17	11.23
7%	SnO_2	1.90; 2; 2.21;	31.91
20%	SnO_2	1.90; 2; 2.25	24.71
Rome in field exposition from January 2010 to June 2010			
3%		1.88; 2.13; 2.81	5.73
7%		1.85; 2.17; 2.47	5.74
20%		1.88; 2; 2.25; 2.34; 2.48; 2.63	17.33
Samples immersed in synthetic acid solution			
3%	Cu_2O SnO_2 $Cu_4SO_4(OH)_6$	(1.93); 2.53	6.69
7%	Cu_2O SnO_2 $Cu_4SO_4(OH)_6$	(1.93); 2.10; 2.53;	5.50
20%	Cu_2O SnO_2 $Cu_4SO_4(OH)_6$ $Cu_2NO_3(OH)_3$	1.90; 2; 2.18; 2.30; 2.53; 3.02	2.62
Samples immersed in 0,1M H_2SO_4			
3%	Cu_2O SnO_2	2.03; 2.75	6.56
7%	Cu_2O SnO_2	2.06; 2.75	2.66
20%	Cu_2O	1.90; 2.10; 2.73	14.16
Samples immersed in 0,1M HNO_3			
3%	SnO_2	1.89; 2.17; 2.53	11.89
7%	Cu_2O SnO_2	1.90; 2.13; 2.53	25.15
Samples sprayed with synthetic acid solution			
3%	Cu_2O SnO_2	2.10; 2.75	13.23
7%	Cu_2O	2.10; 2.78	15.16

	SnO_2		
20%	Cu_2O	1.87; 1.99; 2.25; 2.34	22.46
	$Cu_2NO_3(OH)_3$		
Fiumicino in field exposition from January 2010 to May 2010			
3%		3.10	1.52
7%		(2.03); 2.63	4.60
20%		(1.93); 2.13; 2.53; 2.81	6.57
Samples sprayed with synthetic sea water			
3%	Cu_2O	(1.93); 2.13; 2.20; 2.43; 2.91	12.19
	SnO_2		
7%	Cu_2O	(1.96); 2.22, 2.57; 2.94	13.98
	SnO_2		
	$Cu_2Cl(OH)_3$		
20%	Cu_2O	(2.07); 2.95	5.37
	$Cu_2Cl(OH)_3$		
	CuS		